ARTIFICIAL METALLOPROTEIN

BASED ON BIOTIN-(STREPT)AVIDIN TECHNOLOGY:

THERMODYNAMIC, KINETIC & SELECTIVITY CONSIDERATIONS

Thèse présentée à la Faculté des Sciences

Institut de Chimie

de l'Université de Neuchâtel

Pour l'obtention du titre de Docteur ès Sciences

Par

Untung Edy Rusbandi

Ingénieur diplômé de l'ENSIACET (F)

Acceptée sur proposition du jury composé de:

Prof. Dr. Thomas R. Ward (Directeur de thèse)

Prof. Dr. Thomas Bürgi (Université de Neuchâtel, expert interne)

Prof. Dr. Martin Albrecht (Université de Fribourg, expert externe)

Soutenue le 9 Novembre 2007

Université de Neuchâtel

2007

Université de Neuchâtel

FACULTE DES SCIENCES
Secrétariat-Décanat de la faculté
- Rue Emile-Argand 11
- CP 158
- CH-2009 Neuchâtel

IMPRIMATUR POUR LA THESE

Artificial Metalloprotein based on Biotin-(Strept)avidin Technology : Thermodynamic, Kinetic and Selectivity Considerations

Edy RUSBANDI

UNIVERSITE DE NEUCHATEL

FACULTE DES SCIENCES

La Faculté des sciences de l'Université de Neuchâtel,
sur le rapport des membres du jury

MM. T. Ward (directeur de thèse),
T. Bürgi et M. Albrecht (Fribourg)

autorise l'impression de la présente thèse.

Neuchâtel, le 27 novembre 2007

Le doyen

T. Ward

UNIVERSITE DE NEUCHATEL
FACULTE DES SCIENCES
Secrétariat-décanat de la faculté
Rue Emile-Argand 11 - CP 158
CH-2009 Neuchâtel

Mots clés en français: hydrogénation énantioselective, technologie biotine-avidine, streptavidine, métalloprotéine, immobilisation, composé biotinylé.

Mots clés en anglais: asymmetric hydrogenation, biotin-avidin technology, streptavidin, metalloprotein, immobilization, biotinylated coordination compound.

Résumé

Catalyses homogènes et enzymatiques se situent dans un premier rang pour la création des catalyseurs efficaces plus souvent utilisés dans l'hydrogénation énantioselective (industrie et académique). Nos efforts étaient axés sur la création de metalloenzymes artificielles basées sur la technologie biotine-(strept)avidine. L'ancrage d'un complexe-aminodiphosphine biotinylé dans la (strept)avidine permet de créer un catalyseur « hybride » efficace possédant les avantages de catalyseur homogène et enzyme. Introduction d'éspaceur chiral dans le composé biotinylé (nouvelle génération de métalloenzymes artificielles) montre quelques résultats intéressants.

Le catalyseur le plus efficace était la combinaison de [Rh(COD)**Biot-(*R*)-Pro-1**]$^{+}$ ⊂ S112W Sav (95% (*S*)) pour la réduction de *N*-α-acetamidoacrylique acide et *N*-α-acetamidocinammique acide. Ainsi la nouvelle génération de métalloenzymes artificielles montre la résistance en présence de la quantité importante du solvant organique. De plus, il est possible d'immobiliser les métalloenzymes artificielles sur le support biotine-sepharose grâce aux 4 sites actifs de la (strept)avidine. Une étude cinétique réalisée montre que la présence de la protéine peut accélérer la vitesse de la réaction (jusqu'à 3 fois par rapport au catalyseur sans protéine). Enfin, une étude thermodynamique exploitant l'incorporation de composé biotinylé [Ru(bpy)$_2$(Biot-bpy)]$^{2+}$ dans la (strept)avidine a été réalisée pour le but de déterminer les constantes d'affinité de composé biotinylé dans la protéine (5-7 ordres de magnitude plus faible par rapport à la biotine).

Abstract

The present work describes our efforts in the design of artificial metalloenzymes based on biotin-(strept)avidin technology. The metal biotinylated-precursor ensures the activity of the catalyst, whereas the host protein governs the enantioselectivity of artificial metalloenzymes. This study focused on the introduction of chiral spacer between metal precursor and biotin anchor (second generation of artificial hydrogenases), as well as chemo-genetic strategy for screening. The best result of the second-generation artificial hydrogenases is combination of [Rh(COD)**Biot-(*R*)-Pro-1**]$^{+}$ ⊂ S112W Sav (95% (*S*)) for the reduction of *N*-α-acetamidoacrylic acid et *N*-α-acetamidocinammic acid. The second-generation artificial hydrogenases displayed high selectivity in the presence of high concentration of organic solvent. In addition, as (strept)avidin possesses 4 binding sites, it was demonstrated that it is possible to immobilize one binding site leaving 3 free sites for the incorporation of the biotinylated precursor. The immobilization was achieved using commercially available biotin-sepharose.

Kinetic study shows an increase of reaction rate (up to three fold) using artificial metalloenzymes compared to the free-protein catalyst. Moreover, the incorporation of biotinylated coordination compounds [Ru(bpy)$_2$(Biot-bpy)]$^{2+}$ in (strept)avidin displays a significant decrease of binding affinity (5-7 orders of magnitude) than biotin.

REMERCIEMENT

Ce travail a été réalisé au laboratoire de Metalloenzymes Artificielles dirigé par Prof. Thomas R. Ward. Je le remercie, en tant que directeur et jury de thèse, pour m'avoir accueilli dans son groupe de recherche à l'Université de Neuchâtel. Je le remercie notamment pour ses innombrables conseils et son soutien durant mes 4 ans de travail de thèse.

Je tiens à remercier Professeur Thomas Bürgi (Université de Neuchâtel) et Professeur Martin Albrecht (Université de Fribourg), jury de thèse, pour avoir corrigé la rédaction de thèse ainsi donnés leurs conseils pendant examen de thèse.

J'aimerais remercier à tous les membres du groupe Ward, au passé et à présent :

Andreas Loosli, Cheikh Lo, Julieta Gradinaru, Myriem Skander, Christophe Thomas, Anca Pordea, Alessia Sardo, Sabina Burazerovic, Christelle Schenk, Yves Casta, Déborah Mathis, Christophe Malan, Thibaud Rossel, Marc Creus, Jérôme Collot, Johannes, Nicolas Humbert, Julien Pierron, Anita Ivanova, Christophe Letondor.

Ainsi que les étudiants de 3ème années à qui j'avais données les TP de Chimie Inorganique Avancée.

Je tiens à remercier mes co-équipiers de badminton, pour le plaisir et la joie que nous avons partagé durant ces dernières 2 années. Bao, Edouard, Annie, Pascal, Dani, Arnaud, Camille, Anne-Laure, Stéphane.

Je remercie tous mes amis de loin et de proche ainsi que mes colocataires, pour leur présence et leur joie ainsi que les moments que nous avons passé ensemble. En particulier : Yuda, Sulung, Sophie Alet, Bernard et Juliani Leuenberger, Pierre et Neta, Cédric et Puji, Rani, Johanna Doummar, Daniela Stingelin, Dominique Bourgeois, Nathalie Grämiger, Raluca, Géraldine, Laurence, Marie, Salomé Müller, Christian Kümin.

Enfin, mes remerciements pour mes chers parents, mes sœurs et mon frère, ainsi que mes proches pour leur amour, soutien, et patience.

TABLE OF CONTENTS

TABLE OF CONTENTS ..... **I**

LIST OF SCHEMES ..... **III**

LIST OF TABLES ..... **V**

INTRODUCTION **1**

1.1. GENERAL ASPECTS 1
1.2. BIOTIN-AVIDIN TECHNOLOGY 2
1.2.1. Biotin, Avidin & Streptavidin *2*
1.2.2. Uses of the biotin-(strept)avidin technology *4*
1.2.2.1. Determination of stability constants 5
1.2.2.2. Cooperativity 8
1.2.3. Conclusion *10*
1.3. ASYMMETRIC HYDROGENATION & DESIGN OF ARTIFICIAL METALLOENZYMES 10
1.3.1. Homogeneous asymmetric hydrogenation *11*
1.3.1.1. Ligand design 11
1.3.1.2. Multiphasic media for asymmetric hydrogenation 14
1.3.2. Heterogeneous asymmetric hydrogenation *15*
1.3.3. Enantioselective hydrogenation in aqueous media *15*
1.3.4. Enzymes *17*
1.3.5. Comparison of enzymes vs. homogeneous catalysts *21*
1.3.6. Artificial Metalloproteins & Artificial Enzymes *22*
1.3.6.1. Covalent anchoring 23
1.3.6.2. Dative Anchoring 25
1.3.6.3. Supramolecular Anchoring 27
1.3.7. Mechanistic study of asymmetric hydrogenation and Michaelis-Menten kinetics *30*
1.3.7.1. Mechanistic study of asymmetric hydrogenation 30
1.3.7.2. Michaelis-Menten Kinetics 31
1.4. OBJECTIVES OF THIS WORK 32

THERMODYNAMIC STUDY OF INCORPORATION RUTHENIUM BIOTINYLATED COORDINATION COMPLEXES WITHIN (STREPT)AVIDIN USING CD SPECTROSCOPY 35

2.1. INTRODUCTION 35
2.2. SYNTHESIS OF BIOTINYLATED COORDINATION COMPLEXES: $[Ru(bpy)_2(Biot\text{-}bpy)]^{2+}$ (1) 35
2.3. TITRATION EXPERIMENTS 38
2.4. DETERMINATION OF STABILITY CONSTANTS 39
2.5. ASSESSMENT OF THE COOPERATIVITY: CREATION & SIMULATION OF ARTIFICIAL DATA 51

APPLICATION OF BIOTIN-AVIDIN TECHNOLOGY IN THE DESIGN OF ARTIFICIAL HYDROGENASES: COMBINATORIAL APPROACH AND KINETIC STUDY 57

3.1. INTRODUCTION 57
3.2. CHEMO-GENETIC OPTIMIZATION 59
3.2.1. Saturation mutagenesis at position S112X combined with enantiopure α-aminoacid spacers 61
3.2.2. Single point mutation (at position 114, 115 and 116) & double point mutation *67*
3.2.2.1. Combination with achiral spacer 68
3.2.2.2. Combination with chiral spacer 71
3.3. SUBSTRATE SCOPE 73
3.4. ORGANIC SOLVENT TOLERANCE 76
3.5. IMMOBILIZATION OF ARTIFICIAL HYDROGENASES 78
3.6. MICHAELIS-MENTEN KINETICS: DETERMINATION OF INDIVIDUAL REACTION RATES 82

SUMMARY & OUTLOOK **89**

4.1. SUMMARY 89
4.2. OUTLOOK 90

SUPPORTING INFORMATION **93**

5.1. MATERIALS, INSTRUMENTATION AND TECHNIQUES. 93
5.1.1. Abbreviation used *93*
5.1.2. Reagents and solvents *94*
5.1.3. Preparative methods: column chromatography *96*
5.1.4. Analysis Instruments *96*
5.1.4.1. Absorption Spectrophotometry (UV/Vis) 96
5.1.4.2. Mass spectrometry (MS) 97
5.1.4.3. Nuclear magnetic resonance (NMR) 97
5.2. SYNTHESIS PROTOCOLS 98
5.3. PRODUCTION AND PURIFICATION OF STREPTAVIDIN 108
5.4. ENANTIOSELECTIVE HYDROGENATION REACTIONS 109
5.4.1. General Aspects *109*
5.4.2. Hydrogenation in Monophasic media (9%, 27%, 45% DMSO) *109*
5.4.3. Hydrogenation in Biphasic Media (EtOAc) *110*
5.4.4. Hydrogenation procedure for Immobilized Artificial Metalloenzymes *110*
5.4.5. Hydrogenation procedure for the determination of Michaelis-Menten parameters *111*
5.4.6. Kinetics experiments using Michaelis-Menten models *112*
5.4.7. Analytical data for reduction products *116*
5.5. TITRATION PROCEDURE 116
5.6. DATA TREATMENT USING SPECFIT/32 117
5.6.1. Spectra of each species *117*
5.6.2. Simulations for the Δ-1 ⊂ streptavidin system using SPECFIT/32 ..... *118*
5.7. EXPERIMENTAL DATA OF ENANTIOSELECTIVE HYDROGENATION 120

REFERENCES **125**

LIST OF SCHEMES

Scheme 1. Structure of (+)-biotin (*D*-biotin) 2
Scheme 2. Schematic structure of monomer of avidin (A) and streptavidin (B). Biotin (shown in stick) is located in the binding pocket of (strept)avidin (hereafter refers to either streptavidin or avidin). Coordinates obtained from PDB: 1AVD and 1SWE. 3
Scheme 3. Schematic structure of homo-tetrameric streptavidin (PDB: 1SWE). 4
Scheme 4. Two class of Ru(II)-phenantroline-biotin complexes (a) and (b) [23] 6
Scheme 5. Schematic illustration of biotin (left side) and HABA (right side) binding to streptavidin. ...7
Scheme 6. Strcture of [Rh(COD)(**Biot-1**)]$^{+}$ complex 8
Scheme 7. Microscopic constants of binding a monovalent-donor ligand into a bivalent-receptor. 8
Scheme 8. Industrial production of (*S*)-dopa (Monsanto Process) using [Rh(camp)$_2$(COD)]$^{+}$. 11
Scheme 9. First and second generations of monodentate ligand for asymmetric hydrogenation. 12
Scheme 10. Privileged ligands are in widespread use in chemical industries affording high TOF/TON and a highly enantioselective reduction. 13
Scheme 11. Industrial scale application of asymmetric hydrogenation of several substrates using privileged ligands. 14
Scheme 12. Structure of water-soluble binap and chiraphos, two ligands used for the enantioselective hydrogenation in aqueous media. 16
Scheme 13. Hydrogenation of (*S*)-naproxen in supported aqueous-phase (SAP) using [Ru(binap-4SO$_3$Na)(benzene)Cl]Cl catalyst. 16
Scheme 14. Kinetic resolutions of racemic amino acid for production of chiral amines by lipase. 17
Scheme 15. Hydrogenation of chalcone by microorganism *C. equi* IFO 3730. 18
Scheme 16. Asymmetric bioreduction of activated alkenes bearing an activating electron-withdrawing group (EWG) by enoate reductase. FMNH$_2$: flavin cofactor. 18
Scheme 17. Hydrolytic kinetic resolution of ester by lipase 19
Scheme 18. Chemoenzymatic DKR of (a) secondary alcohols and (b) diols using ruthenium catalyst as racemization chemocatalyst; immobilized *Candida antartica* lipase B (CALB; Novozym 435) as biocatalyst and *p*-chlorophenyl acetate as acyl donor. 19
Scheme 19. Enzymatic reduction of prochiral ketones using double-enzyme approach. 20
Scheme 20. Biocatalytic redox system using single enzyme approach using high concentration of organic solvents. 20
Scheme 21. Enzymatic reduction of prochiral ketones using a double-enzyme approach. 21
Scheme 22. Stereoview of ALBP-phenantroline complex (PDB: 1A18) (a); Covalent attachment Cu-Phen complex in ALBP (b); Enantioselective hydrolysis of amino acid ester derivatives using ALBP-Phen-Cu(II) (c) 24
Scheme 23. Covalent anchoring of ligands and complexes to papain and lipase. 25
Scheme 24. Molecular structures of heme and Schiff base complexes (M = Cr, Mn, and Fe) used for incorporation in myoglobin. 26
Scheme 25. Structure of achiral Rhodium complex used as hapten in the antibody. 27
Scheme 26. Schematic representation of the DNA-based catalytic enantioselective Diels-Alder reaction (operating conditions: Cu^{II}-ligand (0.3 mM), DNA (1.3 mg/mL), pH 6.5, 33% mol catalyst loading, 3 days). 28
Scheme 27. Schematic structure of ferritin (adapted from PDB code: 1BFR, without any further modification). 28
Scheme 28. Enantioselective hydrogenation of α-acetmidoacrylic acid using complex [Rh(NBD)(**Biot-1**)$^{+}$] ⊂ WT avidin. Inset: structure of Pyrphos by Chan and coworkers [15]. 29
Scheme 29. Catalytic cycle for Rh(dipamp) – catalyzed hydrogenation of methyl-(*Z*)-α-acetamidocinnamate (P-P = (*R*,*R*)-dipamp, S = alcoholic solvent). 30
Scheme 30. Representation of Michaelis-Menten plot for determination of kinetic parameters. 32
Scheme 31. Synthesis of Biot-bpy (**4**) and formation of the corresponding racemic coordination complex *rac*-**1**(PF$_6$)$_2$. 36
Scheme 32. The synthesis of diastereopure biotinylated coordination complex *Λ*-**1** using von Zelewsky's procedure. Inset: CD spectra of diastereopure Δ-**1** and Λ-**1** 37

Scheme 33. Possible binding events for a racemic guest in a tetrameric host protein. 14 binding constants are generated from the interactions of racemic mixture with the homotetrameric protein. (•) and (^{o}) are diastereomers. 40
Scheme 34. Second-generation artificial hydrogenases based on the biotin-avidin technology for the reduction of N-acetamido dehydroaminoacids. The host protein ((strept)avidin, violet) displays high affinity for the anchor (biotin green); introduction of an enantiopure α-aminoacid spacer (blue), combined with a flexible diphosphine ligand (red) allows to chemically optimize both the activity and the selectivity. Site-directed mutagenesis further enables a genetic optimization of the host protein to afford enantioselective artificial hydrogenases. 60
Scheme 35. Structure of biotinylated ligands and standard operating conditions for the hydrogenation of a cocktail mixture containing α-acetamidoacrylic acid and α-acetamidocinnamic acid (50 equivalents of each with respect to the biotinylated ligand). 62
Scheme 36. Fingerprint display of the results for the chemogenetic optimization of α-acetamidoacrylic acid (top triangle) and α-acetamidocinnamic acid (bottom triangle). Combination S112P with **Biot-(*R*)-Pip-1**, **Biot-(*S*)-Pip-1**, **Biot-(*R*)-Glu$^{5\text{-Bz}}$-1** and **Biot-(*S*)-Glu$^{5\text{-Bz}}$-1** was not tested. 63
Scheme 37. Reduction of α-acetamidocinnamic acid using WT Sav as starting point, combined with **Biot-(*R*)-Pro-1** affording 91% ee (*S*) that can be fine-tuned to 63 % ee (*R*) upon combination with **Biot-(*R*)-Phe-1** (red diagram). Genetic optimization yielded high diversity ranging from 79% ee (*S*) to 88% ee (*R*) using the same vector **Biot-(*S*)-Phe-1** (black diagram). Inset: Fingerprint display of the results for the chemogenetic optimization. 65
Scheme 38. Structure of monomeric streptavidin with highlighted position of mutation in position 114 (green), 115 (yellow) and 116 (red). 68
Scheme 39. Achiral biotinylated ligands used in this study and standard operating conditions for the hydrogenation of a cocktail mixture containing α-acetamidoacrylic acid and α-acetamidocinnamic acid (50 equivalents of each with respect to the biotinylated ligand). 69
Scheme 40. Fingerprint display of the results of the chemogenetic optimization of α-acetamidoacrylic acid (top triangle) and α-acetamidocinnamic acid (bottom triangle) using achiral spacer ligands and single point mutation in position 114-116 and dual point mutations. 70
Scheme 41. Structure of MAA (methyl acetamidoacrylate) and MAC (methyl acetamidocinnamate) .. 73
Scheme 42. Asymmetric hydrogenation of ketopantolactone using artificial hydrogenases generated from biotin-avidin technology. 75
Scheme 43. Composition of solutions for monophasic (A) and biphasic (B) conditions in asymmetric hydrogenation. 77
Scheme 44. Flowchart of preparation immobilized artificial hydrogenases using biotin-sepharose as solid support. 78
Scheme 45. Immobilization of a Rh-biotinylated complex using biotin-sepharose. One equivalent of biotin-sepharose binds a biotin-binding site of the host protein leaving up to three binding pockets for anchoring of the biotinylated pre-catalysts. 79
Scheme 46. Synthesis pathway of biotinylated-diphosphine ligands bearing an enantiopure amino acid spacer. 101

LIST OF TABLES

Table 1. Comparison of chemical and biological systems [3, 4] 1
Table 2. Comparison between enzymatic catalysis and homogeneous catalysis 22
Table 3. Summary of refined binding constants between $[Ru(bpy)_2(Biot\text{-}bpy)]^{2+}$ (**1**) and (strept)avidin using a three equilibrium model. Standard deviations are given in parenthesis. 47
Table 4. Influence of the random noise level on the association constant values refined either for the complete (equilibrium 1 to 4) or partial (equilibrium 2 to 4) models[a] 54
Table 5. Numerical summary of previous results of catalytic experiments using artificial hydrogenases. 58
Table 6. Numerical summary of selected results of the catalytic experiments using second-generation artificial hydrogenases. 66
Table 7. Numerical summary of selected results of the catalytic experiments: chemogenetic optimization in position 114, 115, and 116, and dual point mutations. 72
Table 8. Numerical summary of selected results of the catalytic experiments using amino acid esters with the same conditions as catalytic experiments using acid as substrate. 74
Table 9. Numerical catalytic results of enantioselective hydrogenation of ketopentalactone 76
Table 10. Numerical summary of selected results of the catalytic experiments performed in the presence of organic solvents or with immobilized artificial metalloenzymes. 80
Table 11. Numerical summary of selected results of the catalytic experiments using immobilized catayst (with [Rh(COD)**Biot–(*R*)-Pro–1**]$^+$) in the presence of organic solvents 81
Table 12. Experimental kinetic data of [Rh(COD)(**Biot-1**)]$^+$ ⊂ WT Sav. 83
Table 13. Kinetics parameters derived from Michaelis-Menten equations. 84
Table 14. Initial reaction rates obtained from kinetic experiments for [Rh(COD)(**Biot-1**)]$^+$ ⊂ WT Sav and parameters values to construct Lineweaver-Burk and Eadie-Hofstee plots. 86
Table 15. Reagents and solvents used 94
Table 16. Kinetic experiments data of [Rh(COD)(**Biot-1**)]$^+$ ⊂ WT Sav 112
Table 17. Kinetic experiments data of [Rh(COD)(**Biot-1**)]$^+$ 113
Table 18. Kinetic experiments data of [Rh(COD)(**Biot-(*R*)-Pro-1**)]$^+$ ⊂ WT Sav in the presence of 30% DMSO 113
Table 19. Kinetic experiments data of [Rh(COD)(**Biot-(*R*)-Pro-1**)]$^+$ ⊂ WT Sav in the presence of 30% DMSO 113
Table 20. Kinetic experiments data of [Rh(COD)(**Biot-(*R*)-Pro-1**)]$^+$ 114
Table 21. Kinetic experiments data of [Rh(COD)(**Biot-(*R*)-Pro-1**)]$^+$ in the presence of 30% DMSO 114
Table 22. Numerical results of enantioselective hydrogenation 120

INTRODUCTION

1.1. General aspects

Metal ions play an important role in the reactivity and diversity of biochemical transformations. The successful synthesis of novel complexes that allow application of metal ions could have a great impact in many areas of chemistry and biology, including medicinal, organic and material chemistry, as well as biochemistry and cell biology [1, 2].

Obtaining useful catalysts (such as those shown in **Table 1**) remains a major challenge for the multibillion-dollar chemical industries that provide raw materials, such as fertilizers. One such useful catalyst, methane monooxygenase, can be used to obtain alcohol as fuel through either a bio or chemical processes (**Table 1**). The added value of this reaction makes some to consider it a "holy grail" of biochemical transformations. Though the synthetic way to carry out this type of catalysis usually needs extreme reaction conditions, equivalent biological transformations use ambient pressure and temperature. However, an improved synthetic methane monooxygenase remains an attractive pursuit, because the robustness of synthetic substances offers many advantages over a purely biological approach.

Table 1. Comparison of chemical and biological systems [3, 4].

Reaction	Chemical System	Biological System
nitrogen fixation	$\mathbf{N_{2(g)}} + 3\ H_{2(g)} \rightarrow 2\ \mathbf{NH_{3(g)}}$ (α-Fe catalyst, 400-550°C, 100 atm)	$\mathbf{N_2} + 8\ H^+ + 8\ e^- + 16$ MgATP $\rightarrow 2\ \mathbf{NH_3} + H_2 + 16$ MgADP $+ 16\ P_i$ (nitrogenase)
methane hydroxylation	$\mathbf{CH_4} + H_2O \rightarrow CO + 3\ H_2$ (Ni catalyst, 700-900°C, 1–25 bar) $CO + 2\ H_2 \rightarrow \mathbf{CH_3OH}$ (Cu/Zn catalyst, 250-280°C, 70-110 bar)	$\mathbf{CH_4} + O_2 + NADH + H^+ \rightarrow \mathbf{CH_3OH} + H_2O + NAD^+$ (methane monooxygenase)
CO oxidation	$\mathbf{CO} + H_2O \rightarrow \mathbf{CO_2} + H_2$ (Fe/Cu catalyst, >200°C)	$\mathbf{CO} + H_2O \rightarrow \mathbf{CO_2} + 2\ H^+ + 2e^-$ (CO dehydrogenase)
CO insertion	$\mathbf{CH_3}OH + \mathbf{CO} \rightarrow \mathbf{CH_3CO}OH$ $[Rh(I)I_2(CO_2)]^-$, 120°C, 30 atm	$\mathbf{CH_3}–[M] + \mathbf{CO} + HS–CoA \rightarrow \mathbf{CH_3(CO)}–S–CoA + H^+ + [M]^{-[a]}$ (acetyl-CoA synthase)

[a] CH_3–[M] is a corrinoid-iron-sulfur protein that acts in the reaction as a methyl group donor; HS-CoA is coenzyme.

Since this thesis is concerned with catalysis, I will present various aspects of enzymatic and homogeneous catalysis: kinetics and thermodynamics of catalysts, as well as operational condition and organic solvent tolerance. I will also introduce artificial metalloenzymes as a new type of catalyst, which offer an attractive alternative to both enzymes and homogeneous catalysis. One such type of artificial catalyst, investigated in the context of this thesis, uses the biotin-avidin technology; therefore, the biotin-avidin technology will be described first in detail.

1.2. Biotin-Avidin Technology

1.2.1. Biotin, Avidin & Streptavidin

Biotin-avidin, often referred to as *molecular velcro*, is one of the tightest guest ⊂ host interactions present in nature [5, 6], with a binding constant of $K_a \sim 10^{15}$ M^{-1}. To the best of our knowledge, only two systems display comparable affinities: vancomycin ⊂ D-Ala-D-Ala [7], ($K_a \sim 10^{17}$ M^{-1}) and the interaction of an acetophenone derivative in ACEsterase ($K_a \sim 10^{15}$ M^{-1}) [8].

The structure of biotin (vitamin H) is depicted in **Scheme 1**.

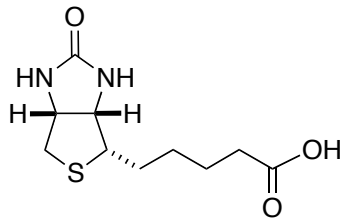

Scheme 1. Structure of (+)-biotin (*D*-biotin)

Avidin is a homo-tetrameric glycosylated protein, positively charged at neutral pH, found in egg white and oviducts of many bird species, at a maximum concentration of about 0.05% of the total protein weight. Like avidin, streptavidin is a

homo-tetrameric protein found in certain gram-negative bacteria, which displays a high affinity for biotin. In contrast to avidin, streptavidin is non-glycosylated and displays a much lower pI = 6.2 [9, 10].

Comparison of the primary structure of these two proteins shows moderate sequence homology, 30% identity and 41% similarity [11]. The tertiary structure of a monomer of avidin and streptavidin is depicted in **Scheme 2**, whereas the quaternary structure of homotetrameric streptavidin is shown in **Scheme 3**.

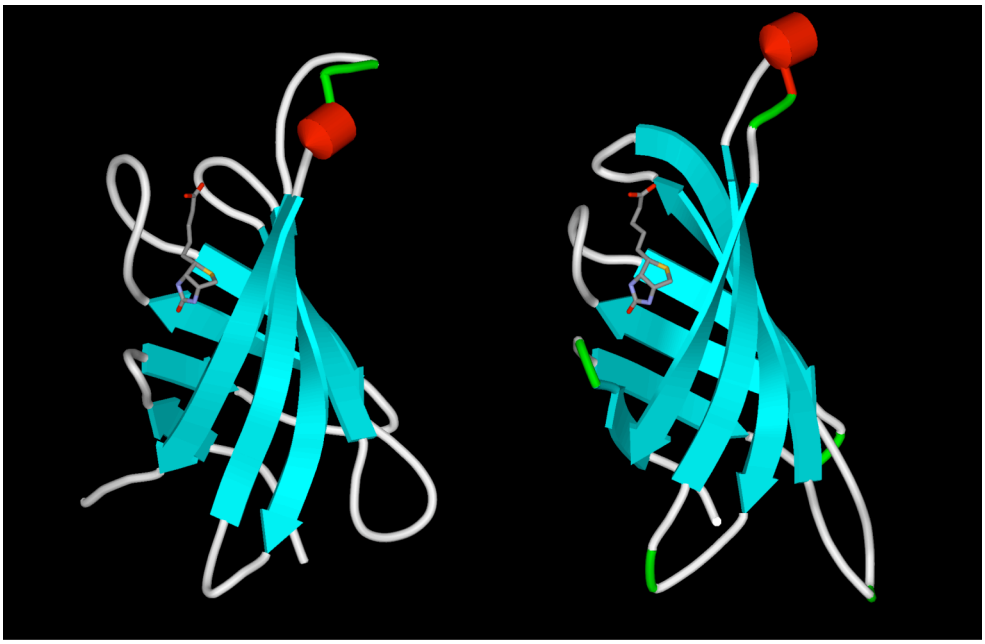

Scheme 2. Schematic structure of monomer of avidin (A) and streptavidin (B). Biotin (shown in stick) is located in the binding pocket of (strept)avidin (hereafter refers to either streptavidin or avidin). Coordinates obtained from PDB: 1AVD and 1SWE.

The origin of the strong binding biotin-streptavidin relies on both hydrophobic and hydrophilic interactions between biotin and several amino-acid residues in the biotin-binding site [11-14].

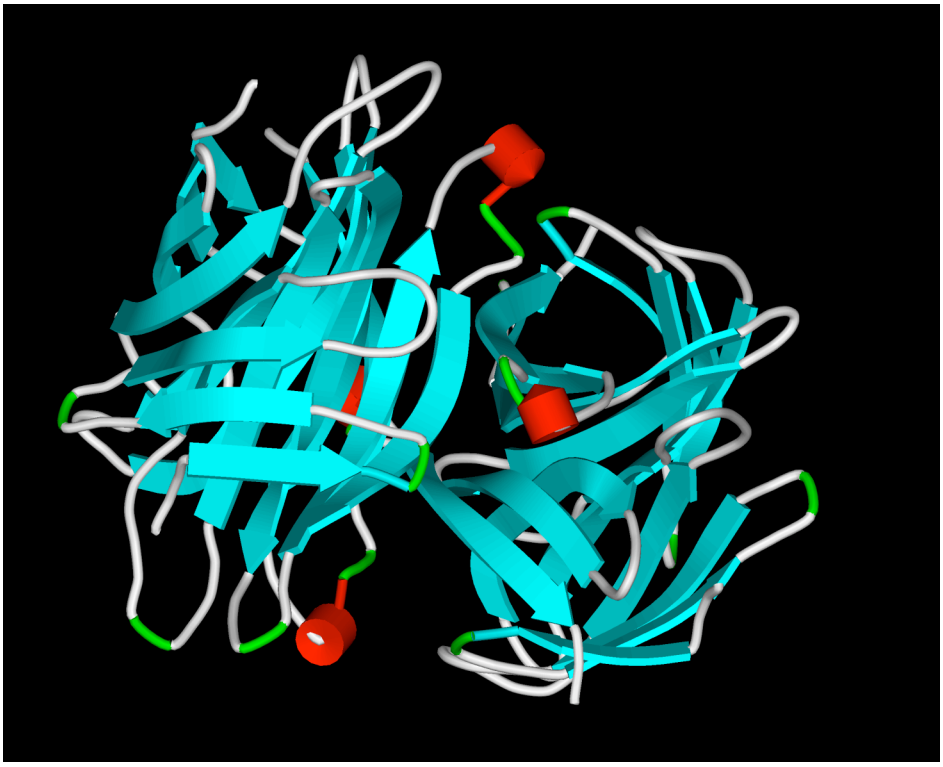

Scheme 3. Schematic structure of homo-tetrameric streptavidin (PDB: 1SWE).

1.2.2. Uses of the biotin-(strept)avidin technology

Many aspects of biotin ⊂ avidin interactions have been extremely well characterized. The most relevant to this thesis are:

- Green and coworkers, as well as many other groups [5, 6, 9-13] have studied biotin-avidin interaction in detail, both thermodynamically and structurally.
- The valeric chain of biotin can be easily modified and conjugated synthetically to a metal cofactor yielding little loss in terms of binding affinity of biotin analog in (strept)avidin [15-28].
- The tetrameric nature avidin allows the attachment of different biotinylated compounds for various purposes (probing, labeling, treatment of disease, marker, and so forth) [29-34].

It is noteworthy that the strong interaction between biotin or biotinylated compounds and (strept)avidin has found many applications in medical diagnostics,

immunoassays, cytochemistry, nanoscience, biomolecule detection [35-41], as well as in radiolabeling techniques, enzymatic reactions, and fluorescence for visualization [16-19, 42, 43].

1.2.2.1. Determination of stability constants

The determination of stability constants in biotin (or biotin analogs)-(strept)avidin systems has emerged as a critical issue recently, especially in the growing field of molecular recognition. Among the available techniques to determine association constants, fluorescence-based assays are some of the most straightforward, rapid and sensitive detection techniques [44-48]. This technique could be achieved by linking covalently a fluorescent dye to biotin, followed by fluorescence detection of the biotinylated molecule through cross-linking with (strept)avidin. However, biotinylated organic dyes have been shown to lose their luminescence intensity upon binding to avidin due to the resonance energy transfer mechanism [49, 50]. To overcome this problem, long spacer, such as poly(ethylene) glycol, has been used to increase the distance between the biotin-conjugated organic dyes and (strept)avidin.

The design of Re(I)-, Ir(III)-, and Ru(II)-polypyridine conjugated to the biotin moiety was proposed by Lo and coworkers [16-19]. The study relied on the determination of the formation constants of the complex in avidin using spectroscopic titrations. For the titrations of avidin with metal-polypyridine complex, they observed two intense absorption bands, first at *ca*. 288 nm which were assigned to intraligand transition (π-π^*) (bpy and ligand attached to biotin), and absorption bands in the region 423-458 nm which correspond to metal ligand charge-transfer (MLCT) transition.

Using a slightly different structure of biotinylated compounds (**Scheme 4**, phenantroline as ligand instead of bipyridine), Sleiman and coworkers [23] determined

the binding affinity of (poly)phenantroline complexes within (strept)avidin. To determine the stability constants, the HABA assays were performed.

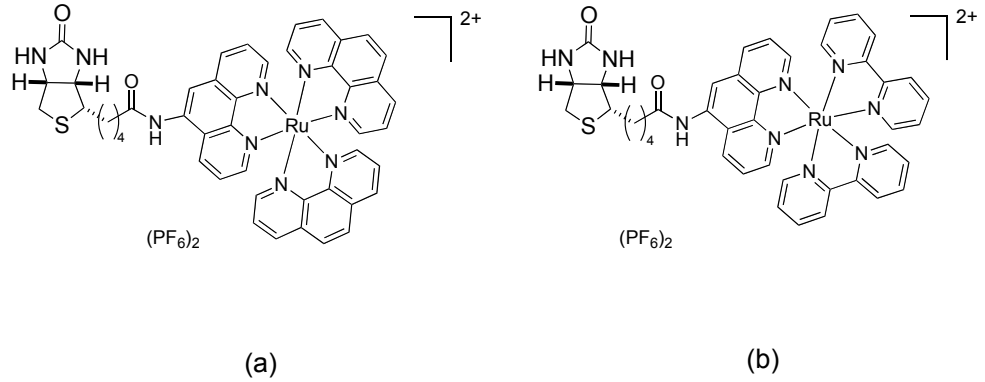

Scheme 4. Two class of Ru(II)-phenantroline-biotin complexes (a) and (b) [23]

HABA (2-(4'-hydroxyazoybenzene)benzoic acid) is an organic dye that binds to (strept)avidin in a similar fashion as native biotin, but with much lower affinity (its binding constant is 9 orders magnitude lower than biotin) [5, 6, 12, 21]. The interactions of HABA with amino acid residues in streptavidin are depicted in **Scheme 5**, as comparison interactions of native biotin are also highlighted [13].

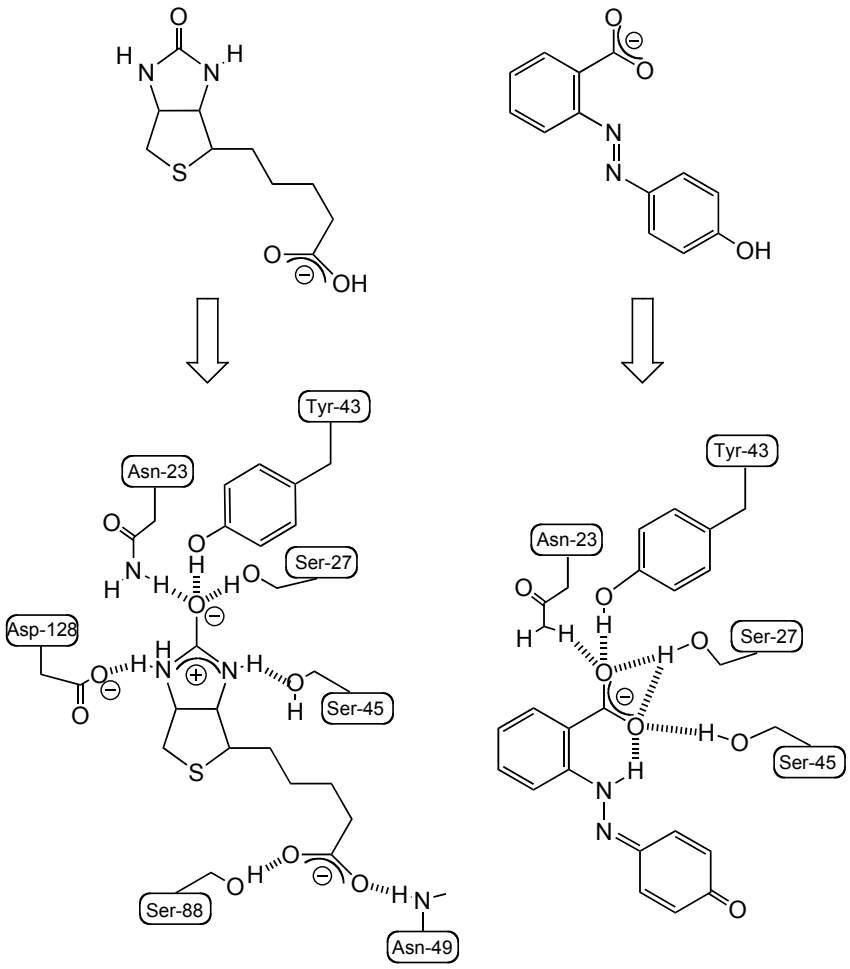

Scheme 5. Schematic illustration of biotin (left side) and HABA (right side) binding to streptavidin.

Upon addition of the biotinylated metal complexes (Scheme 4) to the mixture of HABA ⊂ (strept)avidin, HABA is displaced quantitatively from the biotin binding pocket. This displacement can be followed by UV-vis detection at 500 nm. UV-Vis titrations can be performed to compare the strength of the binding constants of biotinylated conjugates and native biotin. These measurements revealed that the association constant of biotinylated compounds is typically 4-5 orders of magnitude weaker than biotin. It is important to note that the equivalence points of competition titrations using biotinylated compounds with low binding constants (7-8 magnitudes lower than that of biotin) were difficult to observe [16, 19].

Our group [21] reported recently the determination of the binding constant for Rh-diphosphine biotinylated, [Rh(COD)(**Biot-1**)]$^+$ complex (as illustrated in **Scheme 6**) in (strept)avidin. In these studies, the method of HABA displacement was performed and the collected data were treated by the nonlinear least-squares method.

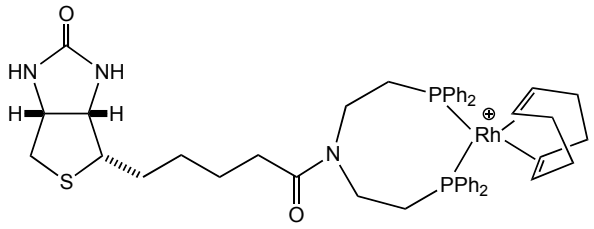

Scheme 6. Strcture of [Rh(COD)(**Biot-1**)]$^+$ complex

The estimated stability constants were *ca*. 7 magnitudes lower compared to those of native biotin. HABA assays suggested that the Rh-diphosphine complex binds to (strept)avidin more tightly than HABA.

1.2.2.2. Cooperativity

The term *cooperativity* refers to the influence of a ligand to the binding strength of the subsequent ligands [51, 52]. A monovalent ligand (ball in **Scheme 7**) can occupy each binding pocket of a bivalent receptor via reversible reaction characterized by the microscopic intermolecular constant (*k*). It is important to distinguish between macroscopic (*K*) and microscopic constants. Microscopic constant characterizes the nature of individual binding events [53].

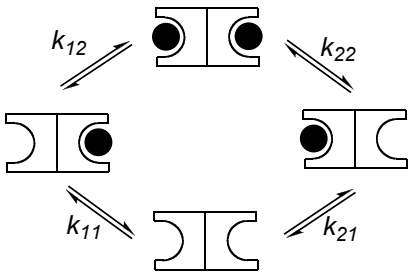

Scheme 7. Microscopic constants of binding a monovalent-donor ligand into a bivalent-receptor.

$$K_1 = \frac{[ML]}{[M][L]} = \frac{[\text{ 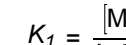 }]+[\text{ 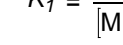 }]}{[M][L]} = k_{11} + k_{21}$$

$$K_2 = \frac{[ML_2]}{[ML][L]} = \frac{[\text{ 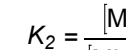 }]}{\{[\text{ 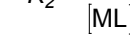 }]+[\text{}]\}[L]} = \frac{k_{12}.k_{11}}{k_{11}+k_{21}}$$

To simplify this system, it is assumed that the 2 binding sites are identical (k_I = microscopic constant when ligand occupies one binding site of bivalent receptor, k_{II} = microscopic constant when both binding sites of receptor are occupied) then $k_{11} = k_{21} = k_I$ and $k_{12} = k_{22} = k_{II}$. Thus for the independent active sites, $k_I = k_{II} = Q$.

Assessment of cooperativity is performed by comparing the ratio of binding constants with a theoretical/statistical one, obtained from equation 2. Non-cooperativity (additive) is found when the equality occurs. In the case that the binding of the ligand favors the binding of the subsequent ligand, then the system is considered positively cooperative/synergistic (K_{i+1}/K_i is higher than the theoretical value). On the contrary, if the binding of a ligand impedes the binding of the subsequent ligand then there is a negative cooperativity (interference), with K_{i+1}/K_i is lower than the statistical value [51-53].

For a general case, with monovalent ligand and *m*-valent receptor, the cooperativity can be assessed through the following equations:

$$K_i = k(m-i+1)/i \qquad (1) \qquad \frac{K_{i+1}}{K_i} = \frac{i(m-i)}{(i+1)(m-i+1)} \qquad (2)$$

A comprehensive example of cooperativity in biology can be found in the following references [54-59].

As the binding constants of biotin in (strept)avidin are extremely high, there are still arguments in *pro* and *contra* concerning the cooperativity in this system. Sano and coworkers [60] suggested that the cooperativity of biotin binding in streptavidin relies on the cooperativity of dimers of streptavidin. In contrast, in 1995 Jones and coworkers [61] revealed that the binding of biotin to tetrameric streptavidin is

noncooperative. This is based on their observation that the differences in affinity of biotin binding to subsequent streptavidin adducts fall within 0.12 kcal·mol^{-1}. This value is too small when compared with positive cooperativity for oxygen binding to hemoglobin $\Delta\Delta G$ = -8 kcal·mol^{-1} between k_1 and k_4 [62]. Nevertheless, as the binding of biotin to streptavidin is extremely tight, the assessment of cooperativity is a non-trivial task. Therefore, the cooperativity of this system remains questionable.

1.2.3. Conclusion

Biotin-avidin technology, based on the strong interaction between the host protein and a covalently bound active cofactor/ligand to biotin, is extremely useful in chemistry and biology for a large number of purposes. Some parameters can influence the affinity of biotinylated compounds in avidin: type and length of the linker, the nature of the cofactor and, in the case of metal complexes, also the steric hindrance of the non-biotinylated chelates.

1.3. Asymmetric hydrogenation & design of artificial metalloenzymes

In the area of enantioselective catalysis, many efforts have been made to reach useful applications and to meet the industry demand, culminating by achievement of the joint nobel prize in 2002 [63-67]. Asymmetric hydrogenation is a core technology in modern synthesis. The recent substantial expansion of this subject has given rise to enormous economic potential in the chemical manufacture of pharmaceutical, health products, agrochemicals, flavors and fragrances [68, 69]. To date, many functional groups can be hydrogenated with high selectivity and high conversion, and scale-up is usually not problematic for industrial application.

The low valent metals such as Rh, Ru, and Ir are known as the most active and versatile catalysts in asymmetric hydrogenations. The first indications of a potentially

useful ligand are catalyst productivity (TON or S/C), catalyst activity (TOF), and selectivity (ee).

1.3.1. Homogeneous asymmetric hydrogenation

1.3.1.1. Ligand design

The first milestone of asymmetric hydrogenation was published in 1966 [70, 71], when Wilkinson reported the preparation of $RhCl(PPh_3)_3$, for homogeneous hydrogenation of alkene. W. S Knowles [72] demonstrated by substituting triphenylphosphine with chiral phoshines, that the phosphorous atom brings the chirality affording efficient catalyst for the asymmetric hydrogenation of α-phenylacrylic acid (88% (*S*) using camp ligand, **Scheme 9**). The sensational finding at that period was the use of camp as ligand for the production of (*S*)-dopa (stabilizer agent of parkinson disease) at industrial scale [73, 74] (**Scheme 8**). The finding of dipamp ligand (**Scheme 10**) improved the selectivity for the production of (*S*)-dopa (95 %(*S*)).

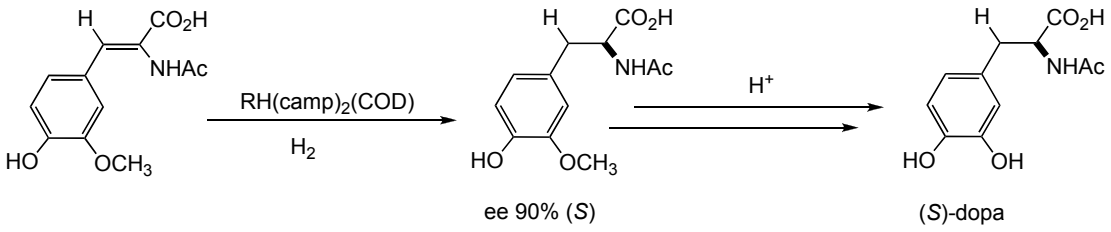

Scheme 8. Industrial production of (*S*)-dopa (Monsanto Process) using $[Rh(camp)_2(COD)]^+$.

Later on, Kagan & Dang [75] demonstrated that a chiral at phosphorous ligand is not necessary if a chiral bidentate ligand is used, such as C_2-symmetric diphosphine ligand diop (**Scheme 10**).

In principle, ligands for asymmetric hydrogenation can be classified into two classes, monodentate ligands and bidentate ligands. For some particular cases, tridentate ligands may also be designed.

Monodentate class of ligands (as shown in **Scheme 9**) displays some interesting features [76] such as being highly active in hydrogenation catalysis, able to achieve equal or better ee than bidentate analogues. Furthermore, monodentate ligands can be prepared from cheap and readily available starting material.

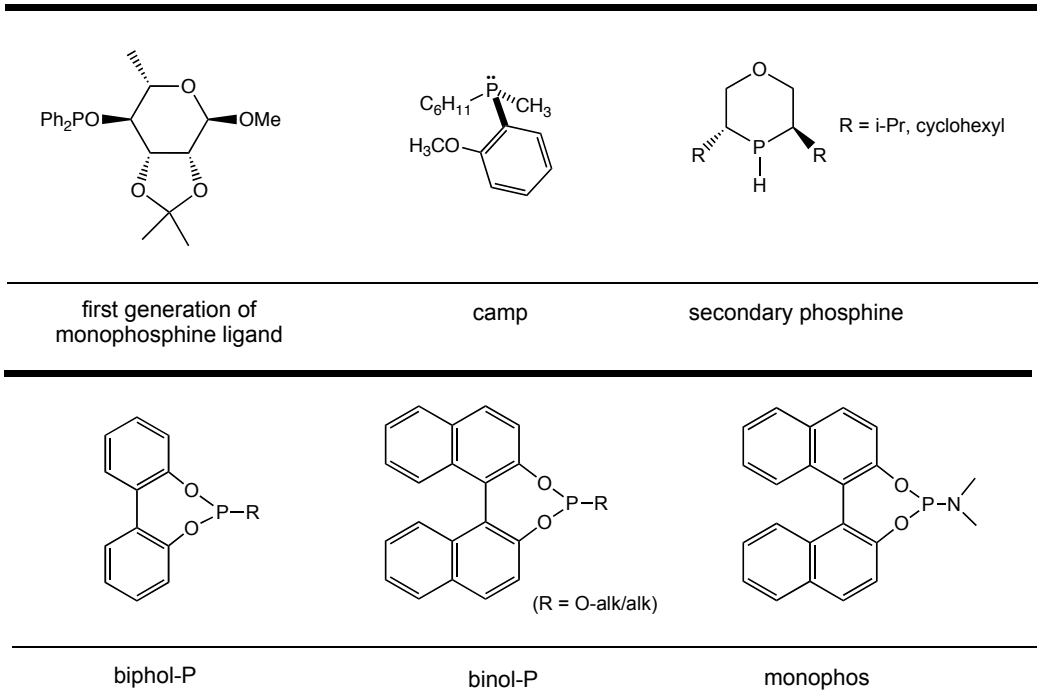

Scheme 9. First and second generations of monodentate ligand for asymmetric hydrogenation.

Bidentate ligands comprising axially chiral biaryl ligands (binap family) were discovered by Noyori and coworkers [77] in early 80's. Thereafter, binap became one of the most versatile class of chiral ligands for hydrogenations of a wide variety of substrates with Ru complexes [66], from activated ketones to α,β-unsaturated acids, allylic alcohols, and enamides [78-82]. Other ligands that achieved successful application are biphep and biphep derivatives (**Scheme 10**) [83]. The finding of the

diphosphine/diamine ligand by Noyori [84] has broadened the substrate scope of asymmetric hydrogenation.

Kumada and Hayashi [85] were the first to introduce the ferrocenyl-based diphosphine ligands, based on the pioneering work of Ugi [86, 87] related to synthesis of enantiopure substituted ferrocenes. Later, Togni and Spindler [88] improved the performance of this ligand by introducing the second phosphino group at the stereogenic center of Ugi's amine. Since then, the josiphos ligand of Solvias (**Scheme 10**) is known as the most versatile and successful ligand from the ferrocenes family [89].

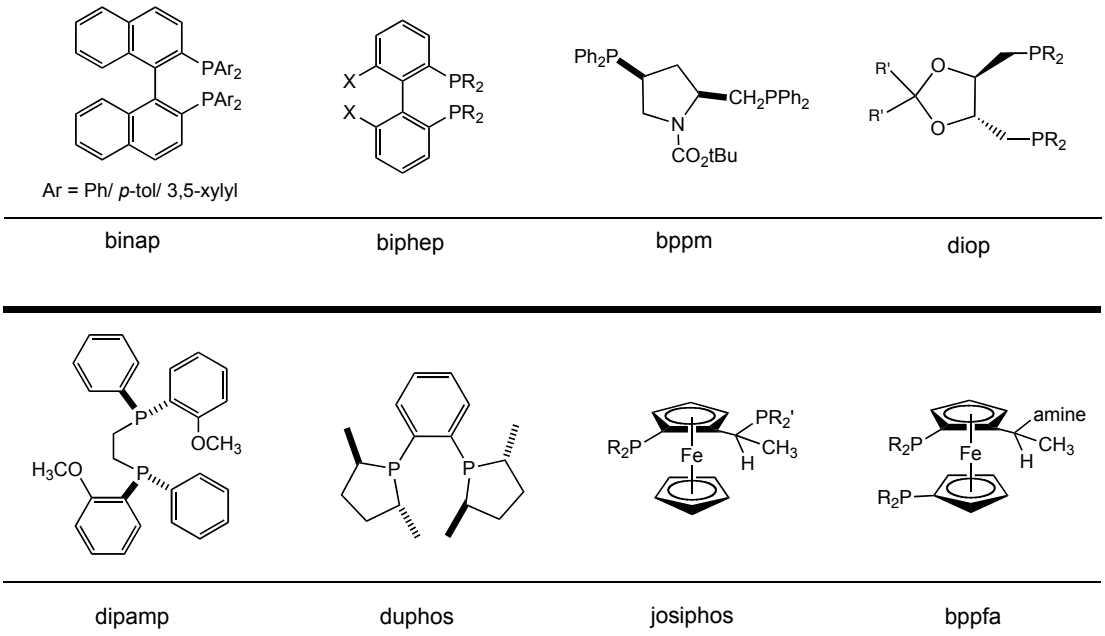

Scheme 10. Privileged ligands are in widespread use in chemical industries affording high TOF/TON and a highly enantioselective reduction.

Burk in the early 90's [89] designed and introduced a novel backbone – phospholane type ligands. The success of duphos ligands (**Scheme 10**) has created considerable activity in other laboratories and a number of interesting variants have been published in the last few years [90, 91].

Scheme 11 highlights some examples of asymmetric hydrogenation at an industrial scale (small scale production to pilot process) [76, 92, 93].

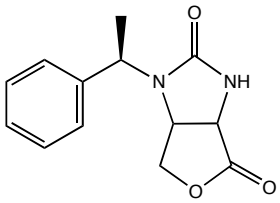	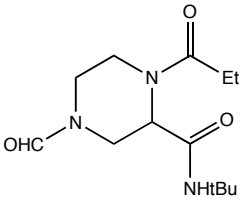	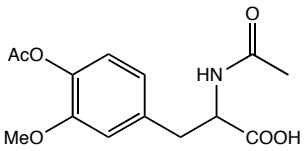
Rh/josiphos: ee 99% TON 2'000; TOF n.a medium-scale production LONZA	Rh/josiphos: ee 97% TON 1'000; TOF 450 h^{-1} pilot process, >200kg LONZA	Rh/dipamp: ee 95% TON 20'000; TOF 1'000 h^{-1} small-scale production MONSANTO
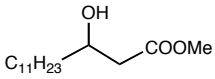	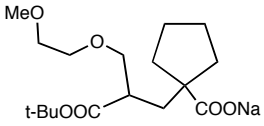	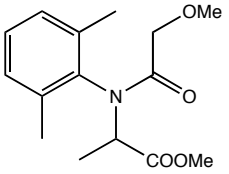
Ru/biphep: ee>98% TON 50'000; TOF 12'500 h^{-1} pilot process, 240kg batch ROCHE	Rh/me-duphos; ee>99% TON 3'500; TOF 1'200 h^{-1} pilot process, >200kg CHIROTECH	Ru/me-duphos: ee 96% TON 50'000; TOF 200 h^{-1} pilot process, kg scale CIBA-GEIGY/SOLVIAS

Scheme 11. Industrial scale application of asymmetric hydrogenation of several substrates using privileged ligands.

1.3.1.2. Multiphasic media for asymmetric hydrogenation

In order to improve the work-up in the experiments, usually the enantioselective hydrogenations are performed in biphasic (multiphasic) media. The advantage of this process, in one hand is to avoid product separation from reaction media, and in the other hand to allow recycling and reusing the catalysts. However in industrial practice, the use of multiphase media is rarely found [94].

1.3.2. Heterogeneous asymmetric hydrogenation

The tremendous progress in asymmetric transformation in both homogeneous and enzymatic catalysis is leaving a significant gap with their heterogeneous counterpart. The non-trivial ligand design and the need for "sophisticated" equipment make the heterogeneous transformations as a major challenge for the chemists. However, in the past few years, some groups [95-98] have successfully designed a lab-scale design for heterogeneous asymmetric transformations, although optimizing conditions are difficult to achieve.

1.3.3. Enantioselective hydrogenation in aqueous media

The chemical industry is under considerable pressure to replace volatile organic compounds that are currently used as solvents in organic synthesis. The toxicity, hazardous properties and expensive remediation of these solvents, notably chlorinated hydrocarbons, are making their use limited and even prohibitive. Thus, the use of "alternative – more environment friendly" solvent becomes increasingly important [99]. Some factors that determine the "greenness" of a reaction are: E factor (weight of the waste/weight of the product, E > 100), V productivity (gram product/liter reaction medium), and solvents [100].

Asymmetric transformation in aqueous media is becoming increasingly attractive as the demand for environmentally benign solvents increases. However, asymmetric transformation in water remains challenging. The use of sulfonated phosphine ligand for hydrogenation using aqueous media began in 1973 with a paper by Joo and Beck [101]. Since then, the numbers of studies dealing hydrogenation in aqueous media is growing rapidly. One of some examples: Davies and coworkers [102, 103] focused on the design of water soluble ligands, by attaching a hydrophilic group,

such as sulfonate to binap ligand (**Scheme 12**) affording good ees (82% (*R*)) of reduction (Z)-α-methyl acetamidocinnamate. α-acetamidoacrylic acid and its methyl ester can be hydrogenated conveniently using water soluble chiraphos (ee up to 94% (*S*)) [104-106].

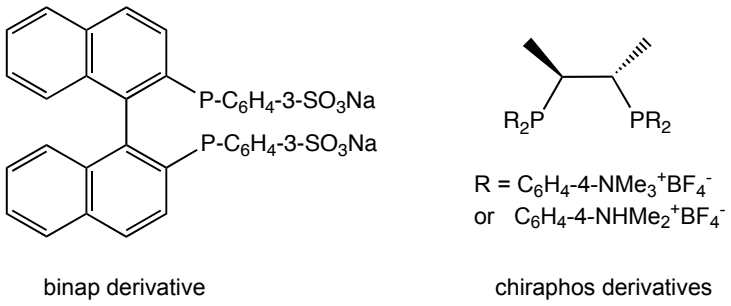

Scheme 12. Structure of water-soluble binap and chiraphos, two ligands used for the enantioselective hydrogenation in aqueous media.

Ruhrchemie/Rhône-Poulenc is the industrial process that introduced and still uses sulfonated triaryl phosphine ligands to afford water-soluble rhodium catalyst for propene hydroxylation.

Davis and coworkers demonstrated the design of chiral-water-soluble ligand (binap-4SO_3Na) for asymmetric hydrogenation of naproxen (**Scheme 13**) in supported aqueous-phase (SAP) yielding high ee up to 96% (*S*) [107].

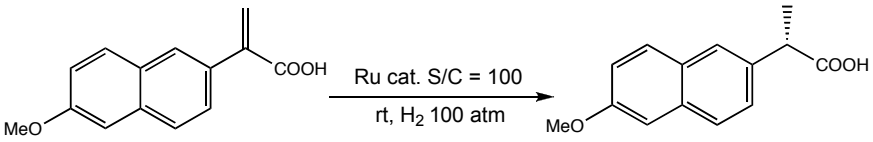

Scheme 13. Hydrogenation of (*S*)-naproxen in supported aqueous-phase (SAP) using [Ru(binap-4SO_3Na)(benzene)Cl]Cl catalyst.

Another promising but challenging media for asymmetric hydrogenations include the use of alternative media such as: ionic liquids [108, 109] and supercritical CO_2 [110].

1.3.4. Enzymes

Linus Pauling [111] rationalized the basic principle underlying enzyme catalysis "*enzyme increases the rate of chemical reaction by binding and stabilizing the transition state of its specific substrate tighter than ground state*". Enzymes are natural catalysts that have high specificity towards compatible substrates. Usually, enzymes catalyze a reaction with high TON/TOF, and require mild condition reactions (room temperature, neutral pH) and water as media.

A wide variety of chemical transformations (hydrolases, lyases, isomerases, and ligases) [112] can be performed by natural enzymes. The active site of enzymes plays a determinant role in catalytic activity and selectivity. One of the most successful enzymes used in industry is a lipase for the production of amino acid (BASF) [113] (**Scheme 14**).

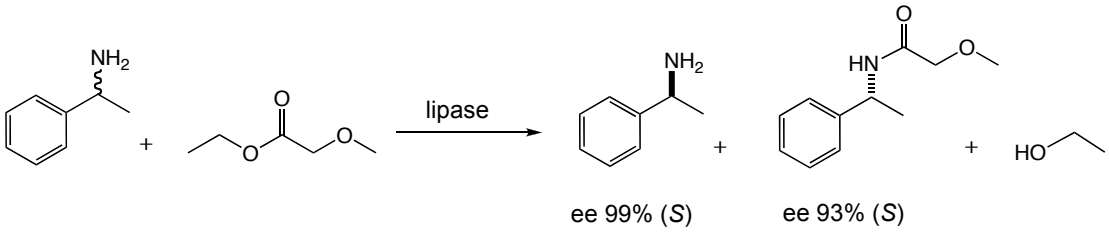

Scheme 14. Kinetic resolutions of racemic amino acid for production of chiral amines by lipase.

This process is applicable to a broad spectrum of amines, which are of considerable interest as chiral building blocks or as auxiliaries for the synthesis of bioactive ingredients.

In 1974, Neumann and coworkers [114] reported stereoselective hydrogenation using microorganisms as catalysts. *Clostridium kluyveri* was used to hydrogenate α,β-unsaturated carboxylic acid and *Bacillus polymyxa* (NCR-9035) to obtain diols from

α-hydroxyketones or α-hydroxyketones and diols from α-oxo acids. In 1983, Ohta [115, 116] demonstrated that *Corynebacterium equi* IFO 3730 can hydrogenate double bond of chalcones (**Scheme 15**), the conversion was reported quantitative after 3 h at 30°C.

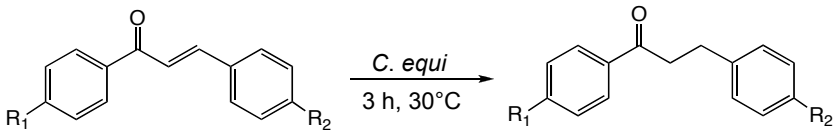

Scheme 15. Hydrogenation of chalcone by microorganism *C. equi* IFO 3730.

In the area of asymmetric bioreduction, recently Faber & coworkers [117] reported the asymmetric reduction of C=C bonds using enzymes. This reaction is catalyzed by enoate reductase, commonly denoted as the "old yellow enzyme" family (**Scheme 16**). Alkenes bear electron-withdrawing group (EWG = ketone, aldehyde, carboxylic acid or anhydride, lactone, imide or nitro).

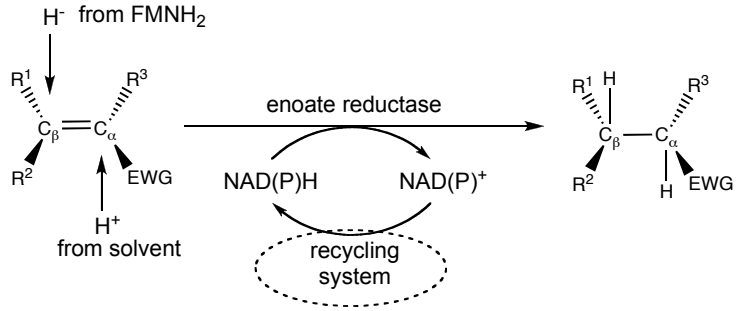

Scheme 16. Asymmetric bioreduction of activated alkenes bearing an activating electron-withdrawing group (EWG) by enoate reductase. $FMNH_2$: flavin cofactor.

Reetz [118] demonstrated that the selectivity factor in kinetic resolution of esters by the lipase of *Pseudomona aeruginosa* (**Scheme 17**) could be enhanced by directed evolution and site directed mutagenesis.

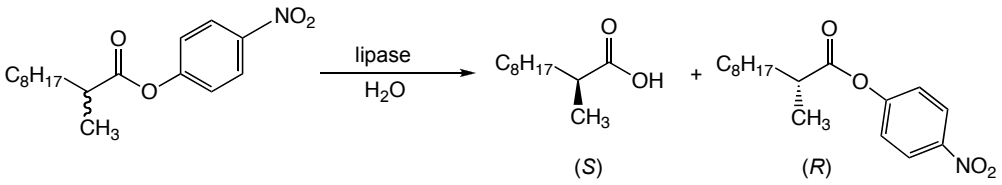

Scheme 17. Hydrolytic kinetic resolution of ester by lipase.

More recently, Bäckvall and coworkers [119-121] demonstrated that the combination of a catalytic racemization procedure and an enzymatic resolution could lead to a dynamic kinetic resolution (DKR) if the enzyme and racemization catalyst are compatible with one another (**Scheme 18**).

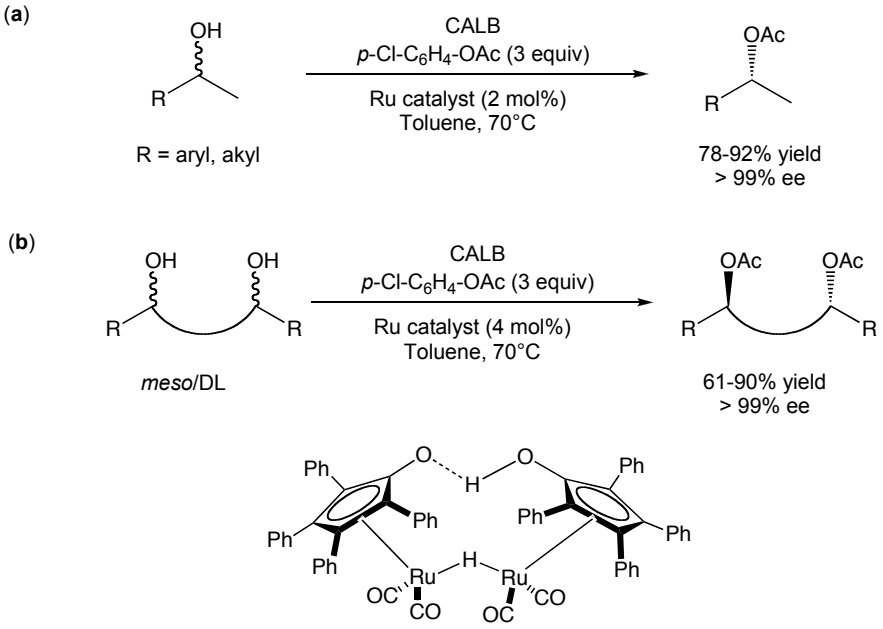

Scheme 18. Chemoenzymatic DKR of (a) secondary alcohols and (b) diols using ruthenium catalyst as racemization chemocatalyst; immobilized *Candida antartica* lipase B (CALB; Novozym 435) as biocatalyst and *p*-chlorophenyl acetate as acyl donor.

With the same strategy, DKR of primary amines using enzyme and metal-catalyst, was also successfully demonstrated [122]. Temperature is an important parameter when planning a DKR. As the racemization is usually faster at higher temperatures, while enzymes undergo denaturation at elevated temperatures. However, it has been shown in recent years that thermostability of lipases can be

increased by immobilization on certain supports. In addition, immobilization also favors the recovery and subsequent reuse of the lipase

Wandrey and coworkers [123] reported a double-enzyme approach (as shown in **Scheme 19**) for reduction of prochiral ketones to the corresponding secondary alcohols affording ee > 99%.

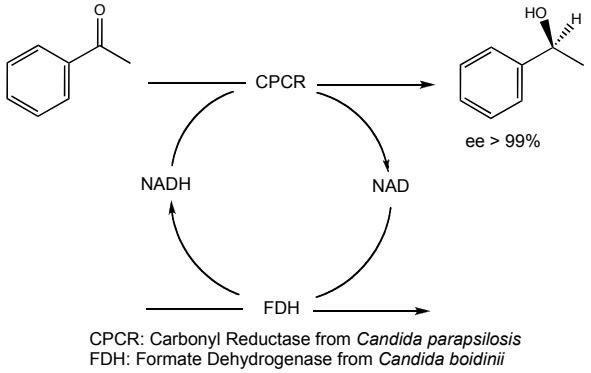

Scheme 19. Enzymatic reduction of prochiral ketones using double-enzyme approach.

Interestingly, Faber and coworkers [124] reported a "coupled-substrate" approach (**Scheme 20**) based on the use of a single enzyme for reduction of ketones and kinetic resolution by oxidation of secondary alcohols (biocatalytic redox system).

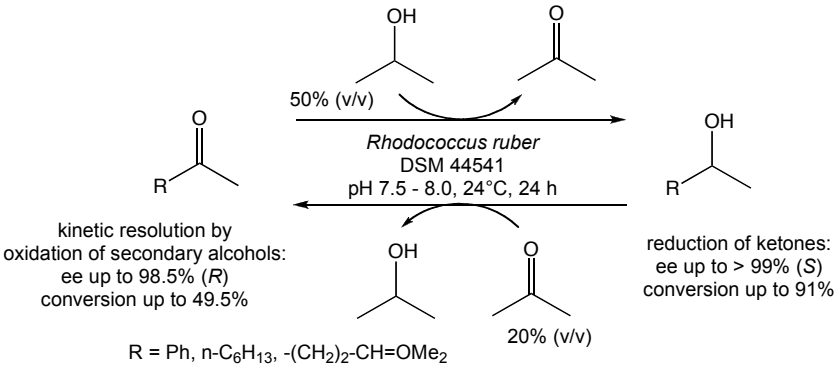

Scheme 20. Biocatalytic redox system using single enzyme approach using high concentration of organic solvents.

The implementation of whole cell biocatalysts (designer cells) in enantioselective reduction of ketones was reported for the first time by Gröger and coworkers (as illustrated in **Scheme 21**) [125]. The "tailor-made" whole-cell catalyst was designed for a desired asymmetric reduction: alcohol dehydrogenases (ADHs) with a high specific activity were chosen (an ADH from *Lactobacillus kefir* as *R*-specific alcohol dehydrogenase and an ADH from *Rhodococcus erythropolis* as *S*-specific). A one-plasmid strategy was applied: genes that encode the alcohol dehydrogenase from *R. erythropolis* and glucose dehydrogenase from *B. subtilis* were ligated into one plasmid (pNO14c).

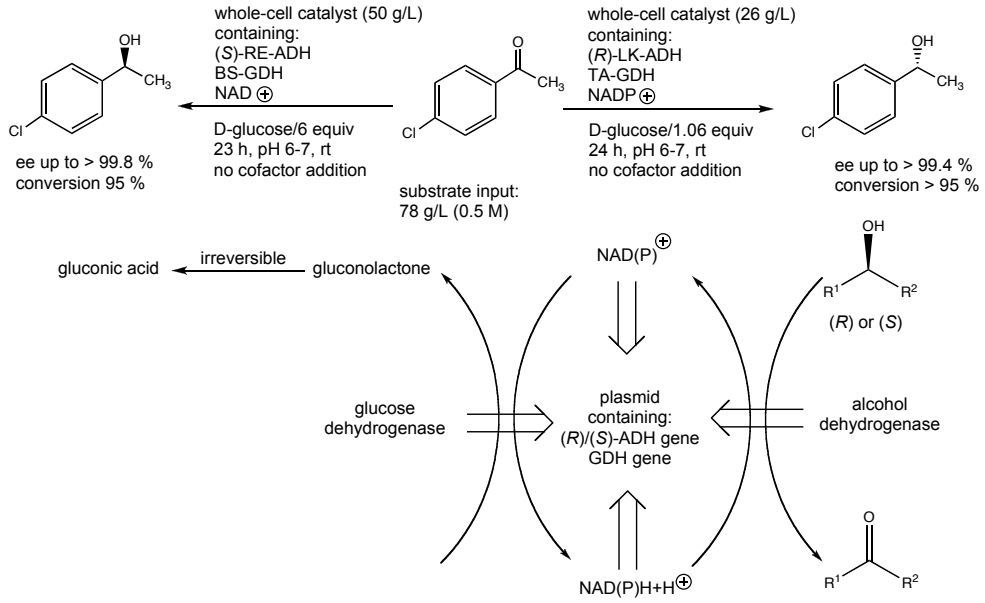

Scheme 21. Enzymatic reduction of prochiral ketones using a double-enzyme approach.

1.3.5. Comparison of enzymes vs. homogeneous catalysts

As stated in the previous section, each class of catalyst (homogeneous or enzymatic) is complementary, in several features: in enantiomeric recognition, reactions' repertoire, TON/TOF, optimization, tolerance to the organic solvents, and in second sphere of coordination. One may wonder about the possibility of creating a

"perfect"- hybrid catalyst combining the advantages of each class of catalysts. Recapitulating, the hybrid catalyst should possess advantages of both homogeneous and enzyme catalysts. These properties are highlighted and summarized in **Table 2**.

Table 2. Comparison between enzymatic catalysis and homogeneous catalysis

Parameters	Homogeneous catalysis	Enzymatic catalysis
Substrate scope	Large	Limited
Enantiomers	2 enantiomers	1 enantiomer
Tolerance to organic solvents	Excellent	Poor
Substrate concentration	High	Low to moderate
MW of catalyst	Low	High
TON/TOF	Average	High
Optimization	Chemical synthesis	Genetic
Repertoire of reaction	Large	Restricted
Second sphere coordination	Ill-defined	Well-defined
Reactions condition	High temperature and pressure	Room temperature and atmospheric pressure
Environmental impact	Hazardous	Friendly

1.3.6. Artificial Metalloproteins & Artificial Enzymes

One of the remarkable features in the recent development of bioinorganic chemistry is the creation of artificial metalloprotein. This section outlines the design of metalloenzymes (and metalloproteins) based on the incorporation of a guest within host. The design and engineering of this type of metalloproteins has several advantages:

- Of only 20 natural amino acids, less than half are capable of coordinating to metal ions. In addition, nature has only a limited repertoire of metal containing cofactors.

By introduction of unnatural amino acids/ non-native metal-containing cofactors into proteins, one can elucidate more precisely the roles of key residues important in protein structures and function precisely.

- The design and engineering of metalloproteins aim at fine-tuning the protein properties to an unprecedented level, expanding the repertoire of protein functionalities, and their range of application.

The artificial metalloproteins presented here are classified according to the nature of the metal fragment-host protein interaction: covalent, dative, and supramolecular.

1.3.6.1. Covalent anchoring

E.T. Kaiser [126] demonstrated for the first time that novel catalytic function could be created by covalent modification of an amino acid residue with appropriately modified coenzyme analogues. In his seminal work, it was shown that papain could be converted into a highly effective oxidoreductase by attaching covalently thiol group of cysteine residue C25 with flavins.

Other pioneer studies in semisynthetic covalent anchoring were those of Distefano and coworkers [127]. The attachment of Cu (II) 1,10-phenantroline complex to a single cysteine residue in adipocyte lipid-binding protein (ALBP) as shown in **Scheme 22**afforded high ee for the stereoselective hydrolysis of several unactivated amino acid ester derivatives (86% ee).

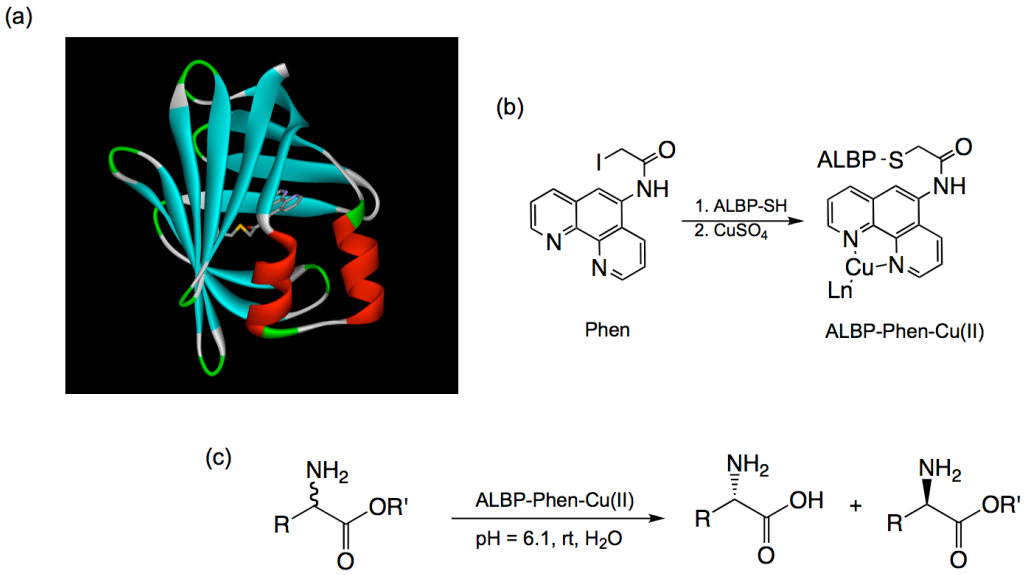

Scheme 22. Stereoview of ALBP-phenantroline complex (PDB: 1A18) (a); Covalent attachment Cu-Phen complex in ALBP (b); Enantioselective hydrolysis of amino acid ester derivatives using ALBP-Phen-Cu(II) (c)

The covalent anchoring approach in artificial metalloenzymes has also been pursued by Reetz and coworkers [128]; Mn (Salen) complexes were linked to papain through Michael additions of the cysteine C25 to the maleinimide-derivatized Schiff base (**Scheme 23**-A), though the catalytic results were moderate (ee less than 10%). Similar results were obtained in the catalytic hydrogenation using $RhCl_3$(bis-pyridine) ⊂ papain (**Scheme 23-B**). Alternatively, diphosphine (**Scheme 23-D**) was covalently attached to a serine within a lipase through phosphonate and catalyst localization was unambiguously established by enzyme inhibition experiments. Recently, de Vries and Feringa [129] reported the reduction of methyl acetamidoacrylate using the covalent attachment of monophosphite (**Scheme 23-C**) to cysteine C25 in papain. Good activity but no enantioselectivity was observed.

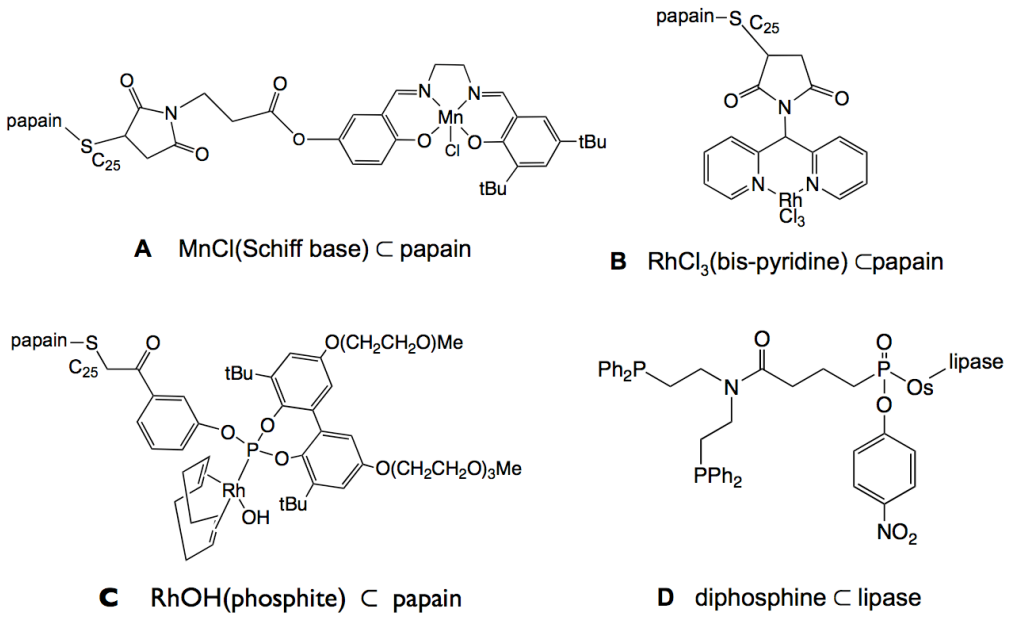

Scheme 23. Covalent anchoring of ligands and complexes to papain and lipase.

Double-point covalent attachment of a metal cofactor in myoglobin was used by Lu and coworkers [130] to produce artifical metalloenzymes for the oxidation of thioanisole affording thioanisole sulfoxides (51% ee). A recent example of covalent anchoring was reported by Fontcave and coworkers [131], who linked covalently a tricarboxylmanganese(I)-aquo complex containing a monodentate organic ligand into lysozyme to generate a binuclear Ni-Mn complex.

1.3.6.2. Dative Anchoring

Kaiser and coworkers [132] demonstrated dative modification of the active site of an enzyme resulting in an artificial metalloenzyme with novel catalytic properties. Non-covalent insertion of Schiff base complexes into the apomyoglobin cavity was reported by Watanabe and coworkers [133]. Two advantages of Schiff base complexes (**Scheme 24**) for the heme substitution are that their molecular size and coordination

geometry are similar to heme and that it is easy to modify the ligand size and hydrophobicity. Watanabe and coworkers demonstrated that the insertion of Schiff base complexe into apomyoglobin, after removal of protoporphyrin IX (original heme in myoglobin), improved catalytic reactivity in enantioselective thioanisole sulfoxidation albeit with moderate ee (32% (*S*)).

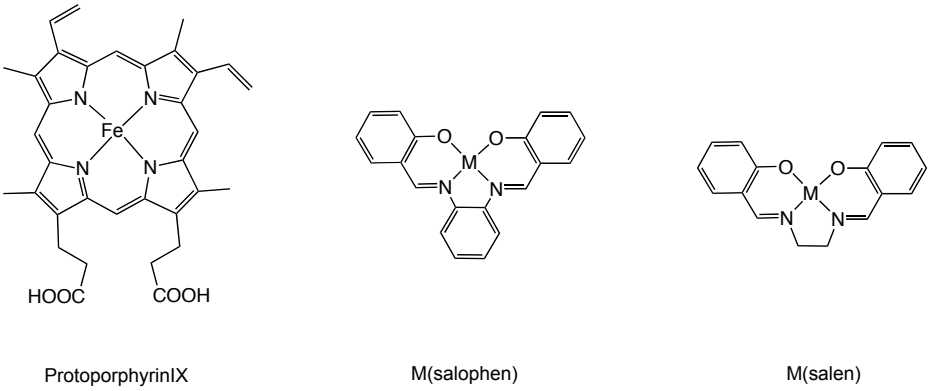

ProtoporphyrinIX M(salophen) M(salen)

Scheme 24. Molecular structures of heme and Schiff base complexes (M = Cr, Mn, and Fe) used for incorporation in myoglobin.

The native hemin of myoglobin can be reconstituted with floavohemin affording reductive activation of O_2, mimicking P450 by dative modification. Myoglobin (Mb) and P450 have the same prosthetic group, protoheme IX, but bound dioxygen on the heme is utilized in a different way [134].

Other examples of dative modification in the area of artificial metalloenzymes comprise the following reactions: oxidation [135], dihydroxylation [136], sulfoxidation [137] and epoxidation [138, 139]. Additionally, some enzymes are shown to catalyze more than one distinct chemical transformation, known as catalytic promiscuity, a term that has been introduced by Kazlauskas [140, 141].

An antibody can be considered a unique type of host that can be tailored to bind desired ligands via immunization with an appropriately chosen hapten. The design of metal-containing hapten is a nontrivial task because the hapten should have

considerable hydrolytic stability under the physiological conditions during the immunization process. In this area, a few promising results have been obtained using robust porphyrin-containing haptens for immunization.

A first example of asymmetric hydrogenation of α-acetamidoacrylic acid using an achiral rhodium complex embedded in the antibody was reported by Harada and coworkers [142] affording 98% ee (*S*) *N*-acetyl-L-alanine (**Scheme 25**).

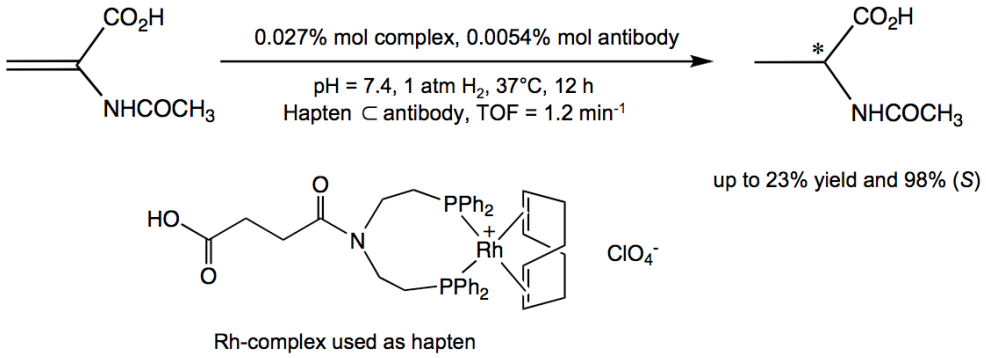

Scheme 25. Structure of achiral Rhodium complex used as hapten in the antibody.

1.3.6.3. Supramolecular Anchoring

Roelfes and Feringa [143] reported the preparation of artificial metalloenzymes built from two classes of ligand, which were non-covalently incorporated in DNA, for Diels-Alder reactions (**Scheme 26**). It is found that the smaller class of ligand was bound in a more favorable orientation affording excellent ee (up to 99% endo). This ligand acts both as intercalator and bidentate ligand.

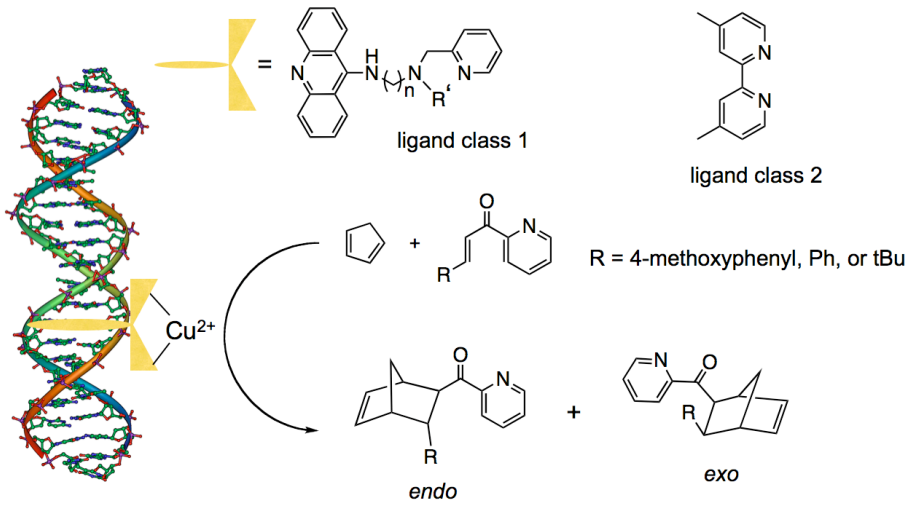

Scheme 26. Schematic representation of the DNA-based catalytic enantioselective Diels-Alder reaction (operating conditions: Cu^{II}-ligand (0.3 mM), DNA (1.3 mg/mL), pH 6.5, 33% mol catalyst loading, 3 days).

Another example of supramolecular anchoring was reported by Watanabe and coworkers [144], who used ferritin to accommodate a Pd-nanoparticle (as illustrated in **Scheme 27**) used for size selective olefin hydrogenation affording better TOF than classic catalysts.

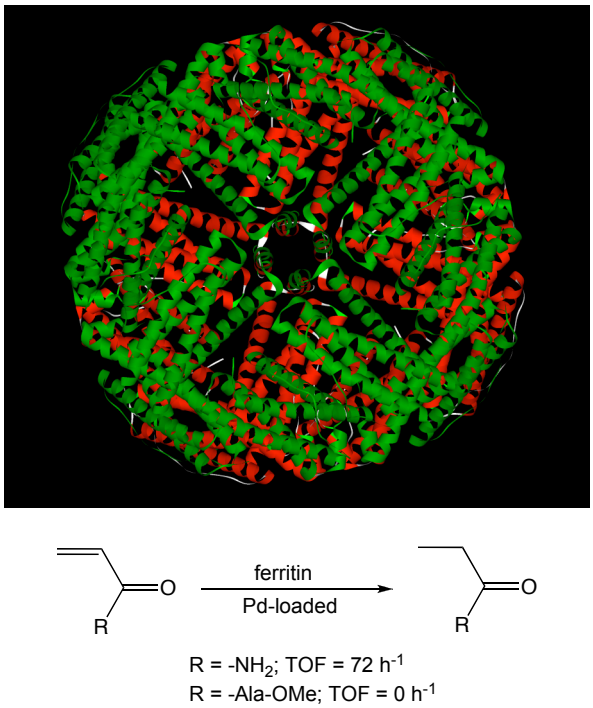

Scheme 27. Schematic structure of ferritin (adapted from PDB code: 1BFR, without any further modification).

Whitesides and Wilson [27] (**Scheme 28**) pioneered in 1978 the asymmetric hydrogenation of α-acetamidoacrylic acid using a biotinylated-Rh precursor embedded in avidin, affording moderate ee (41% (*S*)). Chan and coworkers [15] attempted to use the same principle using other diphoshine ligands: their results displayed moderate enantioselectivities (up to 48% (*R*) and 11% (*S*)). After optimization of operating conditions (pH, pressure, temperature), the selectivity was improved, although ees remained moderate (up to 48% (*R*) and 37% (*S*)).

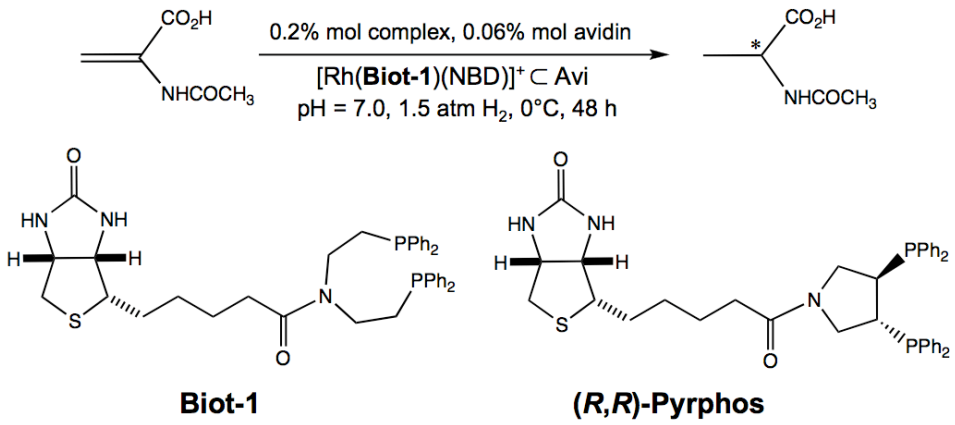

Scheme 28. Enantioselective hydrogenation of α-acetmidoacrylic acid using complex [Rh(NBD)(**Biot-1**)$^{+}$] ⊂ WT avidin. Inset: structure of Pyrphos by Chan and coworkers [15].

Inspired by Whitesides' pioneering work, the biotin-avidin technology has also been successfully applied in our group for transfer hydrogenation of ketones catalyzed by d^6-piano stool complexes [145-147].

1.3.7. Mechanistic study of asymmetric hydrogenation and Michaelis-Menten kinetics

1.3.7.1. Mechanistic study of asymmetric hydrogenation

Halpern and coworkers [148] studied in detail the mechanism of asymmetric hydrogenation of methyl-(*Z*)-α-acetamidocinnamate using (*R*,*R*)-dipamp ligand. They proposed that there are four key steps in this mechanism as depicted in **Scheme 29**:

A. Reversible binding of the substrate to the catalyst via the oxygen atom of the amide group and C=C bond affording rhodium-substrate complex

B. Irreversible oxidative addition of dihydrogen to rhodium-substrate complex

C. Irreversible migratory insertion of the C=C bond into the Rhodium-H bond

D. Irreversible reductive elimination of the product.

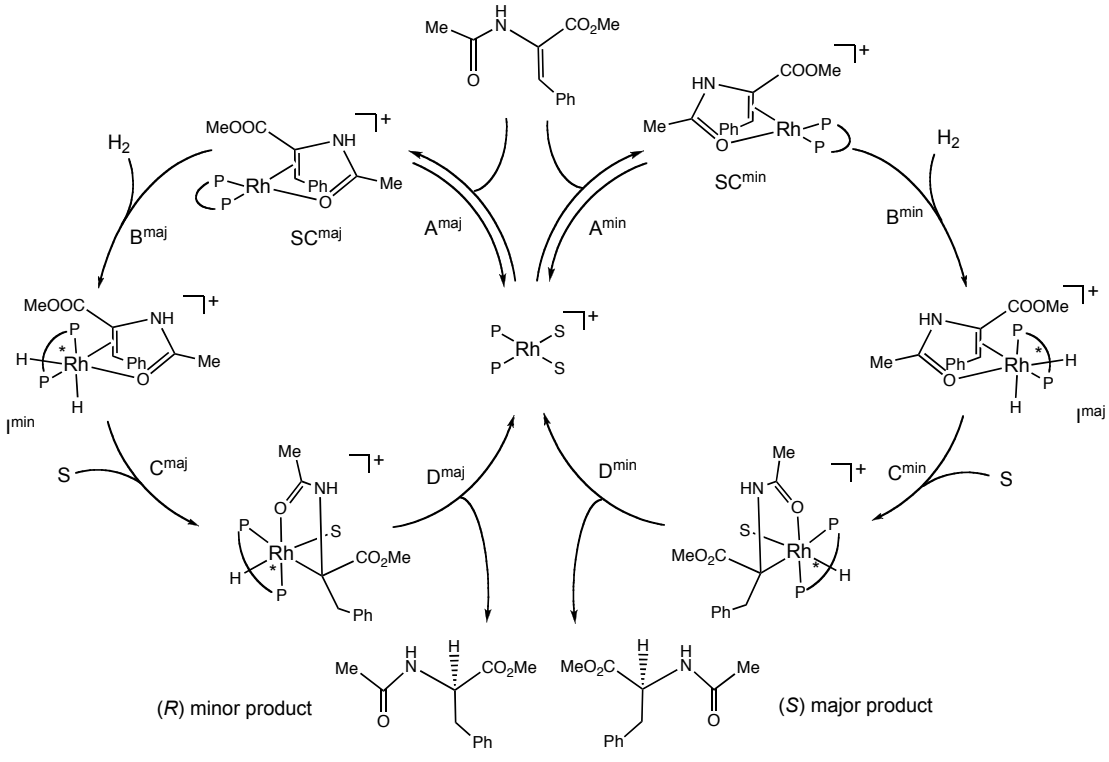

Scheme 29. Catalytic cycle for Rh(dipamp) – catalyzed hydrogenation of methyl-(*Z*)-α-acetamidocinnamate (P-P = (*R*,*R*)-dipamp, S = alcoholic solvent).

Only the first two steps (A and B) were experimentally observable. As the second step (B) is the first irreversible step, it thus dictates the enantioselectivity. Furthermore, these studies revealed that the major intermediate (SC^{maj}) , which is thermodynamically more stable, reacts more slowly with dihydrogen molecule than its minor counterpart (SC^{min}), thus affording minor products at the end of the catalytic cycle. It is noteworthy that the enantioselectivity is determined by the relative rates of the reaction of the diastereomer adducts with dihydrogen rather than by equilibrium constants for binding of the prochiral substrate to the chiral catalyst. Furthermore, it is found that ee decreases with increasing of H_2 partial pressure.

1.3.7.2. Michaelis-Menten Kinetics

Traditionally, in enzymatic catalysis, Michaelis-Menten equations are used to assess and determine the kinetic parameters of a reaction. Leonor Michaelis and Maud Menten laid the foundation for enzyme kinetics as early as 1913 by proposing the following scheme:

$$E + S \underset{k_{-1}}{\overset{k_1}{\rightleftharpoons}} ES \xrightarrow{k_2} E + P$$

The reaction should follow saturation kinetics with respect to the concentration of substrate. The substrate concentration at half the maximal rate, ($V_{max}/2$), is called the K_M. For many simple reactions, K_M is equal to the dissociation constant of ES complex. These steps could be described as follow: $K_M = \frac{k_{-1}}{k_1}$

Where E: enzyme; S: substrate; ES: complex enzyme-substrate, P: product and rate of reaction or turnover number: k_2. Rate of reaction can be described as a function of [S], K_M, and V_{max}, (**Scheme 30**) with $V_{max} = k_{cat}[E]_0$.

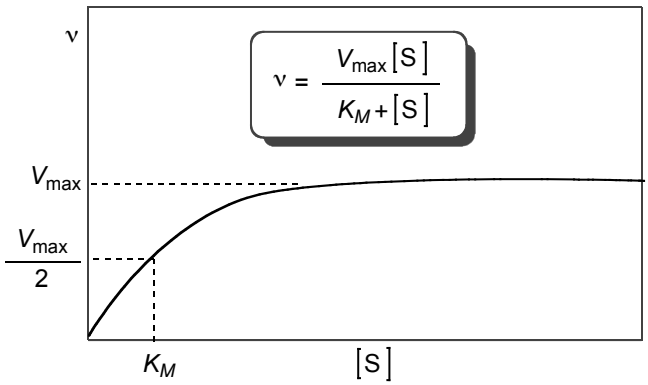

Scheme 30. Representation of Michaelis-Menten plot for determination of kinetic parameters.

The maximum rate of reaction V_{max} is always observed when the substrate concentration is much higher than the enzyme concentration and it is obtained when the enzyme is saturated with substrate. The quantity k_{cat}/K_M is a rate constant that refers to the overall conversion of substrate into product. The ultimate limit of the value is therefore set by the rate constant for the initial formation of the ES complex. This rate cannot be faster than the diffusion-controlled encounter of an enzyme and its substrate, which is 10^8 to 10^9 per mole per second.

Donna G. Blackmond and coworkers [149, 150] stated that the kinetics of the hydrogenation reaction depends to the concentration of hydrogen in liquid rather than gas pressure, as the reaction occurs in the liquid bulk [151].

1.4. Objectives of this work

The present work focuses on the interactions of metal complex and protein in the context of artificial metalloenzymes based on the biotin-avidin technology. The cavity of the protein, which is chiral, is expected to induce chirality upon incorporation of the metal complexes into the protein. This interaction has been exploited for the investigation of catalysts for asymmetric hydrogenation. The

thermodynamic, kinetic and selectivity of these asymmetric hydrogenation reactions will be discussed.

As for thermodynamic studies, the work focused on the design of the diastereopure of $[Ru(Biot)_2(Biot\text{-}bpy)]^{2+}$ to elucidate the enantiodiscrimination upon incorporation of the biotinylated complexes in the host protein, (strept)avidin. Determination of the binding constants was performed through CD spectrophotometric titrations and the data were treated using SPECFIT/32 package. The assessment of the cooperativity between binding sites was performed and is described in detail.

Application of biotin-avidin technology is promising, but challenging. In the past few years, our group has demonstrated that incorporation of achiral/chiral spacer-biotin conjugated-Rh complexes in the (strept)avidin generated highly (*R*)-selective and (*S*)-selective artificial hydrogenases. For this thesis, progress focused on the chemogenetic optimization of second-generation artificial hydrogenases. The chapter is devoted to describe in the first part: results from saturation mutagenesis in position S112 and in the second, results from a single (and double) point mutation of other amino acid residues in the host protein.

Organic solvent tolerance is known to be a major problem in the area of enzymatic catalysis. Another aim of the thesis was to investigate whether the new class of the artificial hydrogenases may give an improved resistance towards organic solvents than the first generation.

In the present work, a straightforward protocol to immobilize the artificial hydrogenase by using biotin-sepharose was proposed. This protocol was inspired by the fact that, first, (strept)avidin has four binding-sites and, second, when varying the occupancy of biotinylated-complex with respect to the protein, 1–3 occupancies of

binding site does not affect the catalytic result significantly (1-2% lower ee was observed) [152, 153]. By saturating biotin-sepharose (wet beads) with streptavidin, only one binding site is occupied on average, allowing the rest of binding sites to attach the metal precursor for performing heterogeneous/immobilized catalysis.

Finally, the kinetic study of asymmetric hydrogenation using Michaelis-Menten approach was also carried out. To build Michaelis-Menten equations, a series of individual kinetic experiments with varying the concentration of substrates, were performed and will also be described.

THERMODYNAMIC STUDY OF INCORPORATION RUTHENIUM BIOTINYLATED COORDINATION COMPLEXES WITHIN (STREPT)AVIDIN USING CD SPECTROSCOPY

2.1. Introduction

The incorporation of biotin ⊂ (strept)avidin has been studied extensively since three decades. In this context, the binding constant of biotinylated compounds within (strept)avidin plays an important role. To date, only few reports have been issued for the determination of binding affinities, and even less to study the cooperativity of binding of biotinylated ligands in (strept)avidin. In this chapter, we present a straightforward determination of binding constants of biotinylated compounds in (strept)avidin using CD spectroscopy. The assessment of the cooperativity of incorporation biotinylated compounds within (strept)avidin will be presented and discussed.

2.2. Synthesis of biotinylated coordination complexes: $[Ru(bpy)_2(Biot\text{-}bpy)]^{2+}$ (1)

The synthesis of biotinylated bipyridine ligand Biot-bpy (**4**) was achieved by mixing equimolar amounts of biotinylated ethylenediamine (**2**) [154] with the activated ester (**3**) [155] in the presence of triethylamine in DMF. *rac*-$[Ru(bpy)_2(Biot\text{-}bpy)](PF_6)_2$ (*rac*-**1**$(PF_6)_2$) [156] was achieved by refluxing $[Ru(bpy)_2Cl_2]$ in the presence of a slight excess of Biot-bpy (**4**), followed by precipitation with NH_4PF_6 (**Scheme 31**).

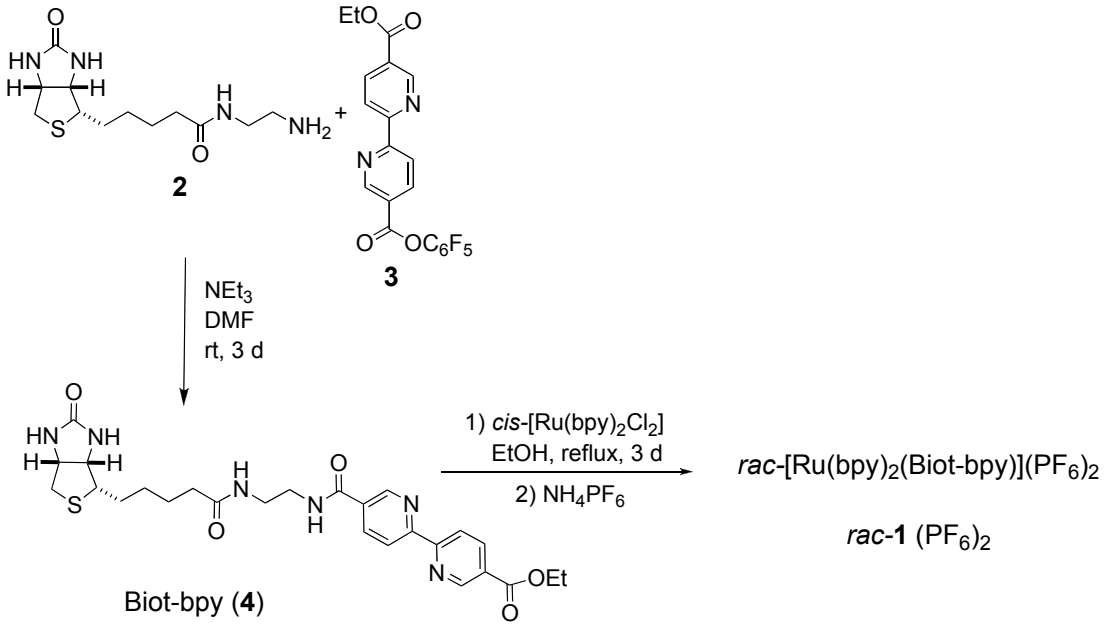

Scheme 31. Synthesis of Biot-bpy (**4**) and formation of the corresponding racemic coordination complex *rac*-**1**$(PF_6)_2$.

The preparation of diastereopure Λ-$[Ru(bpy)_2(Biot\text{-}bpy)]^{2+}$ (Λ-**1**) was achieved using von Zelewsky's procedure [157, 158]. Refluxing of Λ-$[Ru(bpy)_2(py)_2]$[(-)-*O,O'*-dibenzoyl-L-tartrate] with Biot-bpy (**4**) in ethyleneglycol-water mixture in the dark affords Λ-$[Ru(bpy)_2(Biot\text{-}bpy)]^{2+}$ (Λ-**1**). The diastereomeric purity of biotinylated complex Λ-**1** was assessed by subjecting a quantity of crude sample to ion exchange chromatography (Sephadex C-25) using potassium nitrate (0.05 M, pH = 5.0) as eluent. The entire elution peak was collected in three fractions; each of these was analyzed by UV-Vis and CD spectroscopy. Plotting the ratio of the signals (UV-Vis/CD) for each fractions results in a horizontal line, thus suggesting that the entire elution peak is diastereopure.

These steps are summarized in **Scheme 32**.

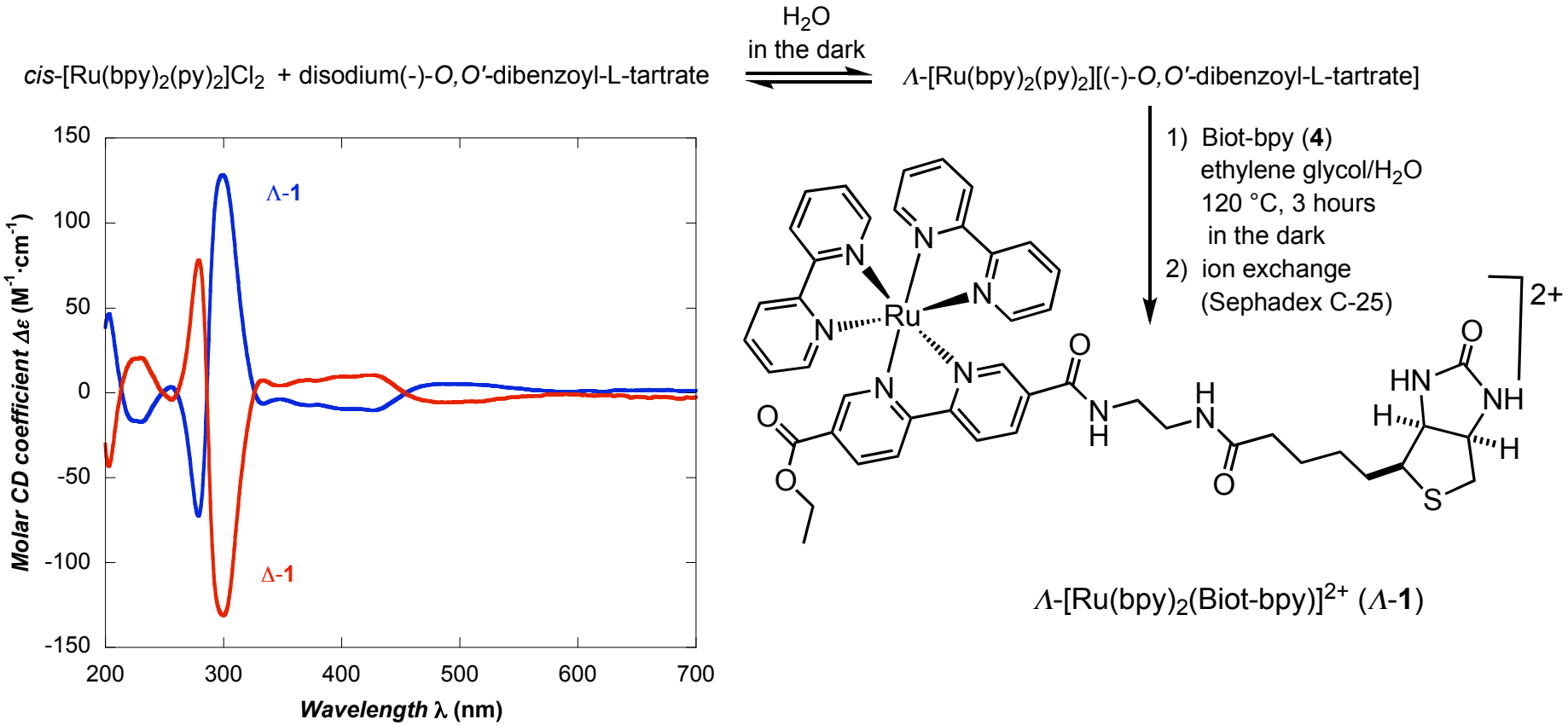

Scheme 32. The synthesis of diastereopure biotinylated coordination complex *Λ*-**1** using von Zelewsky's procedure. Inset: CD spectra of diastereopure Δ-**1** and Λ-**1**.

2.3. Titration experiments

The activity of (strept)avidin was determined using Gruber's protocol [159] based on the fluorescence quenching of biotinylated fluorescein upon incorporation in (strept)avidin.

In the first attempt, the determination of binding constants was performed by titrations of apo-protein with *rac*-**1**. The titrations were carried out at 25°C and buffered at pH = 7 aqueous medium (KH_2PO_4/Na_2HPO_4). The ellipticity changes induced by the incremental addition of a *rac*-$[Ru(bpy)_2(Biot\text{-}bpy)]^{2+}$ (*rac*-**1**) solution in 5.0 μL aliquots (0.25 equiv) were monitored up to 6.0 equiv vs. the tetrameric protein in 250–500 nm range by circular dichroism (CD) spectroscopy.

The CD spectra resulting from the titration of *rac*-$[Ru(bpy)_2(Biot\text{-}bpy)]^{2+}$ (*rac*-**1**) with avidin are depicted in **Figure 1**.

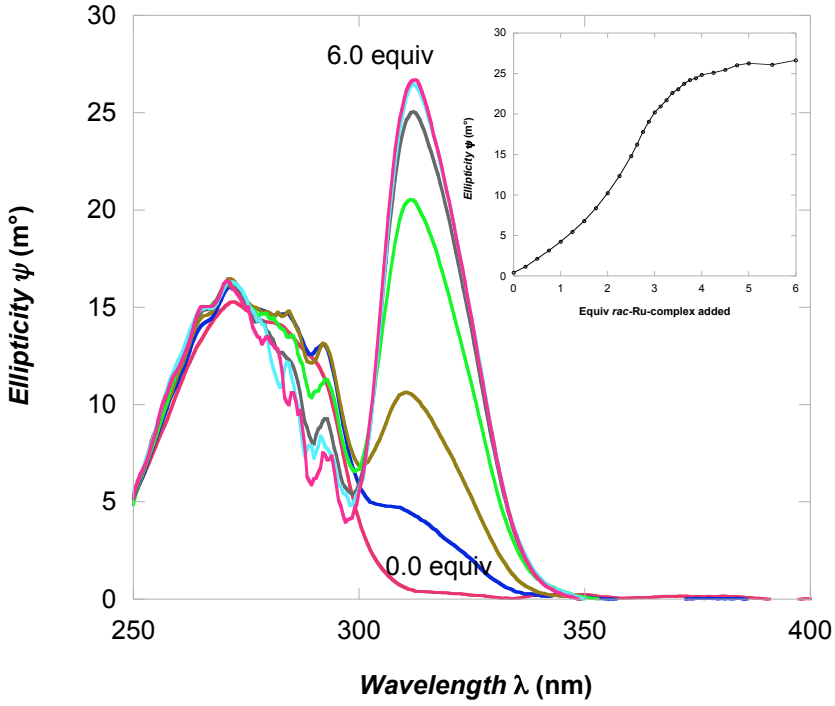

Figure 1. CD titration profile obtained for the addition of aliquots of *rac*-**1** to avidin. Inset: titration profile monitored at 313 nm (I = 0.15 M; KH_2PO_4/Na_2HPO_4; pH = 7.00; T = 298.1 K).

Similar results were obtained with streptavidin [156]. Figure 1 suggests that the biotinlyated coordination compound can occupy four binding sites of (strept)avidin. Since the biotinylated guest is racemic, the appearance of a strong band centered at 313 nm can be attributed to an induced CD signal resulting from second coordination sphere interaction between the host-protein and the guest (*rac*-**1**).

2.4. Determination of stability constants

In order to determine the stability constants, the spectroscopic data were analyzed using SPECFIT/32 package [160-162] with a theoretical model with up to four binding constants. However, this attempt failed, as reflected by the lack of convergence in the fitting procedure. This is probably due to the presence of both diastereomers of the biotinylated coordination complexes within a single tetrameric (strept)avidin.

The following simplified model points out the complexity of this system, taking into account the following assumptions:

i.) A second guest molecule enters exclusively in *trans*-position to the first guest.

ii.) The two remaining free binding sites in (strept)avidin are identical.

iii.) The affinity of the guest depends on the presence or absence of a guest in an adjacent binding site.

This procedure affords 14 different binding constants to be fitted for *rac*-$[Ru(bpy)_2(Biot\text{-}bpy)]^{2+} \subset$ (strept)avidin. This situation is summarized in **Scheme 33**.

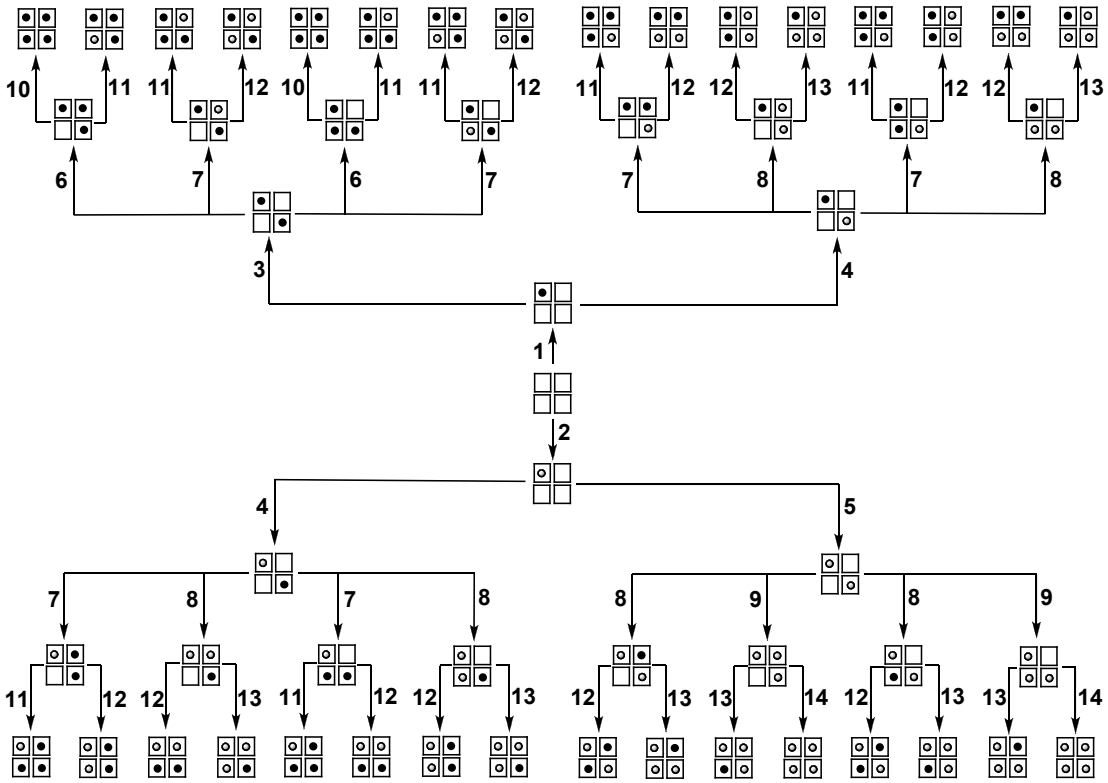

Scheme 33. Possible binding events for a racemic guest in a tetrameric host protein. 14 binding constants are generated from the interactions of racemic mixture with the homotetrameric protein. (•) and (^{o}) are diastereomers.

In order to reduce the number of unknown binding constants, the spectrophotometric titrations were repeated with the diastereopure biotinylated ruthenium complexes (Δ-**1** and Λ-**1**). The spectra of these titrations are depicted in the Figures 2-5. As expected, considering the structural similarity of avidin and streptavidin, both titration spectra closely resemble each other (**Figure 2** vs. **Figure 3**, and **Figure 4**vs. **Figure 5**).

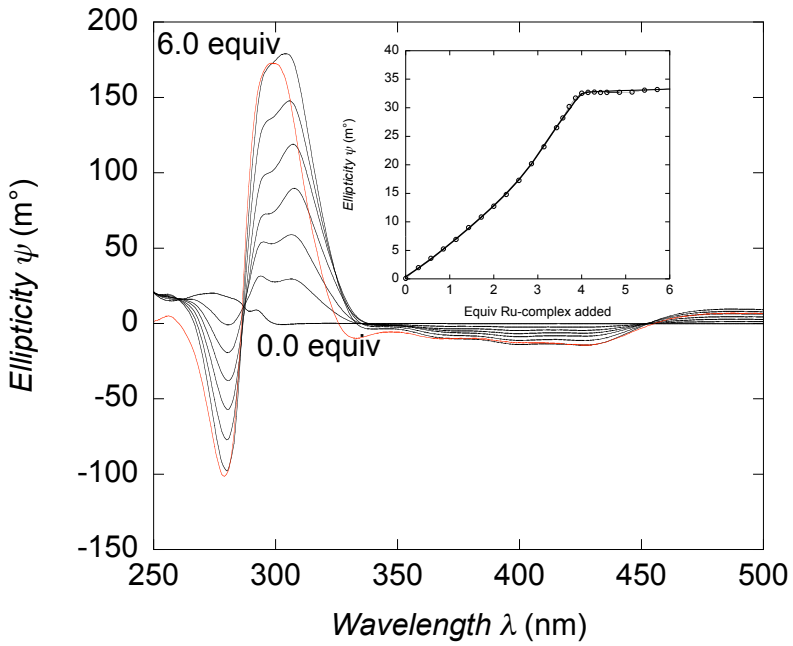

Figure 2. CD titration profile obtained for the addition of aliquots of Λ-**1** to streptavidin. The red lines correspond to the CD spectra of the diastereopure biotinylated complex (Λ-**1**) in the absence of streptavidin (I = 0.15 M; KH_2PO_4/Na_2HPO_4; pH = 7.00; T = 298.1 K). Inset: titration monitored at 324 nm.

Upon inspection of the spectra, one can observe that both apo-proteins show weak absorption bands occurring below 300 nm with a positive Cotton effect ascribing to tryptophan-centered transitions, both apo-proteins are spectroscopically silent above 310 nm. Upon addition of the Λ–**1** diastereomer, a negative band at 280 nm progressively appears accompanied by a more intense and positive signal centered around 300 nm that tails out in the visible region as broad, albeit much weaker. Ellipticity features a negative (340–455 nm) and, at higher wavelengths, a positive (455–500 nm) Cotton effect.

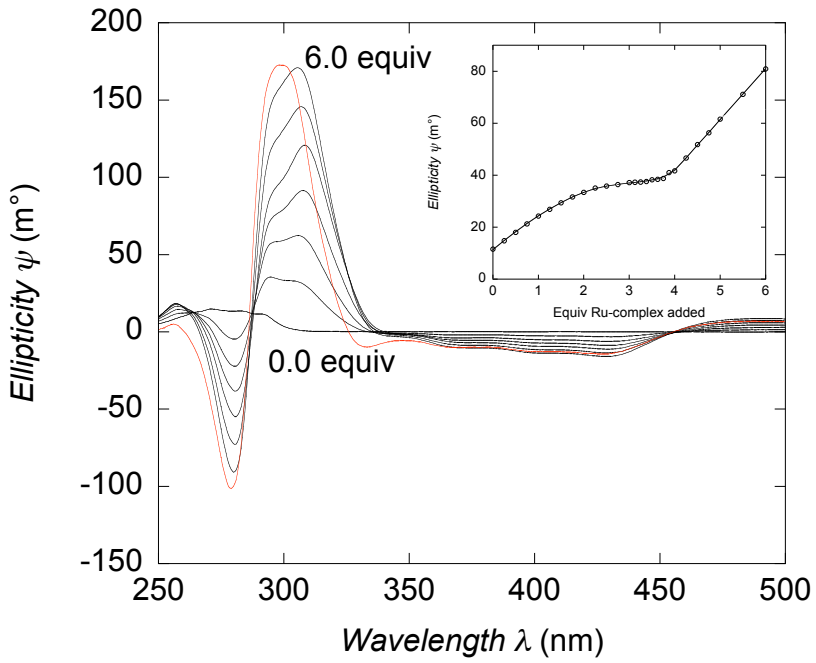

Figure 3. CD titration profile obtained for the addition of aliquots of Λ-**1** to avidin. The red lines correspond to the CD spectra of the diastereopure biotinylated complex (Λ-**1**) in the absence of avidin (I = 0.15 M; KH_2PO_4/Na_2HPO_4; pH = 7.00; T = 298.1 K). Inset: titration monitored at 290 nm.

As the titration proceeds, the CD-induced ellipticity bands undergo subtle morphological changes in the UV region, without showing sharply defined isodichroic points. This behavior is best exemplified by the steady intensity increase of the low- at the expense of the high-energy component of the positive envelope peaking at 308 nm (*ca*. 10 nm shift) at the end of the titration of (strept)avidin. The non-monotonic variation of the ellipticity measured at selected wavelengths further confirms the one-by-one sequential uptake of the biotinylated ruthenium tris(bipyridine) complexes (Δ-**1** and Λ-**1**) by the protein.

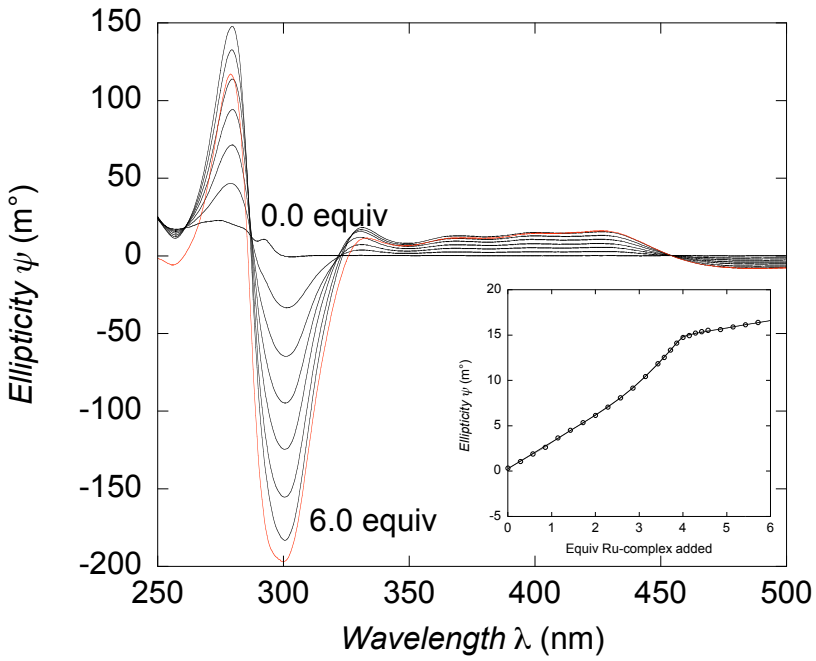

Figure 4. CD titration profile obtained for the addition of aliquots of Δ-**1** to streptavidin. The red lines correspond to the CD spectra of the diastereopure biotinylated complex (Δ-**1**) in the absence of streptavidin (I = 0.15 M; KH_2PO_4/Na_2HPO_4; pH = 7.00; T = 298.1 K). Inset: titration monitored at 329.5 nm.

Despite opposite Cotton effects and some similarities in the general morphology, interestingly the spectra pertaining for a given host-protein (avidin and streptavidin) to both diastereomer Λ-**1** and Δ-**1** are not reflecting the similar effect of induction (as shown in Scheme 2, the CD spectra of Λ-**1** and Δ-**1** are superimposable to the mirror image of each other).

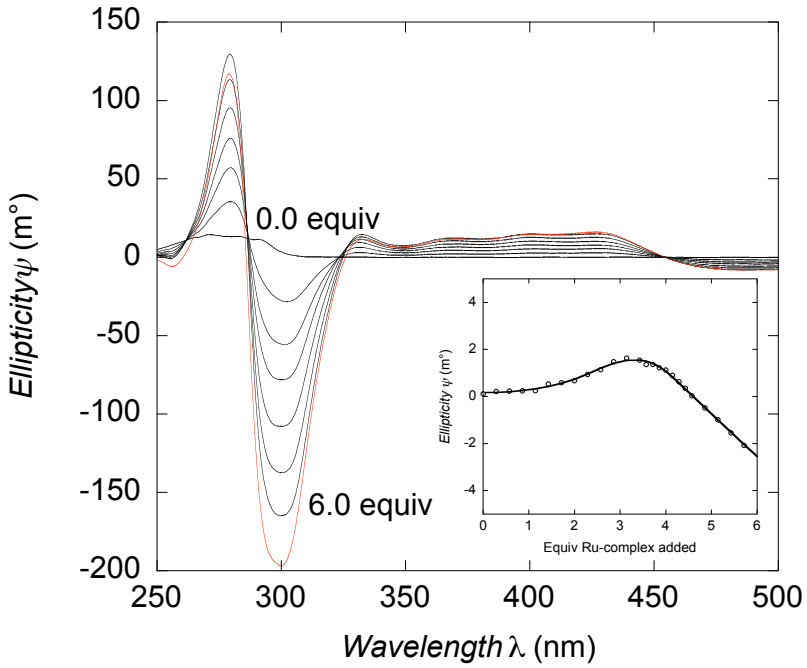

Figure 5. CD titration profile obtained for the addition of aliquots of Δ-**1** to avidin. The red lines correspond to the CD spectra of the diastereopure biotinylated complex (Δ-**1**) in the absence of avidin (I = 0.15 M; KH_2PO_4/Na_2HPO_4; pH = 7.00; T = 298.1 K). Inset: titration monitored at 324 nm.

The major differences appear in the region around 300 nm. Whereas the positive feature is clearly resolved into two components in the case of Λ-**1** diastereomer (**Figure 2** and **Figure 3**), for the Δ-**1** complex (**Figure 4** and **Figure 5**), the negative feature evidences no visible splitting. In addition, development of a much weaker band with positive Cotton effect at 331 nm is observed only for the binding of Δ-**1** diastereomer. This electronic transition is characteristic for complex formation since it is absent in the spectrum of free Δ-**1**.

Each data sets of titration were imported into the SPECFIT/32 package. Factor analyses were calculated from preliminary examination in SPECFIT/32, representing the approximate number of absorbed components present in the solution. This can be achieved via singular-value decomposition (SVD) procedure, which is integrated in the software package. The spectroscopy data, comprising 27 spectra and 501

distributed wavelengths can be extracted to not more than five eigenvalues without losing information other than instrumental noise. The overall binding constants were subsequently refined by nonlinear least squares using Marquardt's algorithm [163].

$$\text{(strept)avidin} + x\,\mathbf{1} \rightleftharpoons \mathbf{1}_x \subset \text{(strept)avidin} \quad (1)$$

$$\beta_x = \frac{[\mathbf{1}_x \subset \text{(strept)avidin}]}{[\text{(strept)avidin}]\cdot[\mathbf{1}]^x} = \prod_{i=1}^{x} K_i \quad (2)$$

$$x = 1 - 4$$

Considering that both streptavidin and avidin are homotetrameric proteins constructed from identical, single domain subunits consisting of eight-stranded, antiparallel β-barrels, the most obvious chemical model to be considered should include six absorbing species, namely the four inclusion complexes (x = 1 – 4) in addition to both reactants. However, all attempts to determine these four stability constants failed, as reflected by the lack of convergence of the fitting procedure. The rough overview of the success of the determination of binding constants may be obtained by comparing the theoretical number of component existing in the system with the significant factor analysis obtained from Evolved Factor Analysis (EFA).

As an example, the eigenvalues/significant factor analysis obtained after importing the data using SPECFIT/32 package for **Δ-1** ⊂ streptavidin system are depicted in **Figure 6**:

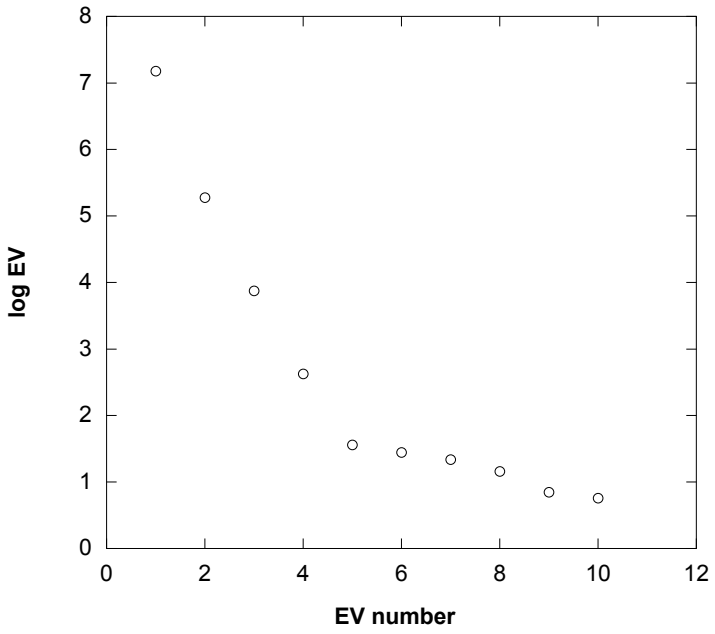

Figure 6. Eigenvalues/factor analysis obtained from SPECFIT/32 package for titration data of **Δ-1** ⊂ streptavidin system (EV = eigenvalue(s)).

A critical examination to define the number of component present in the system is therefore essential. From **Figure 6**, we speculate for the first attempt to take into account only the first 5 eigenvalues being introduced in the equilibrium model. This procedure yields 3 equations of equilibrium by excluding the first equilibrium; the results of this iteration were compiled in the **Table 3**. For the second attempt, we consider that there are six absorbant species, representing the complete 4 equilibrium equations, however the nonlinear least square minimization failed. We reasoned that the sixth eigenvalue is less significant compared to the systematic equipment error.

The encountered numerical difficulties are a direct consequence of a very shallow, badly defined error hypersurface and were systematically associated with divergence of the first equilibrium constant β_1.

On the basis of the lack-of-fit parameter σ expressed as the residual standard error and by the physical meaning of the calculated CD spectra pertaining to each species, only the model with three inclusion complexes was evaluated ($x = 2 - 4$).

A comparison of the calculated and experimental spectra recorded for the apo-(strept)avidin and complex was of particular value in discarding models with similar σ values that were not statistically different from each other at the 95% probability level according to a Fischer–Snedecor F-test. As expected, the optimal fit was obtained after excluding β_1 from the set of refined constants.

The estimations of the stepwise binding constants are summarized in Table 1, together with their standard deviations derived from the variance/covariance matrix. The refined equilibrium constants log β_x are highly correlated with correlation coefficient systematically exceeding 0.99, while stepwise constants (log K_x) are less correlated (the highest correlation coefficient in the range of 0.75, found between log K_1K_2 and log K_3).

Table 3. Summary of refined binding constants between $[Ru(bpy)_2(Biot\text{-}bpy)]^{2+}$ (**1**) and (strept)avidin using a three equilibrium model. Standard deviations are given in parenthesis.

Host-guest complex	log K_1K_2	log K_3	log K_4
(Δ-$[Ru(bpy)_2(Biot\text{-}bpy)]^{2+}$)⊂avidin	15.1(5)	6.8(2)	6.7(1)
(Λ-$[Ru(bpy)_2(Biot\text{-}bpy)]^{2+}$)⊂avidin	15.7(3)	7.2(1)	7.4(1)
(Δ-$[Ru(bpy)_2(Biot\text{-}bpy)]^{2+}$)⊂streptavidin	18.9(9)	8.9(2)	8.4(2)
(Λ-$[Ru(bpy)_2(Biot\text{-}bpy)]^{2+}$)⊂streptavidin	18.8(6)	9.5(2)	8.1(1)

[a] $I = 0.15$ M (KH_2PO_4/Na_2HPO_4), pH = 7.00 , $T = 298.1$ K.

The refined CD spectra corresponding to each absorbing species for the investigated systems are displayed in **Figure 7** (for Λ-**1** ⊂ avidin) and in **Figure 8** (for Δ-**1** ⊂ streptavidin). For all theses cases, molar CD coefficient $\Delta\varepsilon$ values calculated for the apo-proteins and free diastereopure complexes are in excellent agreement with the experimentally measured values. In addition, almost perfect mirror image coincidence was found for the computed spectra of both Δ-**1** and Λ-**1** diastereomers, providing further confidence in the refinement results.

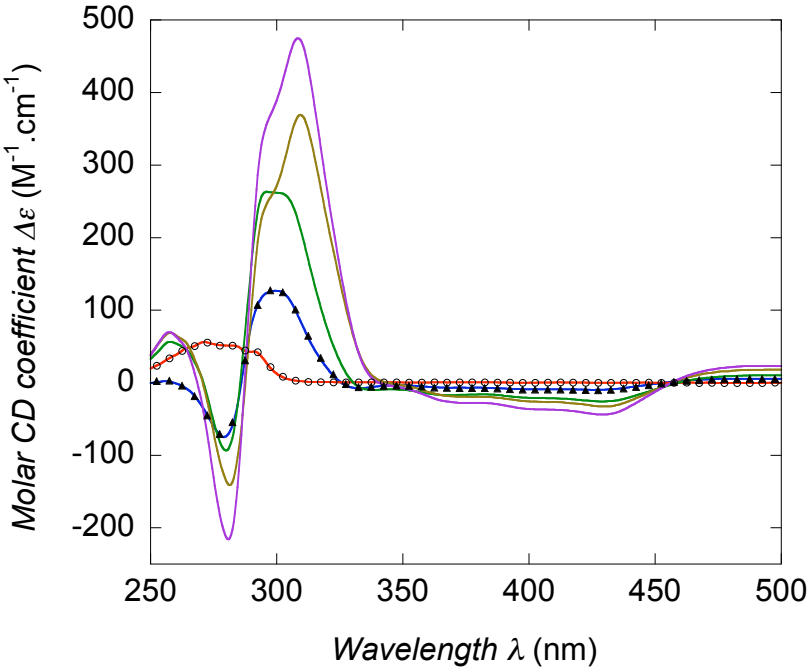

Figure 7. Refined CD spectra for each absorbing species for (Λ-**1**)$_x$ ⊂ avidin, x = 0: red line, x = 2: green line, x = 3: brown line and x = 4: violet line. For comparison, the measured spectra for the host protein and for the biotinylated guest Λ-**1** are displayed as open circles and full triangles respectively, overlaid with the corresponding refined spectra (thin lines).

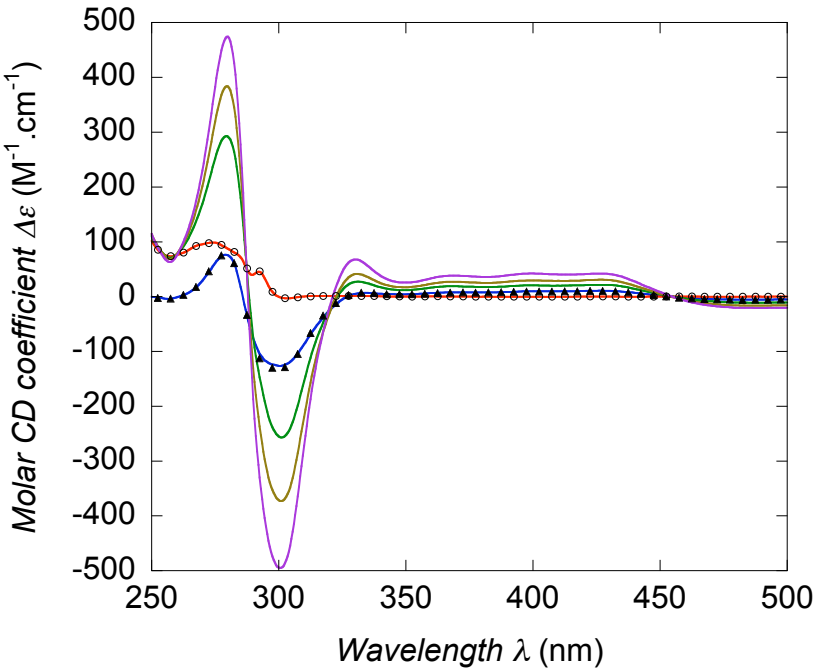

Figure 8. Refined CD spectra for each absorbing species for (Δ-**1**)$_x$ ⊂ streptavidin, .x = 0: red line, x = 2: green line, x = 3: brown line and x = 4: violet line. For comparison, the measured spectra for streptavidin and for Δ-**1** are displayed as open circles and full triangles respectively, overlaid with the corresponding refined spectra (thin lines).

The species distribution diagram for the four investigated systems are depicted in **Figure 9**. A close view to these distribution diagrams, avidin showed a more regular fashion in the formation of the complexes. Up to a two-fold of Ru-complex (Δ-**1** or Λ-**1**), the presence of bis-species is pre-dominant in the solution. However, in streptavidin, the competition between bis- and tris-species was already observed from the beginning of the titration (this observation is clearly shown for (Λ-**1**)$_x$ ⊂ streptavidin system, **Figure 9**(a)). Though, this indication is still questionable if this phenomenon could be related to the cooperativity of the binding sites.

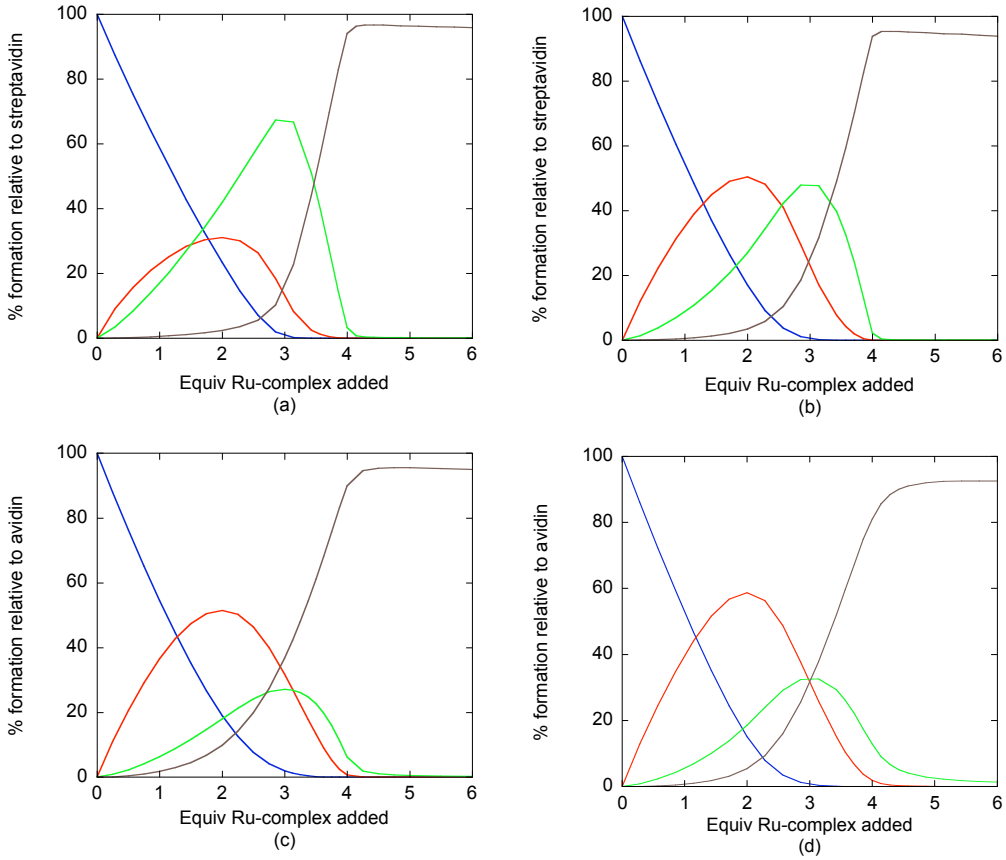

Figure 9. Species distribution diagram for (Λ-**1**)$_x$ ⊂ streptavidin (a); (Δ-**1**)$_x$ ⊂ streptavidin (b); (Λ-**1**)$_x$ ⊂ avidin (c) and (Δ-**1**)$_x$ ⊂ avidin (d) .x = 0: blue line, x = 2: red line, x = 3: green line and x = 4: brown line.

The attempts to determine the first binding constants K_1, including addition of smaller aliquots of biotinylated complex **1** as well as titration of biotinylated complexes with aliquots of (strept)avidin failed. To rationalize this observation, one may put forward the following arguments:

i.) The impossibility to identify the (Λ-**1**/Δ-**1**) ⊂ (strept)avidin complex during the titration is a direct consequence of very similar spectra signatures of both mono and bis-species making them indistinguishable by CD spectroscopy. This argument is plausible considering the high similarity of the four binding pockets found in the crystal structure of both proteins in the loaded and unloaded state.

ii.) A strong cooperativity of the formation of the bis-species (**Δ-1 or Λ-1**)$_2$ ⊂ (strept)avidin, so that the concentration of the mono-species (**Δ-1 or Λ-1**) ⊂ (strept)avidin at any stage of titration remains below the detection limit of the CD spectrophotometer.

2.5. Assessment of the cooperativity: creation & simulation of artificial data

A quantitative assessment of cooperativity for the four systems under investigation is complicated by the errors associated with the equilibrium constants and most importantly by the fact that K_1 remains experimentally inaccessible. It proved particularly intricate to circumvent this difficulty just by tuning the titration conditions while maintaining the measured signal below the saturation level of the CD detector. Although the spectral contribution of the mono-adduct species to the overall measured CD signal is similar or even below the instrumental noise level, exclusion of the first equilibrium from the chemical model raises some important concerns from a computational standpoint.

To appreciate the extent of the bias on the refined values of the equilibrium constants introduced when the formation constant of a minor species is ignored, a series of artificial data sets with known values of binding constants and molar CD absorption coefficients were generated at different, but constant noise levels using the simulation routine implemented in SPECFIT/32 package.

The conditions were chosen so as to reproduce accurately the actual titration conditions. We focused this examination for **Δ-1** ⊂ streptavidin system. The refined spectra and rounded-off values of the equilibrium constants corresponding to the free components and inclusion species displayed in Figure 8 were used as input for each simulation. As far as the uncharacterized mono-species is concerned, its molar CD

absorption $\Delta\varepsilon$ were arbitrarily set to half the molar CD absorption coefficient calculated for the bis-species (Δ-**1** or Λ-**1**)$_2$ $\subset$ (strept)avidin (**Figure 10**), which seems a reasonable assumption considering the similar spectral morphologies displayed by the three inclusion complexes (for Δ-**1** species, while considering only the similarity of the tris- (Λ-**1**)$_3$ $\subset$ (strept)avidin and (Λ-**1**)$_4$ $\subset$ (strept)avidin for Λ-**1** species).

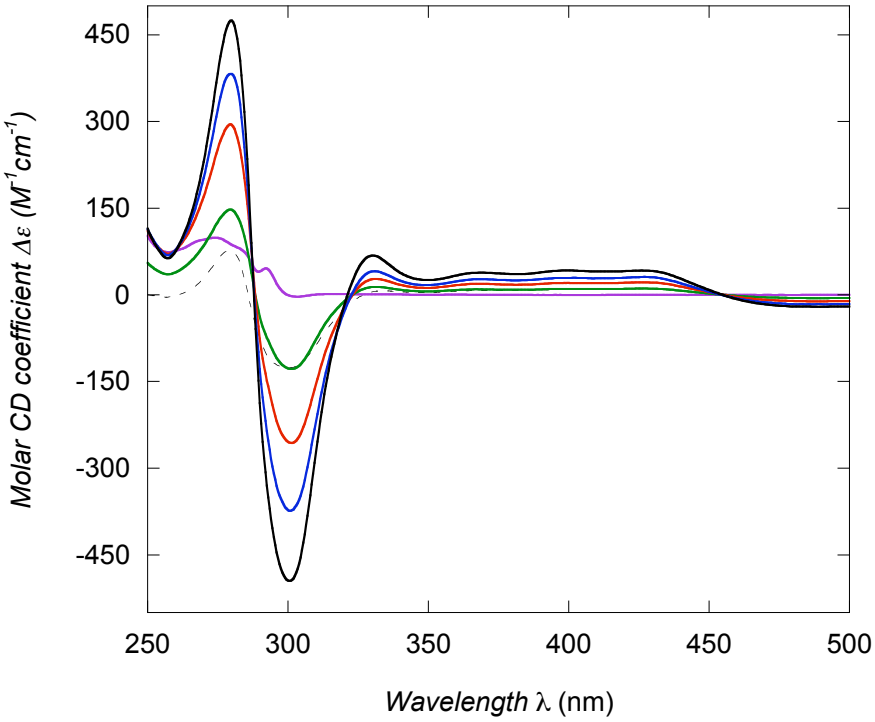

Figure 10. Fixed CD spectra used to generate the artificial data sets. For each absorbing species for (Δ-**1**)$_x$ $\subset$ streptavidin. x = 0: violet line, x = 1: green line, x = 2: red line, x = 3: blue line and x = 4: black solid line. The spectrum of Δ-**1** is displayed as a dotted black line.

A global analysis of the artificial data sets, first with the full model and then with the sub-model ignoring the formation of the minor mono-species, allow one to check the robustness of the minimization algorithm with increasing random noise.

Referring to these calculations, unbiased estimates of the four association constants in full agreement with the true values were computed as long as the noise level remained below 0.001%, although the concentration of Δ-**1** $\subset$ streptavidin does

not exceed 1.5% throughout the titration (Figure 11). With increasing noise level (~0.1%), the same refinement difficulties as those experienced for the real data were encountered, leading to exclude β_1 from the model.

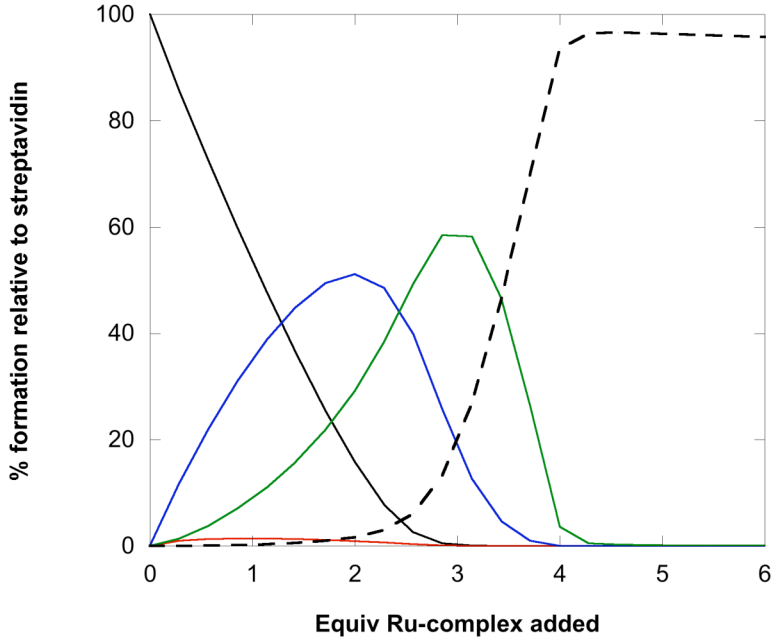

Figure 11. Species distribution diagram calculated for the above mentioned conditions (For each absorbing species for $(\Delta\text{-}[Ru(bpy)_2(Biot\text{-}bpy)]^{2+})_x \subset$ streptavidin ($(\Delta\text{-}\mathbf{1})_x \subset$ streptavidin). $x = 0$: black solid line, $x = 1$:red line, $x = 2$: blue line, $x = 3$: green line and $x = 4$: black dotted line. The fraction of the $(\Delta\text{-}\mathbf{1}) \subset$ streptavidin species does not exceed 1.5%.

Interestingly, the most important outcome was obtained when the simulated data were analyzed with the incomplete model. As long as the spectral contribution is significantly greater than the random noise level, a sizeable but approximately constant bias close to 0.25 logarithmic units affects the refined β_2, β_3, and β_4 equilibrium constants, while the visual examination of the residual plot evidences systematic trends. More surprisingly, the deviation of the parameter estimates from their nominal values become larger and larger as the noise level increases and the contribution of the minor species is vanishing in the spectral background. Unpredictable errors that could be larger than one order of magnitude were obtained

for the noisiest data sets (0.1% random noise), while the residues were approximately randomly distributed around zero.

Table 4. Influence of the random noise level on the association constant values refined either for the complete (equilibrium 1 to 4) or partial (equilibrium 2 to 4) models[a]

Noise level	0%	0.001%	0.01%	0.1%	0.2%	0.5%
Nb. of factors	5	5	5	4	4	3
			4 equilibrium model			
$\log \beta_1$	8.002(3)	8.01(3)	8.2(2)	8.2(8)	< 0 [b]	<0 [b]
$\log \beta_2$	19.0000(5)	19.000(5)	19.00(5)	19.1(3)	18.7(4)	20(1)
$\log \beta_3$	28.0000(7)	28.000(7)	28.00(7)	28.2(4)	27.7(5)	30(1)
$\log \beta_4$	36.0000(9)	36.000(9)	36.00(8)	36.2(5)	35.7(5)	38(1)
σ	2.337×10^{-5}	2.286×10^{-4}	2.27×10^{-3}	2.207×10^{-2}	2.843×10^{-2}	1.1×10^{-1}
$\Delta\theta_{min/max}$ (m°)	$\pm 2.3 \times 10^{-4}$ [c]	$\pm 2.3 \times 10^{-3}$ [c]	$\pm 2.3 \times 10^{-2}$ [c]	$\pm 2 \times 10^{-1}$ [c]	$\pm 5 \times 10^{-1}$ [c]	± 1 [c]
			3 equilibrium model			
$\log \beta_2$	19.2(1)	19.2(2)	19.2(2)	19.2(4)	19.2(4)	21(1)
$\log \beta_3$	28.2(2)	28.2(2)	28.2(2)	28.3(5)	28.2(5)	30(1)
$\log \beta_4$	36.2(2)	36.2(2)	36.2(2)	36.3(5)	36.3(6)	39(1)
σ	7.240×10^{-3}	7.363×10^{-3}	7.837×10^{-3}	2.431×10^{-2}	2.972×10^{-2}	1.157×10^{-2}
$\Delta\theta_{min/max}$ (m°)	–0.03/0.075 [d]	–0.03/0.075 [d]	–0.03/0.075 [d]	$\pm 2 \times 10^{-1}$ [c]	$\pm 5 \times 10^{-1}$ [c]	± 1 [c]

[a] σ : residual standard deviation; $\Delta\theta_{min/max}$: range of the residual ellipticities expressed in millidegrees. [b] The refinement procedure converges but β_1 is poorly defined and becomes negative (multiple minima). The calculated spectra become unrealistic although the estimates of β_2–β_4 are well defined and unique. [c] The residues are randomly distributed around zero. [d] The plot of residues shows systematic trends.

Pertinent results of the singular value decomposition (number of significant eigenvalues) and subsequent nonlinear least-squares refinement of the artificial data sets to which a constant noise level has been superimposed, are summarized in Table 4. As can be seen in Table 3 and Table 4, if the standard error in the ellipticity measurements is within < 0.1%, as it is the case in all experiments carried out in the present work, it is then safe to trust that the maximal concentration of mono-adduct (Δ-**1** or Λ-**1**) $\subset$ (strept)avidin does not exceed 4% during the entire titration. Most importantly, this higher limit is a sufficient criterion to assess the cooperative

formation of the bis-biotinylated adduct (Δ-**1** or Λ-**1**)$_2$ ⊂ (strept)avidin starting from the apo-protein.

It has therefore to be concluded that the occurrence of the minor species throughout a single titration results not only in poorly defined spectra and equilibrium constants for those species, but more importantly, the entire global nonlinear least squares analysis fails to produce reliable precise estimates of the unknown parameters corresponding to the major species. The effective rank deficiency evidenced by the singular value decomposition is a direct consequence of the unavoidable experimental noise. Thus, the values reported in Table 3 that pertain to the analysis of the experimental CD spectra with only three equilibria, should be considered as approximate and spoilt by systematic errors at least as large as the standard errors returned by the Marquardt procedure (bias about 0.25 logartihmic units affects the refined β_2, β_3 and β_4). On the basis of this observation, the formation of the bis-species occurs with strong cooperativity, precluding the determination of the first binding constant K_1.

As comparison between host-proteins- streptavidin and avidin, in terms of binding constants: an enhanced overall stability constant when streptavidin is employed as the host protein. We reasoned that this may be due to Coulomb/repulsion interactions of streptavidin (pI = 6.4). Moreover, since streptavidin has a deeper binding pocket compared to avidin, this cavity seems to facilitate stabilizing the conformation of the complexes in the biotin binding pockets. Interestingly, in terms of chiral discrimination, avidin displays a modest preference for Λ-**1**, while streptavidin binds nearly indiscriminately both Δ-**1** and Λ-**1**. Considering the large standard deviations, this last conclusion is subject to caution however.

Having investigated the discrimination of biotinylated coordination compounds upon incorporation within (strept)avidin, in the next chapter we will present the application of biotin-avidin technology in the area of artificial metalloenzymes.

APPLICATION OF BIOTIN-AVIDIN TECHNOLOGY IN THE DESIGN OF ARTIFICIAL HYDROGENASES: COMBINATORIAL APPROACH AND KINETIC STUDY

3.1. Introduction

Inspired by Whitesides' early report [27], our group has demonstrated that incorporation of a biotinylated-diphosphine Rh complex, embedded in the active site of either avidin or streptavidin can afford artificial hydrogenases [21, 22, 26, 152, 164-166]. The previous studies by Dr. A. Loosli [22, 156] revealed that incorporation of biotinylated-diphosphine Rh complex to (strept)avidin yields a quantitative incorporation guest ⊂ host (estimated binding constant is 10^7 M^{-1}). It is thus clear that the biotinylated compounds occupy the same binding pocket with a significantly reduced affinity as native biotin ($K_a = 10^{14}$ M^{-1}).

Despite all efforts (computer calculation, kinetic experiments, and so forth), nowadays it still remains difficult to predict the outcome of a metal-catalyzed enantioselective reaction. As described by Knowles [167]:

"*Since achieving 95 % ee only involves energy differences of about 2 kcal, which is no more than the barrier encountered in a simple rotation of ethane, it is unlikely that before the fact one can predict what kind of ligand structures will be effective*".

To get round the difficulty of predicting enantioselectivity, asymmetric catalysis relies more and more on combinatorial approach to optimize the selectivity of new catalysts. With the same spirit, our group relies by both chemical and genetic strategies. Chemical optimization consists in varying the spacer (length, achiral/enantiopure, aliphatic/arylic) between a biotin anchor and a diphosphine moiety, whereas the genetic optimization relies on modifying the amino acid residues responsible for the interaction with the metal catalyst.

Initial studies focused on a chemogenetic optimization relying on the design of achiral amino acid spacers-ligand and saturation mutagenesis in position S112X. It was shown that the ligand scaffold plays a critical role on the performance of the resulting artificial hydrogenases [21]. In addition, the reaction conditions such as: solvent, counter ion, added salts, have a significant and unpredictable influence on the enantioselectivity [168]. These weak interactions between catalyst and its non-bonded environment are commonly referred to second coordination sphere interactions [21].

General trends obtained from the previous studies are as follows: combination of achiral spacer and twenty streptavidin isoforms revealed that chemical optimization creates more diversity than genetic counterpart (**Table 5**, entry 1-7) [165]. Introduction of enantiopure spacer (natural α-amino acids) in combination with WT streptavidin resulted artificial hydrogenases with increased organic solvent tolerance and improved (*S*)-selectivity (**Table 5**, entry 11-13) [22]. The selected results from initial studies are collected in **Table 5**.

Table 5. Numerical summary of previous results of catalytic experiments using artificial hydrogenases.

Entry	Ligand	Protein	ee[a] *N*-AcPhe	Conv. *N*-AcPhe	ee[a] *N*-AcAla	Conv. *N*-AcAla
1[c]	**Biot-1**	WT Sav	93	84	94	quant. [b]
2[c]	**Biot-1**	S112A	94	94	93	quant. [b]
3[c]	**Biot-1**	S112G	94	77	93	quant. [b]
4[c]	**Biot-4^{meta}-1**	S112K	-88	89	-63	quant. [b]
5[c]	**Biot-4^{meta}-1**	S112R	-86	71	-63	quant. [b]
6[c]	**Biot-3^{1}-2**	S112Y	-42	10	-55	quant. [b]
7[c]	**Biot-3^{4}-2**	S112Q	92	77	87	quant. [b]

8[d]	**Biot-(*R*)-Phe-1**	WT Sav	64	quant. [b]	66	quant. [b]
9[d]	**Biot-(*S*)-Phe-1**	WT Sav	-64	88	-73	quant. [b]
10[d]	**Biot-(*S*)-Pro-1**	WT Sav	23	quant. [b]	23	quant. [b]
11[d]	**Biot-(*R*)-Pro-1**	WT Sav	-91	quant. [b]	-86	quant. [b]
12[d]	**Biot-(*R*)-Pro-1** (45%DMSO)	WT Sav	-86	94	-87	quant. [b]
13[d]	**Biot-(*R*)-Pro-1** (biphasic EtOAc)	WT Sav	-87	85	-86	90

[a]ee in %, positive ee values in favor of the (*R*)-enantiomer, negative ee values in favor of the (*S*)-enantiomer; [b]quantitative; [c]according reference [165]; [d]according reference [22]; *N*-AcPhe = *N*-acetamidophenylalanine, *N*-AcAla = *N*-acetamidoalanine.

The next section of this chapter highlights the chemogenetic optimizations of the second generation of artificial hydrogenases using biotin-avidin technology. The chemogenetic optimization is divided into two strategies: combination of chiral spacers with saturation mutagenesis in position S112X and combination of both chiral and achiral spacers with single/double point mutation. The design of the new class of ligands using non-natural α-amino acids will be described as well as the results of catalytic experiments. This new class of ligands has proven to be highly tolerant towards organic solvents. The results of enantioselective hydrogenation using immobilized artificial hydrogenases will be presented and followed by a detailed kinetic study using Michaelis-Menten model.

3.2. Chemo-Genetic optimization

In the preliminary study, Dr. Myriem Skander [22, 168] had identified that the introduction of natural α-amino acids as spacer displays some interesting features:

protein free precursors afforded little enantioselectivity (ee < 10%) and high tolerance towards organic solvents (up to 45% organic solvent content). Proline and phenylalanine were selected for this purpose. We reasoned that the phenylalanine spacer may display stabilizing π-π stacking effects upon interaction with the hydrophobic (strept)avidin binding pockets, which possess four of five aromatic residues for streptavidin and avidin, respectively.

The studies presented herein focus on incorporation of enantiopure amino acid spacers (natural and non-natural). For screening purposes, the standard enamides for enantioselective hydrogenation were selected. A general scheme is presented in **Scheme 34**.

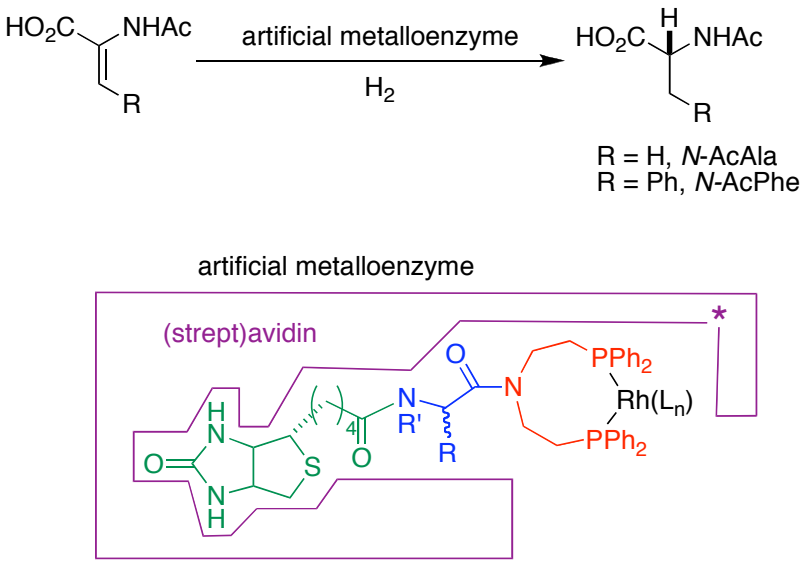

Scheme 34. Second-generation artificial hydrogenases based on the biotin-avidin technology for the reduction of N-acetamido dehydroaminoacids. The host protein ((strept)avidin, violet) displays high affinity for the anchor (biotin green); introduction of an enantiopure α-aminoacid spacer (blue), combined with a flexible diphosphine ligand (red) allows to chemically optimize both the activity and the selectivity. Site-directed mutagenesis further enables a genetic optimization of the host protein to afford enantioselective artificial hydrogenases.

3.2.1. Saturation mutagenesis at position S112X combined with enantiopure α-aminoacid spacers

On the basis of docking studies, it was found that position S112 is situated in proximity of the metal center (for systems bearing a short spacer). It was thus interesting to perform saturation mutagenesis at this position affording twenty streptavidin isoforms. Furthermore, as introduction of proline and phenylalanine residues displayed interesting features, we proceeded to screen other enantiopure α-amino acid spacers. As proline spacer afforded the highest (*S*)-selectivity, a proline analog was then chosen as spacer in order to investigate the role of the ring size in catalytic performance. For this purpose, we chose a pipecolinic acid as "expanded" proline. In addition, glutamic acid 5-benzyl ester was chosen because it bears different properties compared to previously studied amino acids, proline and phenylalanine, spacers. The synthetic pathway for preparation of these new ligands was very similar to the previous ones (the detailed synthetical pathways are presented in Chapter 5).

The performance of the extended chiral spacer ligands in the absence of the (strept)avidin was tested first. In all cases, the control experiments revealed that the ee for the reduction product did not exceed 10% (**Table 6**, entries 12-13). The structure of the ligands and typical reaction conditions are displayed in **Scheme 35**.

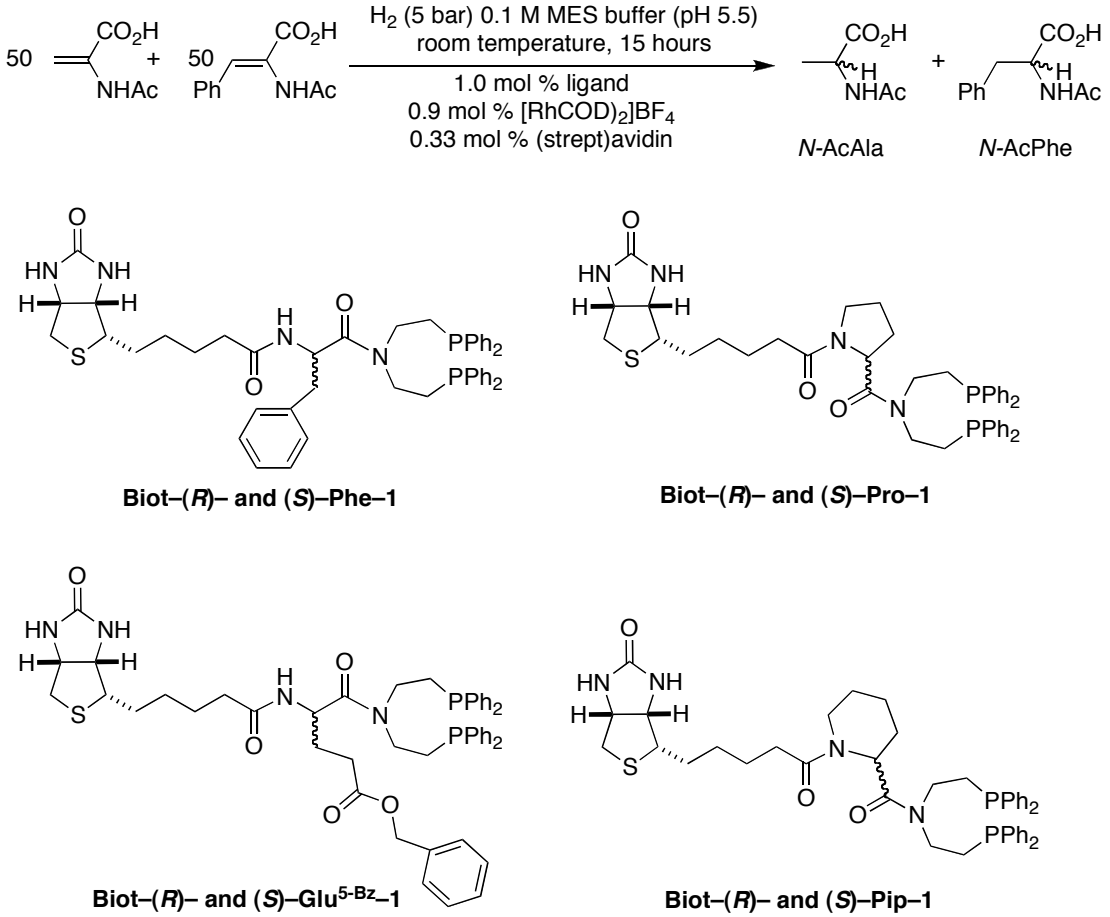

Scheme 35. Structure of biotinylated ligands and standard operating conditions for the hydrogenation of a cocktail mixture containing α-acetamidoacrylic acid and α-acetamidocinnamic acid (50 equivalents of each with respect to the biotinylated ligand).

The results of the hydrogenation using eight chiral-spacer ligands and twenty isoforms of streptavidin are collected and presented in fingerprint display allowing rapid identification of the trends (**Scheme 36**). The results of catalytic experiments using single and double point mutations will be discussed in section 3.2.2.

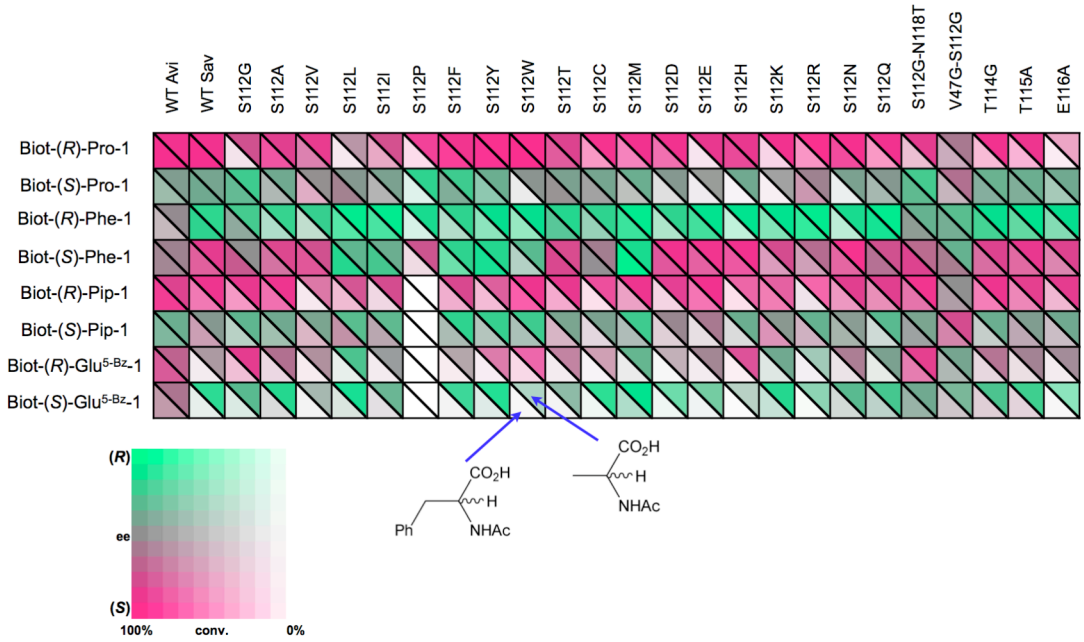

Scheme 36. Fingerprint display of the results for the chemogenetic optimization of α-acetamidoacrylic acid (top triangle) and α-acetamidocinnamic acid (bottom triangle). Combination S112P with **Biot-(*R*)-Pip-1**, **Biot-(*S*)-Pip-1**, **Biot-(*R*)-Glu$^{5\text{-Bz}}$-1** and **Biot-(*S*)-Glu$^{5\text{-Bz}}$-1** was not tested.

Inspection of the fingerprint reveals several interesting trends.

- The absolute configuration of the aminoacid spacer by-and-large determines the absolute configuration of the reduction product: **Biot–(*R*)-Pro–1** and **Biot-(*R*)-Pip-1** strongly favor formation of (*S*)-reduction products, while **Biot–(*S*)-Pro–1** and **Biot–(*R*)-Phe–1** produce preferentially (*R*)-reduction products, **Biot–(*S*)-Pro–1** produces moderate selectivities (10-30% ee). Interestingly, **Biot–(*S*)-Phe–1**, **Biot-(*S*)-Glu$^{5\text{-Bz}}$-1**, **Biot-(*R*)-Glu$^{5\text{-Bz}}$-1**, and **Biot-(*S*)-Pip-1** give more diversity (**Figure 12**), the reduction products vary from high (*S*)-enantiomer to (*R*)-enantiomer depending on the streptavidin isoform.
- Compared to the phenylalanine and proline linkers, the introduction of pipecolinic acid and glutamic acid 5-benzyl ester residues afforded substrate selective artificial hydrogenase (high activity towards smaller substrate). For example, combination of **Biot-(*S*)-Glu$^{5\text{-Bz}}$-1** and Sav S112C yielded 33% (*R*) and 12% conversion for *N*-

AcPhe, whereas 72% (*R*) and 96% conversion for *N*-AcAla (**Table 6**, entry 17 and 23). This trend has been observed in the catalytic results of the first generation of artificial hydrogenases (using achiral spacers) [165].

Interestingly, some catalytic results show that incorporation of ligands in avidin competes with the results obtained with WT sav, which in general performs best (**Table 6**, entry 14 vs. 16 and entry 15 vs. 17).

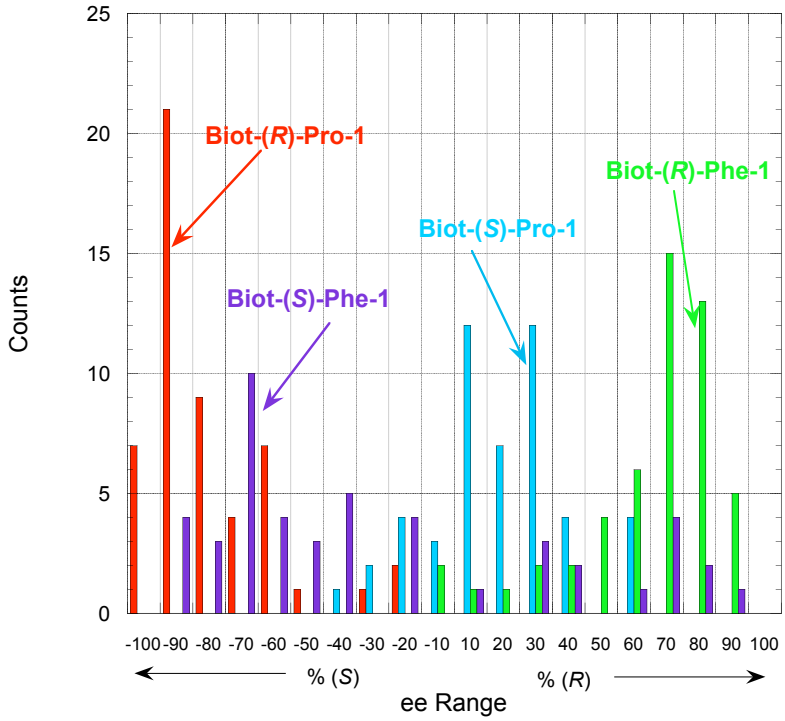

Figure 12. Enantioselectivity histogram as a function of chemical component in the presence of twenty streptavidin isoforms (catalytic results combining mutation in position 112, 114-116 and double point mutations are included).

- Combining **Biot–(*R*)-Pro–1** with Sav mutants bearing aromatic residues at position S112X (S112W and S112Y) affords the most (*S*)-selective artificial hydrogenases (up to 95% ee for both substrates, **Table 6**, entries 3-4).

- The hybrid catalysts derived from **Biot–(*S*)-Phe–1** afford both (*R*)- and (*S*)-reduction products. For example, [Rh(COD)**Biot–(*S*)-Phe–1**]$^+$ ⊂ Sav S112M and [Rh(COD)**Biot–(*S*)-Phe–1**]$^+$ ⊂ Sav S112H yield quantitatively *N*-AcPhe in 88% ee

(*R*) and 79% ee (*S*) respectively (**Scheme 37**, and **Table 6**, entries 10-11). For a single mutation, this represents a difference in transition state free energy $\Delta\Delta G^{\ddagger} > 2.6$ kcal·mol^{-1} at room temperature. Irrespective of the absolute configuration of the phenylalanine spacer, hybrid catalysts derived from S112F, S112L, S112M, S112W and S112Y streptavidin mutants afford preferentially the same enantiomer.

- Both [Rh(COD)**Biot–(*R*)-Phe–1**]$^+$ ⊂ Sav S112M and [Rh(COD)**Biot–(*S*)-Phe–1**]$^+$ ⊂ Sav S112M yield quantitatively (*R*)-*N*-AcAla in 86% ee and 73% ee respectively (**Table 6**, entries 7 and 11). We speculate that the presence of a bulky residue at position S112 outrules the preference imposed by the enantiopure Phe-spacer. This may be achieved either by inverting the preferred enantioenriched ligand conformation or by forcing the prochiral substrate to present its *si*-face to the biotinylated catalyst.

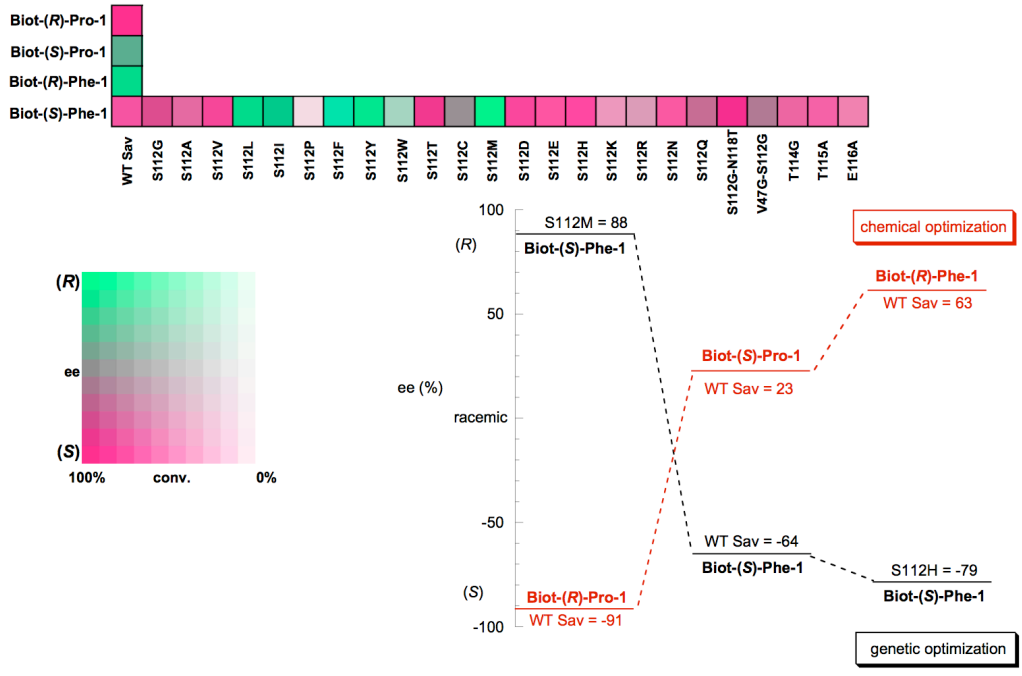

Scheme 37. Reduction of α-acetamidocinnamic acid using WT Sav as starting point, combined with **Biot-(*R*)-Pro-1** affording 91% ee (*S*) that can be fine-tuned to 63 % ee (*R*) upon combination with **Biot-(*R*)-Phe-1** (red diagram). Genetic optimization yielded high diversity ranging from 79% ee (*S*) to 88% ee (*R*) using the same vector **Biot-(*S*)-Phe-1** (black diagram). Inset: Fingerprint display of the results for the chemogenetic optimization.

- Both substrates afford comparable enantioselectivities. However, slightly better conversions are generally obtained for the smaller product *N*-AcAla. Significant substrate discriminations are found for catalysts derived from **Biot–(*R*)-Pro–1**. For example, [Rh(COD)**Biot–(*R*)-Pro–1**]$^+$ ⊂ Sav S112K affords quantitatively (*S*)-*N*-AcAla (88% ee), while the conversion for the larger (*S*)-*N*-AcPhe remains modest (36% conversion, 84% ee, **Table 6**, entry 2).
- Regardless the configuration of enantiopure amino acid, the introduction of glutamic acid as spacer afforded substrate specific artificial hydrogenases (**Table 6**, entries 17, 21-23), compared to the others spacers (phenylalanine, proline, and pipecolinic acid).
- Combining **Biot–(*R*)-Pro–1** with WT Avi affords, for the first time, good levels of enantioselection (89% ee for *N*-AcPhe quantitative conversion, **Table 6** entry 1). This may be of interest for future developments as WT Avi is significantly cheaper than WT Sav.

Table 6. Numerical summary of selected results of the catalytic experiments using second-generation artificial hydrogenases.

Entry	Ligand	Protein	ee[a] *N*-AcPhe	Conv. *N*-AcPhe	ee[a] *N*-AcAla	Conv. *N*-AcAla
1[c]	**Biot–(*R*)-Pro–1**	WT Avi	-89	quant.[b]	-87	quant.[b]
2	**Biot–(*R*)-Pro–1**	S112K	-84	36	-88	quant.[b]
3	**Biot–(*R*)-Pro–1**	S112W	-95	quant.[b]	-95	quant.[b]
4	**Biot–(*R*)-Pro–1**	S112Y	-93	97	-92	quant.[b]
5	**Biot–(*R*)-Phe–1**	S112I	74	80	84	quant.[b]
6	**Biot–(*R*)-Phe–1**	S112L	74	88	83	quant.[b]
7	**Biot–(*R*)-Phe–1**	S112M	75	94	86	quant.[b]

8	**Biot–(*R*)-Phe–1**	S112Q	76	82	81	quant.[b]
9	**Biot–(*R*)-Phe–1**	S112R	82	75	84	quant.[b]
10	**Biot–(*S*)-Phe–1**	S112H	-78	65	-87	quant.[b]
11	**Biot–(*S*)-Phe–1**	S112M	87	quant.[b]	73	quant.[b]
12	**Biot–(*R*)-Pip–1**		-4	80	-8	quant.[b]
13	**Biot–(*R*)-Glu$^{5\text{-Bz}}$–1**		-9	28	-7	quant.[b]
14	**Biot–(*R*)-Pip–1**	WT Avi	-85	96	-68	quant.[b]
15	**Biot–(*R*)-Glu$^{5\text{-Bz}}$–1**	WT Avi	-60	92	-38	quant.[b]
16	**Biot–(*R*)-Pip–1**	WT Sav	-82	69	-81	quant.[b]
17	**Biot–(*R*)-Glu$^{5\text{-Bz}}$–1**	WT Sav	-30	15	-11	86
18	**Biot–(*R*)-Pip–1**	S112W	-90	78	-82	quant.[b]
19	**Biot–(*R*)-Pip–1**	S112E	-86	69	-87	quant.[b]
20	**Biot–(*S*)-Pip–1**	S112F	11	69	64	quant.[b]
21	**Biot–(*R*)-Glu$^{5\text{-Bz}}$–1**	S112W	-70	22	-78	78
22	**Biot–(*S*)-Glu$^{5\text{-Bz}}$–1**	S112M	41	51	79	quant.[b]
23	**Biot–(*S*)-Glu$^{5\text{-Bz}}$–1**	S112C	33	12	72	96
24	**Biot–(*S*)-Glu$^{5\text{-Bz}}$–1**	S112L	-28	79	41	quant.[b]

[a]ee in %, positive ee values in favor of the (*R*)-enantiomer, negative ee values in favor of the (*S*)-enantiomer; [b]quantitative; all listed experiments were performed at least in duplicate (see Supporting Information); [c]according reference [168]; *N*-AcPhe = *N*-acetamidophenylalanine, *N*-AcAla = *N*-acetamidoalanine.

3.2.2. Single point mutation (at position 114, 115 and 116) & double point mutation

To elucidate the role of the proximal amino acid residues in the binding pocket of (strept)avidin, we performed a docking study to determine the closest amino acid residues around metal center responsible to perturb the interaction of the metal center with binding pocket environment. The docking studies suggest that position 114, 115,

and 116, which is situated in loop 7 and 8 of streptavidin could be potentially interesting to be modified. For this purpose, in position 114, we have introduced glycine instead of threonine, in position 115, we have replaced threonine by alanine and in position 116, alanine replaced glutamic acid. The position 114, 115 and 116 in loop 7 and 8 of monomeric streptavidin is depicted in **Scheme 38**.

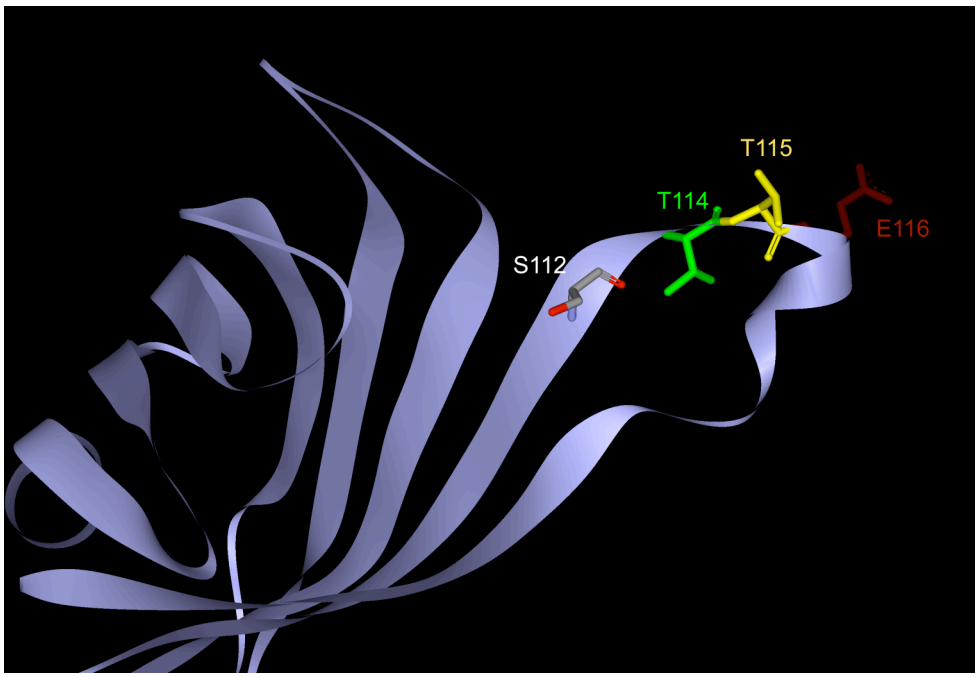

Scheme 38. Structure of monomeric streptavidin with highlighted position of mutation in position 114 (green), 115 (yellow) and 116 (red).

3.2.2.1. Combination with achiral spacer

The first attempt was to attach the first generation of artificial hydrogenases within the modified host protein. Two ligand scaffolds, **Biot-1** and **Biot-2** were used in this preliminary test. A cocktail mixture of α-acetamidoacrylic acid and α-acetamidocinnamic acid was used. The detailed operating conditions, together with the structure of the ligands used, are depicted in **Scheme 39**.

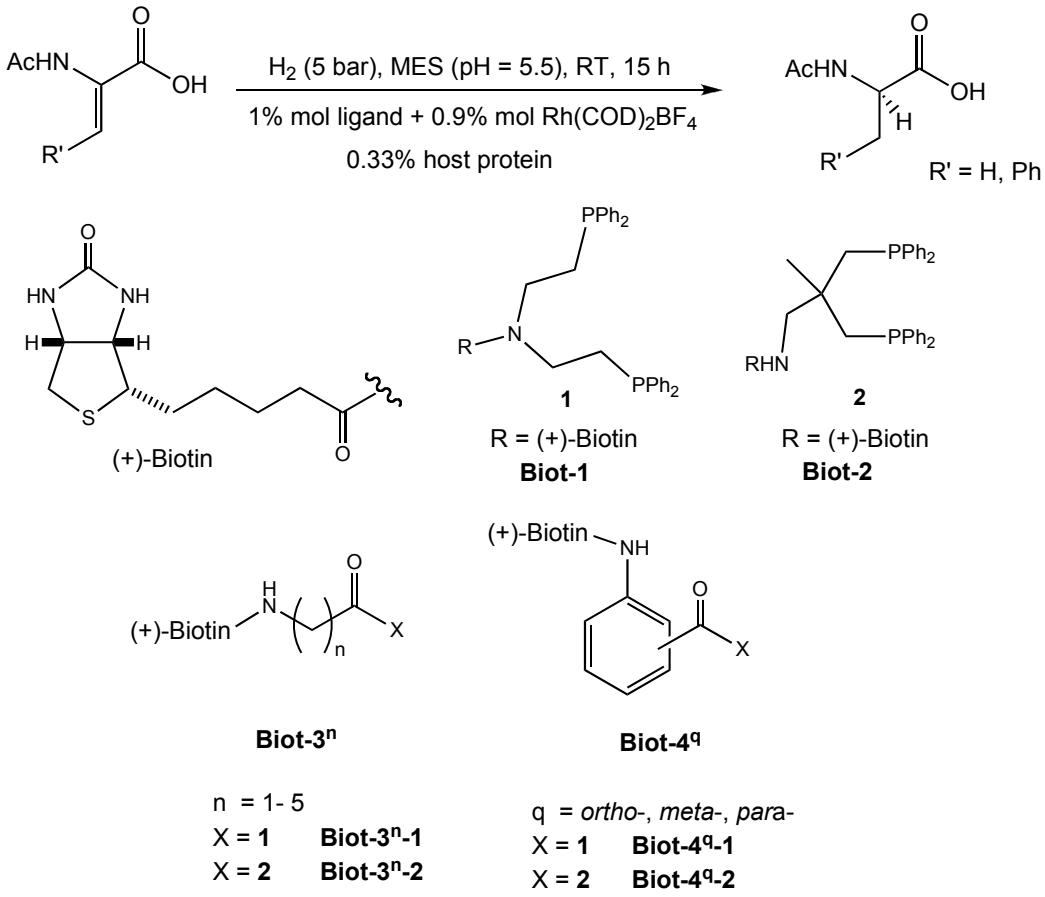

Scheme 39. Achiral biotinylated ligands used in this study and standard operating conditions for the hydrogenation of a cocktail mixture containing α-acetamidoacrylic acid and α-acetamidocinnamic acid (50 equivalents of each with respect to the biotinylated ligand).

The results of the catalytic run were collected and compiled in the fingerprint presentation as depicted in **Scheme 40**.

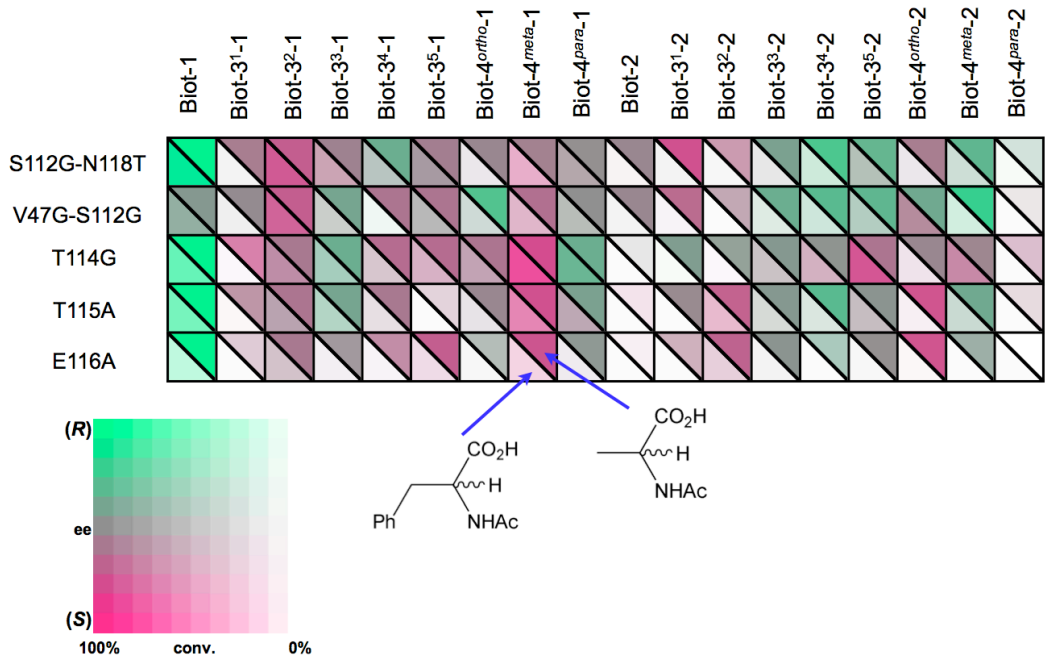

Scheme 40. Fingerprint display of the results of the chemogenetic optimization of α-acetamidoacrylic acid (top triangle) and α-acetamidocinnamic acid (bottom triangle) using achiral spacer ligands and single point mutation in position 114-116 and dual point mutations.

Scheme 40 suggests that ligand scaffold 1 outperforms ligand scaffold 2. In principle, the smaller substrate, α-acetamidoacrylic acid was hydrogenated with better performance compared to the bulky one, α-acetamidoncinammic acid. It is known that in the enantioselective homogeneous hydrogenation of enamide with cationic rhodium complexes, that increasing substitution in alkene part drive to a direct and negative effect on the performance of the catalyst. Although similarity of the substrates displaying a real steric difference, due to the presence of the phenyl ring on the prochiral C=C double bond of α-acetamidocinammic acid. Steric interactions within the binding pocket of (strept)avidin are therefore unavoidable, thus the smaller substrate may have better access to the cavity of the binding pocket of (strept)avidin than more bulky substrate α-acetamidocinnamic acid.

Mutation of amino acids in two different positions displayed an advantage to finely tune the reduction product of hydrogenation. For example, using **Biot-3^{1}-2** as ligand, in combination with S112G-N118T afforded 54% (*S*) reduction product, whereas 59% (*R*) reduction product was obtained upon combination with V47G-S112G (**Table 7**, entry 4 and 8). It is noteworthy that for some combinations, double points mutations does not seem to influence the inversion of reduction product (**Table 7**, entries 2-3, 6-7).

In the case of single point mutation in position 114, 115 and 116, with exception in combination with **Biot-3^{5}-2** and **Biot-3^{1}-1**, all catalytic result yielded comparable values of enantioselectivity (**Table 7**, entries 10, 15, 20 and 12, 17, 22). However, a slightly lower enantioselectivity was observed when combining with mutation in position 116 (or 115), in comparison with mutation in position in position 114 (**Table 7**, entries 9, 14, 19 and 11, 16, 21).

3.2.2.2. Combination with chiral spacer

Having identified the outcome of interaction of the double point mutation and single point mutation at position 114, 115, and 116 with the achiral-spacer ligands, the next attempt was to combine these mutants with the chiral-spacer ligands in catalytic experiments. The results were collected and compiled in the fingerprint presentation and some interesting results were outlined in **Table 7**.

Based on **Scheme 35**, it is clear that enantioselectivity is determined by-and-large by spacer between biotin moiety and diphosphine anchor. Again, **Biot-(*R*)-Pro-1**, **Biot-(*S*)-Phe-1** and **Biot-(*R*)-Pip-1** favor the formation of (*S*)-reduction products, whereas **Biot-(*S*)-Pro-1**, **Biot-(*R*)-Phe-1** and **Biot-(*S*)-Glu$^{5\text{-Bz}}$-1** afforded preferentially (*R*)-reduction products.

Single point mutation in position 114, 115 and 116 yielded similar behavior upon incorporation with biotinylated complexes, this observation is valid especially in combination with chiral-spacer ligands (**Scheme 35** and **Table 7**, entries 24-26). Except for a lower conversion, the mutants T114G, T115A, and E116A react indiscriminately to afford the same enantioselectivity level.

Table 7. Numerical summary of selected results of the catalytic experiments: chemogenetic optimization in position 114, 115, and 116, and dual point mutations.

Entry	Ligand	Protein	ee[a] *N*-AcPhe	Conv. *N*-AcPhe	ee[a] *N*-AcAla	Conv. *N*-AcAla
1	**Biot–1**	S112G-N118T	86	93	94	quant.[b]
2	**Biot–3^{2}–1**	S112G-N118T	-53	97	-42	quant.[b]
3	**Biot–4^{meta}–1**	S112G-N118T	-54	49	-14	quant.[b]
4	**Biot–3^{1}–2**	S112G-N118T	-7	10	-54	quant.[b]
5	**Biot–1**	V47G-S112G	15	84	7	quant.[b]
6	**Biot–3^{2}–1**	V47G-S112G	-52	92	-44	quant.[b]
7	**Biot–4^{meta}–1**	V47G-S112G	-30	8	-33	quant.[b]
8	**Biot–3^{1}–2**	V47G-S112G	45	28	59	quant.[b]
9	**Biot–1**	T114G	93	67	94	quant.[b]
10	**Biot–3^{1}–1**	T114G	-56	4	-52	77
11	**Biot–4^{meta}–1**	T114G	-79	88	-59	quant.[b]
12	**Biot–3^{5}–2**	T114G	-59	96	-24	quant.[b]
13	**Biot–4^{ortho}–2**	T114G	-22	20	-8	quant.[b]
14	**Biot–1**	T115A	91	quant.[b]	94	quant.[b]
15	**Biot–3^{1}–1**	T115A	-27	5	-22	80
16	**Biot–4^{meta}–1**	T115A	-62	70	-55	quant.[b]
17	**Biot–3^{5}–2**	T115A	-8	56	4	quant.[b]
18	**Biot–4^{ortho}–2**	T115A	-29	10	-53	quant.[b]
19	**Biot–1**	E116A	91	29	93	quant.[b]

20	**Biot–3^{1}–1**	E116A	-40	3	-26	39
21	**Biot–4^{meta}–1**	E116A	-56	26	-52	quant.[b]
22	**Biot–3^{5}–2**	E116A	0	7	-2	quant.[b]
23	**Biot–4^{ortho}–2**	E116A	-24	5	-53	quant.[b]
24	**Biot-(*R*)-Pro-1**	T114G	-93	79	-94	quant.[b]
25	**Biot-(*R*)-Pro-1**	T115A	-93	68	-89	quant.[b]
26	**Biot-(*R*)-Pro-1**	E116A	-92	32	-86	87
27	**Biot-(*S*)-Pip-1**	V47G-S112G	-47	78	-60	quant. [b]

[a]ee in %, positive ee values in favor of the (*R*)-enantiomer, negative ee values in favor of the (*S*)-enantiomer; [b]quantitative; *N*-AcPhe = *N*-acetamidophenylalanine, *N*-AcAla = *N*-acetamidoalanine.

In summary and in comparison with previous studies relying on achiral spacers, the introduction of enantiopure spacers yields more (*S*)-selective artificial metalloenzymes (best result for the first generation 88% vs. 95% with second generation). In addition, the genetic optimization by saturation mutagenesis at position S112X Sav generates more diversity than previously observed with achiral spacers [165].

3.3. Substrate scope

In our attempt to broaden the substrate scope of artificial hydrogenases, the esters of protected amino acid substrates were used. The structure of these substrates is depicted in **Scheme 41** and the preliminary results of the enantioselective hydrogenations are compiled in **Table 8**.

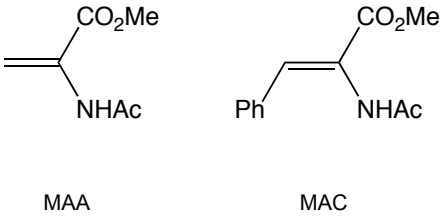

Scheme 41. Structure of MAA (methyl acetamidoacrylate) and MAC (methyl acetamidocinnamate).

Table 8. Numerical summary of selected results of the catalytic experiments using amino acid esters with the same conditions as catalytic experiments using acid as substrate.

Entry	Ligand	Protein	Substrate	Conv.	ee[a]
1	**Biot–1**	WT Sav	MAA	68	61
2	**Biot–1**	WT Sav	MAC	2	17
3	**Biot–(*R*)-Pro–1**	WT Sav	MAA	76	-17
4	**Biot–(*R*)-Pro–1**	WT Sav	MAC	10	-3
5	**Biot–(*R*)-Pro–1**	S112A	MAA	78	-22
6	**Biot–(*R*)-Pro–1**	S112E	MAA	28	-34
7	**Biot–(*R*)-Pro–1**	S112H	MAA	63	-20
8	**Biot–(*R*)-Pro–1**	S112I	MAA	88	-19
9	**Biot–(*R*)-Pro–1**	S112K	MAA	65	-26
10	**Biot–(*R*)-Pro–1**	S112M	MAA	85	-28
11	**Biot–(*R*)-Pro–1**	S112W	MAA	85	-28
12	**Biot–(*R*)-Pro–1**	S112W	MAC	85	-28
13	**Biot–(*S*)-Phe–1**	WT Sav	MAA	88	-39
14	**Biot–(*S*)-Phe–1**	WT Sav	MAC	13	-14
15	**Biot–(*S*)-Phe–1**	S112M	MAA	quant.[b]	8
16	**Biot–(*S*)-Phe–1**	S112M	MAC	22	2
17	**Biot–(*S*)-Phe–1**	S112H	MAA	88	-55
18	**Biot–(*S*)-Phe–1**	S112H	MAC	9	-31

[a]ee in %, positive ee values in favor of the (*R*)-enantiomer, negative ee values in favor of the (*S*)-enantiomer; [b]quantitative; MAA = methyl acetamidoacrylate; MAC = methyl acetamidocinnamate.

As can be appreciated from **Table 8**, the artificial hydrogenases yielded modest enantioselectivity (up to 61% (*R*) and 55% (*S*)) and low to moderate activity for the enantioselective hydrogenation of the esters compared to the corresponding acids. Recently, Reetz [169] reported asymmetric hydrogenation of methyl

acetamidoacrylate with [Rh(COD)(**Biot-1**)]$^+$ ⊂ WT Sav affording ee 23% (*R*). It is noteworthy that Reetz used slightly different condition (pH, substrate concentration, and so forth) for the reaction. In addition, Reetz focused his studies exclusively on the genetic optimization (saturation mutagenesis), the best ees obtained are 65% in favor of (*R*) in combination of **Biot-1** with N49V and 7% in favor of (*S*) in combination of **Biot-1** with N49H-L124F.

Another type of substrate *i.e.* ketopantolactone was tested for the first time for the reduction of C=O bond (shown in **Scheme 42**). For this purpose, the most versatile (*R*)- and (*S*)-selective artificial hydrogenases were selected and tested: [Rh(COD)(**Biot-1**)]$^+$ ⊂ WT Sav (highly (*R*)-selective) and [Rh(COD)(**Biot-(*R*)-Pro-1**)]$^+$ ⊂ S112W (highly (*S*)-selective). The preliminary study suggested that for the reduction of C=O bond, high pressure is required (P > 20 bar).

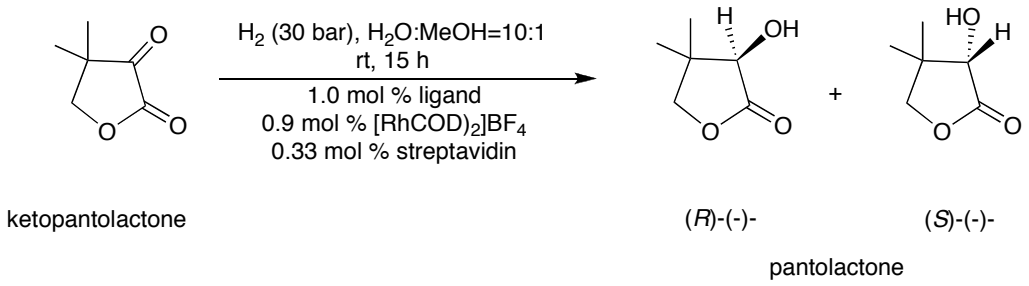

Scheme 42. Asymmetric hydrogenation of ketopantolactone using artificial hydrogenases generated from biotin-avidin technology.

The experimental results are collected in **Table 9**. From this preliminary study, it is interesting to note that artificial hydrogenases were little active and selective for the reduction of C=O bond. As control experiments, [Rh(COD)(**Biot-1**)]$^+$ in WT Sav and [Rh(COD)(**Biot-(*R*)-Pro-1**)]$^+$ in S112W were charged with standard substrates (α-acetamidoacrylic acid and α-acetamidocinnamic acid) and standard

conditions (S/C = 100, catalyst/protein = 3, Rh-complex dissolved in DMSO, except with P = 30 bar instead of 5 bar). The results revealed that **Biot-1** in WT Sav afforded a racemic mixture, whereas [Rh(COD)(**Biot-(*R*)-Pro-1**)]$^+$ in S112W was still highly selective, albeit with a slight decrease in enantioselectivity (total conversion and 86% ee (*S*) vs. total conversion and 95% (*S*) with P = 5 bar). This is the first time that the artificial hydrogenases generated from biotin-avidin interactions showed the high selectivity and activity under high-pressure dihydrogen [152].

Table 9. Numerical catalytic results of enantioselective hydrogenation of ketopentalactone

Entry	Ligand	Protein	Conv.	ee[a]
1	**Biot-1**	WT Sav	9	-2
2	**Biot–(*R*)-Pro–1**	WT Sav	18	-37
3	**Biot–(*R*)-Pro–1**	S112W	31	-61

[a]ee in %, positive ee values in favor of the (*R*)-enantiomer, negative ee values in favor of the (*S*)-enantiomer.

3.4. Organic solvent tolerance

Having identified both (*R*)- and (*S*)-selective (ee > 90%) artificial hydrogenases, we proceeded to test these artificial hydrogenases in the presence of large amounts of organic co-solvents. For this purpose, dimethylsulfoxide (DMSO, miscible with water) and ethylacetate (EtOAc, non-miscible with water) were selected. The results for the screening in the presence of the most selective catalyst ⊂ protein combinations are summarized in **Table 10**.

As can be appreciated from these data, the catalyst derived from **Biot–1** does not tolerate large amounts of either DMSO or EtOAc (**Table 10**, entries 1-2). Introduction of an enantiopure spacer confers significant organic-solvent tolerance in the presence of streptavidin and its mutants. Both (*S*)- and *(R*)-selective catalysts

[Rh(COD)**Biot–(*R*)-Pro–1**]$^+$ ⊂ Sav S112W and [Rh(COD)**Biot–(*S*)-Phe–1**]$^+$ ⊂ Sav S112M perform well in the presence of either 45% DMSO or EtOAc (maximal ee erosion 12%, **Table 10**, entries 12-13 and 15-16).

In contrast to streptavidin isoforms as host proteins, avidin-based artificial metalloenzymes perform poorly in the presence 45% DMSO (**Table 10**, entries 4-5 and 8-9). In the presence of either 27% DMSO or EtOAc, the erosion observed with [Rh(COD)**Biot–(*R*)-Pro–1**]$^+$ ⊂ WT-Avi is minimal (**Table 10**, entries 8 and 10). One of the main limitations of enantioselective catalysis performed in aqueous media is the very limited solubility of many substrates. The organic solvent tolerance should thus contribute to broaden the substrate scope of these artificial metalloenzymes.

The composition of solutions in the reaction mixture is illustrated in **Scheme 43** for both monophasic and biphasic systems.

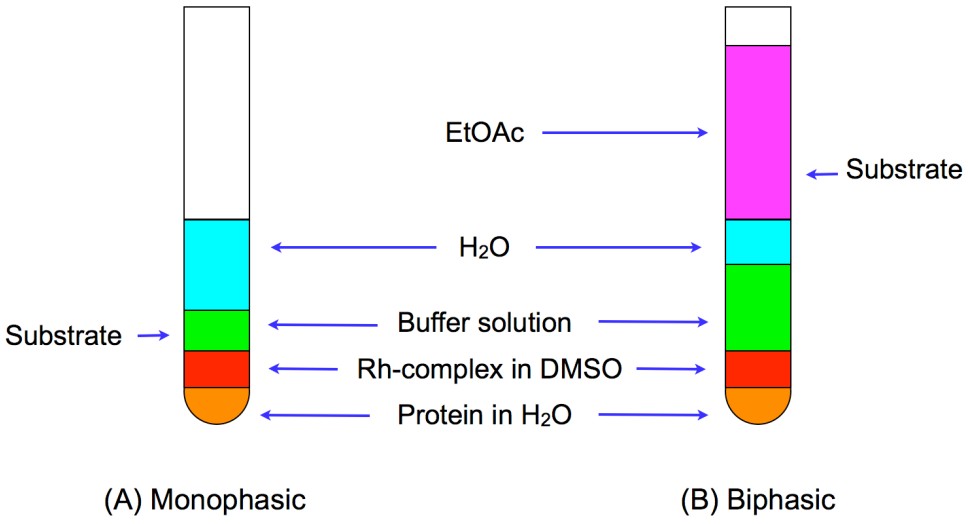

Scheme 43. Composition of solutions for monophasic (A) and biphasic (B) conditions in asymmetric hydrogenation.

3.5. Immobilization of artificial hydrogenases

In the past [152], Dr. J. Collot had shown that an artificial metalloenzyme's selectivity is little affected upon varying the ratio of [Rh(COD)(**Biot–1**)]$^+$ versus WT Sav between one and four, suggesting that the occupancy of one binding site does not significantly affect neighboring sites. As streptavidin is a homo-tetrameric protein, we speculated that it may be possible to exploit one binding site to immobilize the artificial metalloenzyme, leaving three sites for the incorporation of a biotinylated catalyst. A schematic flowchart of the preparation of immobilized catalysts is shown in **Scheme 44**. While **Scheme 45** illustrates the immobilization of Rh-complex using biotin-sepharose.

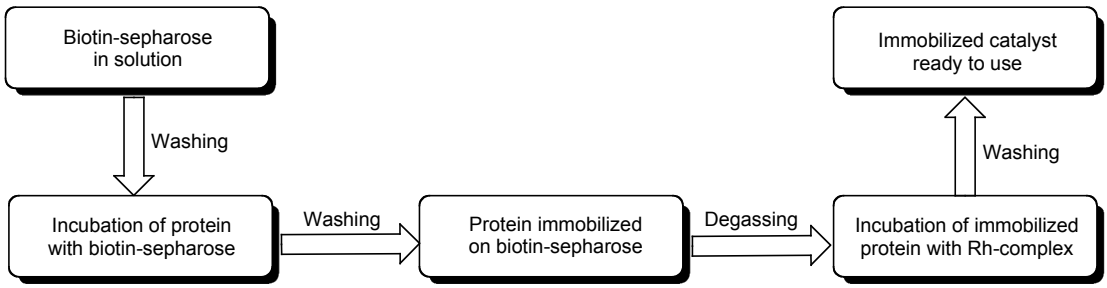

Scheme 44. Flowchart of preparation immobilized artificial hydrogenases using biotin-sepharose as solid support.

For this purpose, one equivalent of commercially available biotin-sepharose was added to tetrameric (strept)avidin prior to the addition of an excess biotinylated catalyst precursor (**Scheme 45**).

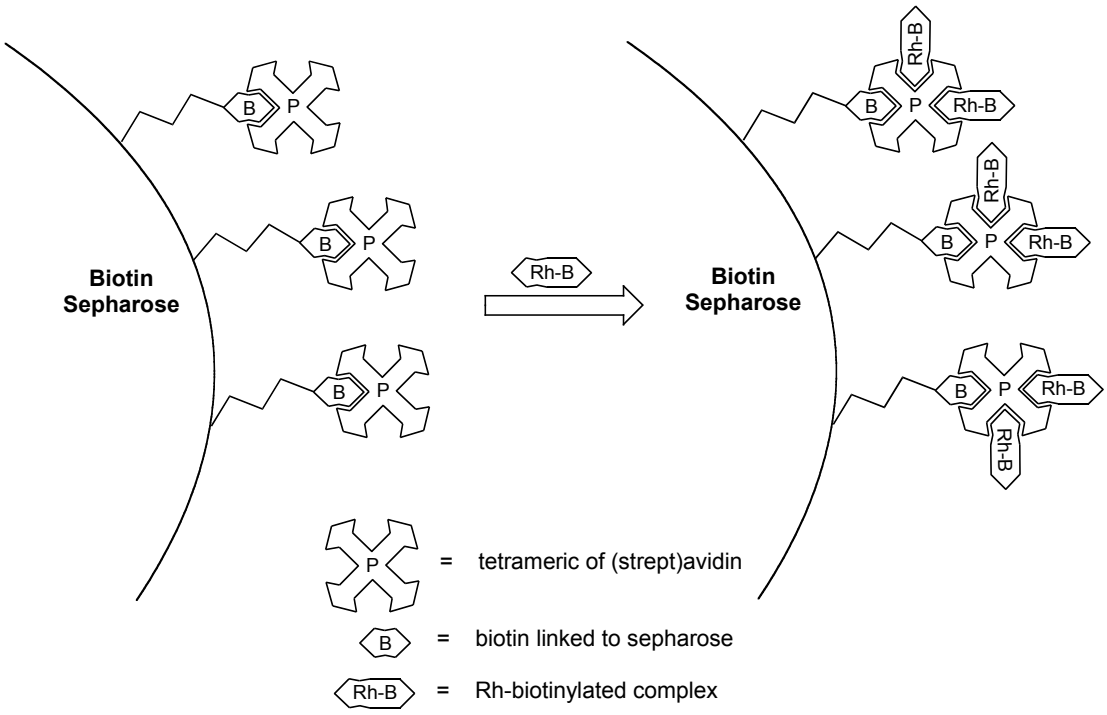

Scheme 45. Immobilization of a Rh-biotinylated complex using biotin-sepharose. One equivalent of biotin-sepharose binds a biotin-binding site of the host protein leaving up to three binding pockets for anchoring of the biotinylated pre-catalysts.

After decanting the immobilized catalyst precursors, thus removing the excess biotinylated rhodium and the unbound protein present in solution, these were tested using the standard reaction conditions. Selected results are collected in **Table 10**. As can be appreciated, the immobilized artificial metalloenzymes are most often nearly as selective as their homogeneous counterparts. However, the activity decreases, especially for the larger α-acetamidocinnamic acid substrate. The most versatile immobilized hybrid catalyst is [Rh(COD)**Biot–(*R*)-Pro–1**]$^+$ ⊂ Sav S112W which is as active and as selective as its homogeneous counterpart (compare **Table 5** entry 3 and **Table 10** entry 14).

Table 10. Numerical summary of selected results of the catalytic experiments performed in the presence of organic solvents or with immobilized artificial metalloenzymes.

Entry	Ligand	Protein	Organic solvent	ee[a] *N*-AcPhe	Conv. *N*-AcPhe	ee[a] *N*-AcAla	Conv. *N*-AcAla
1[b]	**Biot–1**	WT Sav	45 % DMSO	24	9	16	71
2[b]	**Biot–1**	WT Sav	EtOAc	31	5	30	56
3	**Biot–1**	WT Sav	Immob.[d]	93	78	83	quant.[c]
4	**Biot–(*R*)-Pro–1**	WT Sav	27 % DMSO	-91	100	-87	quant.[c]
5[b]	**Biot–(*R*)-Pro–1**	WT Sav	45 % DMSO	-86	94	-87	quant.[c]
6[b]	**Biot–(*R*)-Pro–1**	WT Sav	EtOAc	-87	85	-83	90
7	**Biot–(*R*)-Pro–1**	WT Sav	Immob.[d]	-89	36	-76	76
8	**Biot–(*R*)-Pro–1**	WT Avi	27 % DMSO	-82	94	-86	quant.[c]
9	**Biot–(*R*)-Pro–1**	WT Avi	45 % DMSO	-15	34	-37	quant.[c]
10	**Biot–(*R*)-Pro–1**	WT Avi	EtOAc	-89	77	-87	quant.[c]
11	**Biot–(*R*)-Pro–1**	WT Avi	Immob.[d]	-80	32	-76	quant.[c]
12	**Biot–(*R*)-Pro–1**	S112W	45 % DMSO	-88	56	-85	quant.[c]
13	**Biot–(*R*)-Pro–1**	S112W	EtOAc	-94	86	-94	quant.[c]
14	**Biot–(*R*)-Pro–1**	S112W	Immob.[d]	-94	89	-92	quant.[c]
15	**Biot–(*S*)-Phe–1**	S112M Sav	45 % DMSO	75	68	69	quant.[c]
16	**Biot–(*S*)-Phe–1**	S112M Sav	EtOAc	81	78	64	quant.[c]
17	**Biot–(*S*)-Phe–1**	S112M Sav	Immob.[d]	81	50	33	quant.[c]
18	**Biot–(*R*)-Pro–1**	T114G	Immob.[d]	-94	82	-89	quant.[c]
19	**Biot–1**	T114G	Immob.[d]	94	68	-88	quant.[c]
20	**Biot–3^2–2**	S112Q	Immob.[d]	89	79	72	quant.[c]

[a]ee in %, positive ee values in favor of the (*R*)-enantiomer, negative ee values in favor of the (*S*)-enantiomer; [b]according reference [22]; [c]quantitative; [d]Immobilized; *N*-AcPhe = *N*-acetamidophenylalanine, *N*-AcAla = *N*-acetamidoalanine.

As preliminary study to recover and re-use the immobilized catalysts, we have chosen the most versatile catalyst, [Rh(COD)**Biot–(*R*)-Pro–1**]$^+$ ⊂ Sav S112W system. By removing the reaction mixture at the end of reaction (after *ca*. 15 hours), the substrate solution with the same quantity as the first cycle (S/C = 100) was added into the immobilized catalyst to run the 2nd cycle of catalyst. We observed that the immobilized catalyst could be recovered and reused up to 1 additional catalytic cycle without decreasing significantly the enantioselectivity. For the combination of [Rh(COD)**Biot–(*R*)-Pro–1**]$^+$ ⊂ Sav S112W as catalyst, and α-acetamidocinnamic acid as substrate resulted: 94% (*S*) and quantitative conversion for the 1st cycle, then for the 2nd cycle 94% (*S*) and 81% conversion, 3rd cycle >30% (*S*) and >25% conversion.

To assess the tolerance towards organic solvents of the immobilized catalysts, we attempted to add the ratio of the organic solvent in solution and to run the reaction using the immobilized catalysts. The results are collected in **Table 10**.

Table 11. Numerical summary of selected results of the catalytic experiments using immobilized catayst (with [Rh(COD)**Biot–(*R*)-Pro–1**]$^+$) in the presence of organic solvents.

Entry	condition	Protein	ee[a] *N*-AcPhe	Conv. *N*-AcPhe	ee[a] *N*-AcAla	Conv. *N*-AcAla
1	10% DMSO	WT Avi	-80	32	-76	quant.[b]
2	45% DMSO	WT Avi	-40	12	-31	58
3	EtOAc biphasic	WT Avi	-77	10	-80	64
4	10% DMSO	WT Sav	-89	36	-76	76

5	45% DMSO	WT Sav	-50	14	-71	70
6	EtOAc biphasic	WT Sav	-70	3	-49	5
7	10% DMSO	S112W	-94	89	-92	quant.[b]
8	45% DMSO	S112W	-91	35	-91	96
9	EtOAc biphasic	S112W	-93	83	-94	quant.[b]
10	10% DMSO	T114G	-94	82	-89	quant.[b]
11	45% DMSO	T114G	-56	11	-76	84
12	EtOAc biphasic	T114G	-65	4	-76	13

[a]ee in %, positive ee values in favor of the (*R*)-enantiomer, negative ee values in favor of the (*S*)-enantiomer; [b]quantitative; *N*-AcPhe = *N*-acetamidophenylalanine, *N*-AcAla = *N*-acetamidoalanine.

Incorporation of [Rh(COD)**Biot–(*R*)-Pro–1**]$^+$ in S112W afforded a highly resistant and tolerant artificial hydrogenase towards organic solvent. In addition, its activity and selectivity remains stable upon immobilization with biotin-sepharose. This feature is promising for future studies.

3.6. Michaelis-Menten kinetics: determination of individual reaction rates

In preliminary report, our group has demonstrated that the host protein does not only responsible for inducing enantioselectivity but also for increasing the activity of the catalyst. This phenomenon is called "*protein accelerated catalyst*" [153]. With this spirit, we set out to quantify this phenomenon by determining the individual reaction rates.

For solubility reasons, only α-acetamidoacrylic acid was chosen as substrate. Michaelis-Menten model appeared to be an ideal model for this system. The kinetic data were collected at given time, by performing independent reactions with different initial concentration of substrate. The typical data are collected and compiled in **Table**

12 (the data set of the 3 other systems can be found in the supporting information in Chapter 5).

Table 12. Experimental kinetic data of [Rh(COD)(**Biot-1**)]$^+$ ⊂ WT Sav.

Concentration of substrate (mM)	Time (min)	Conv. (%) by GC	ν (mM.min^{-1})
0	0	0	0
2.83	2	8	0.113
3.96	3	11	0.145
5.09	3	9	0.153
5.65	5	15	0.170
11.30	5	9	0.203
16.95	10	12	0.203
28.25	10	8	0.226
33.90	10	7	0.237

It is noteworthy that only the rate of the reaction in the *pre-steady state* is taken into account in calculation. In order to obtain the kinetics parameters, an initial value, maximum rate and rate constant, are inserted into the Michaelis-Menten equations (equation 1 and 2) to allow non-linear least-squares minimization $(\nu_{calc} - \nu_{obs})^2 = \text{minimum}$.

$$\nu = \frac{V_{\max}[\mathrm{S}]}{K_M + [\mathrm{S}]} \quad (\mathbf{1}), \qquad \text{where: } V_{\max} = k_{cat}[\mathrm{E}]_0 \quad (\mathbf{2})$$

The initial rate was obtained by dividing the conversion (by GC) with time. The ee of the reduction products is constant during the course of the reaction. Moreover, no induction period or catalyst inhibition were observed during the course of the reaction. The comparison of calculated and measured values for the four observed systems is depicted in **Figure 13** as a Michaelis-Menten plot.

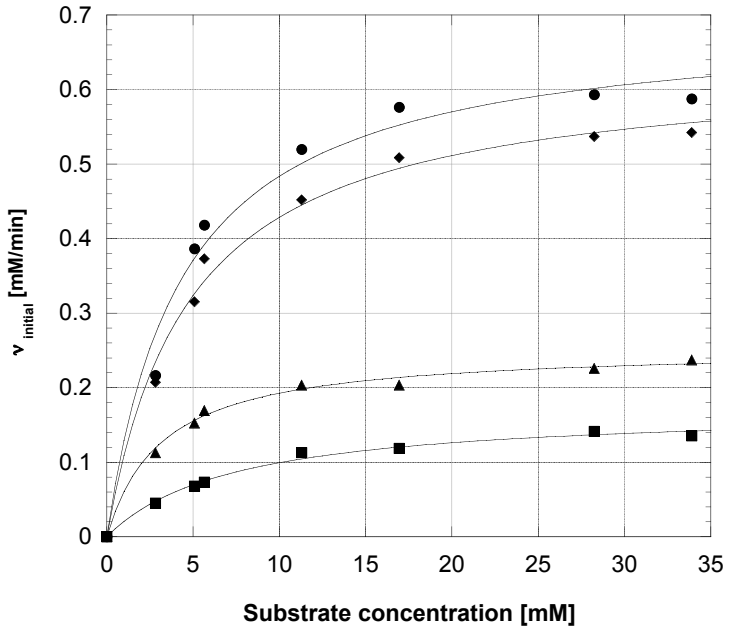

Figure 13. Michaelis-Menten plot for different systems: ● [Rh(COD)**Biot–(*R*)-Pro–1**]$^+$ ⊂ WT Sav ◆ [Rh(COD)**Biot–(*R*)-Pro–1**]$^+$ ⊂ WT Avi ▲ [Rh(COD)(**Biot–1**))]$^+$ ⊂ WT Sav ■ [Rh(COD)(**Biot–1**)]$^+$ free protein.

The calculated values (K_M and V_{max}) obtained from the iteration procedures are compiled in **Table 13**.

Table 13. Kinetics parameters derived from Michaelis-Menten equations.

entry	Ligand	Protein	V_{max} (mM.min^{-1})	k_{cat} (min^{-1})	K_M (mM)	k_{cat}/K_M (min.mM^{-1})
1	**Biot-1**	-	0.173	3.06	7.38	0.42
2	**Biot-1**	WT Sav	0.254	4.49	3.18	1.41
3	**Biot-(*R*)-Pro-1**	WT Sav	0.695	12.30	4.36	2.82
4	**Biot-(*R*)-Pro-1**	WT Avi	0.634	11.23	4.80	2.34

From these observations, interesting features are:

- All catalytic systems follow the Michaelis-Menten model. This behaviour is similar to natural enzymes.
- In comparison to protein-free catalyst, all artifical hydrogenases display higher affinity (up to two fold) and higher rate constants (up to three fold). A plausible reason for this may be the presence of a hydrophobic pocket providing a favourable environment for the mass transfer of dihydrogen to access the active site of the artificial metalloenzymes
- Both host proteins streptavidin and avidin, display the similar kinetics behaviour.
- The presence of DMSO contributes to increase the reaction rates. Some previous studies revealed that the solubility of dihydrogen in organic solvent is significantly higher than in aqueous counterpart [170], thus contributing to the mass transfer of the dihydrogen thus increasing the reaction rate.

To compare the values of the kinetics parameters with different available methods, we have performed evaluation through linearization graphical methods, such as Eaddie-Hofstee [171-173] and Lineweaver-Burk models [172, 174].

A linearization method is commonly used for a graphical representation of the kinetic data. This was performed either by Lineweaver-Burk plot or Eadie-Hofstee plot. These two methods are used routinely in enzymatic catalysis, although the latter is considered to be better and more accurate than the Lineweaver-Burk method. The Lineweaver-Burk or double reciprocal is very useful to analyze data graphically and to detect deviations from an ideal behaviour. By plotting 1/ν vs. 1/[S] curve, one can extract the maximum initial rate, V_{max}, from the inverse of constant of the linear equation (**3**). The slope of this curve corresponds to ratio K_M/V_{max}. As V_{max} is known,

K_M can be extracted. Re-arranging equation (**1**), we obtain equation (**3**) which relates 1/ν and 1/[S].

$$\frac{1}{\nu} = \frac{K_M}{V_{\max}}\frac{1}{[S]} + \frac{1}{V_{\max}} \quad (\mathbf{3})$$

Table 14. Initial reaction rates obtained from kinetic experiments for [Rh(COD)(**Biot-1**)]$^+$ ⊂ WT Sav and parameters values to construct Lineweaver-Burk and Eadie-Hofstee plots.

[S] (mM)	Time (min)	Conv. (%)	ν (mM.min^{-1})	1/[S] (mM^{-1})	1/ν (mM^{-1}.min)	ν/[S] (min^{-1})
0	0	0	0	-	-	-
2.825	2	8	0.113	0.354	8.85	0.040
3.955	3	11	0.145	0.252	6.89	0.037
5.085	3	9	0.153	0.197	6.55	0.030
5.65	5	15	0.169	0.177	5.90	0.030
11.3	5	9	0.203	0.089	4.91	0.018
16.95	10	12	0.203	0.059	4.91	0.012
28.25	10	8	0.226	0.035	4.24	0.008
33.9	10	7	0.237	0.029	4.21	0.007

The graphical representation of the Lineweaver-Burk plot is depicted in **Figure 14**. Kinetic parameters obtained from this linearization are $V_{\max}$ = 0.259 mM.min^{-1} and K_M = 3.43 mM.

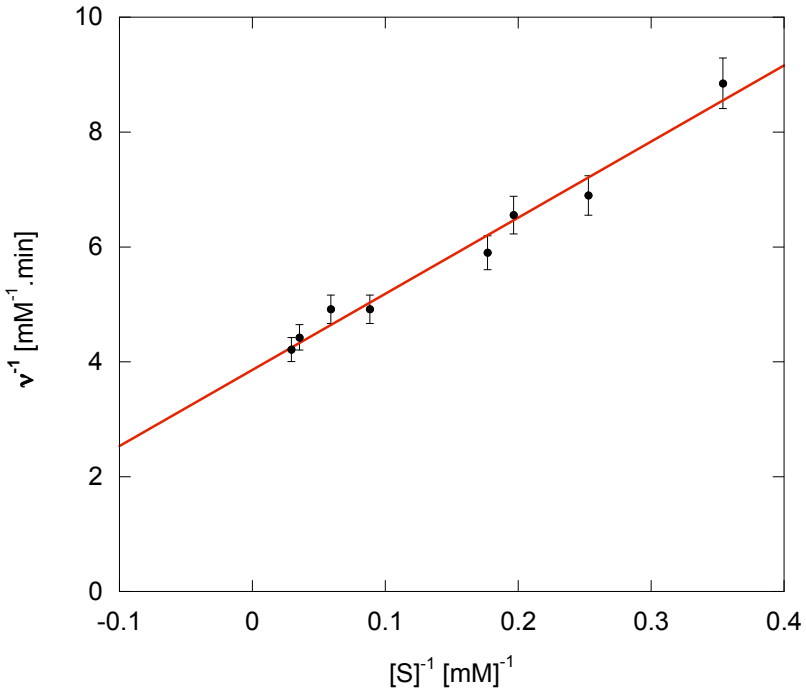

Figure 14. Lineweaver-Burk plot for determination of kinetic parameters for [Rh(COD)(**Biot-1**)]$^+$ ⊂ WT Sav. The fitted equation is highlighted in red with $R^2 = 0.977$.

Another graphical method, the Eadie-Hofstee plot, relating initial rate ν vs. ν/[S], with equation $\nu = -K_M \frac{\nu}{[S]} + V_{max}$ (**4**) affords the following kinetic values: K_M = 3.22 mM and V_{max} = 0.254 mM/min and the plot of this equation is depicted in **Figure 15**. From this example, it is obvious that with the Eadie-Hofstee method, the kinetic parameters can be extracted directly from equation (**4**). Furthermore, it is known that this method has a clear advantage in robustness against error-prone data than the Lineweaver-Burk plot. Particularly, it yields equal weight to data points in any range of substrate concentration or reaction rate, thus the typical measure goodness of fit, correlation coefficient R^2, is no longer applicable.

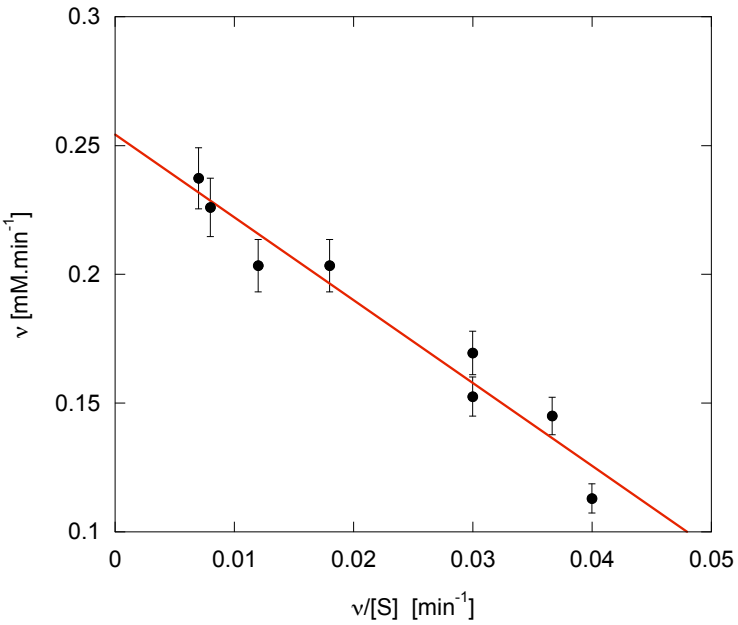

Figure 15. Eadie-Hofstee plot for determination of kinetic parameters for [Rh(COD)(**Biot-1**)]$^{+}$ ⊂ WT Sav.

As stated above, the kinetics parameters obtained from these two linearization methods are slightly different. The Eadie-Hofstee linearization yields quite similar kinetics parameters compared to the Michaelis-Menten model.

SUMMARY & OUTLOOK

4.1. Summary

This work describes the thermodynamic, kinetic and enantioselectivity considerations of artificial metalloenzymes based on the biotin-avidin technology. These studies focused on improving the performance of the first-generation artificial hydrogenases based on biotin-avidin technology.

In chapter 2, a straightforward methodology using CD spectroscopy was used to determine the association constants of biotinylated coordination compounds $[Ru(bpy)_2(Biot\text{-}bpy)]^{2+}$ within (strept)avidin. It was demonstrated that bulky biotinylated coordination compounds can occupy four biotin binding sites of (strept)avidin. The binding affinity, however, is significantly reduced compared to native biotin (*ca*. 5-7 orders magnitude lower: K_a biotin ⊂ streptavidin = 10^{13} M^{-1}). Moreover, no significant chiral discrimination between the Δ– and Λ– diastreomers $[Ru(bpy)_2(Biot\text{-}bpy)]^{2+}$ could be observed upon binding to streptavidin.

In chapter 3 we demonstrated that the biotin-avidin technology could be exploited to create artificial hydrogenases. Building upon previous work within the group, we showed that a second generation of artificial hydrogenases bearing enantiopure amino acid-spacers, affords both (*R*) and (*S*)-selective hydrogenases. The highest ee in favor of (*S*)-reduction product was obtained with [Rh(COD)**Biot-(*R*)-Pro-1**)]$^+$ ⊂ Sav S112W (95% ee (*S*) for both *N*-AcAla and *N*-AcPhe). In addition, combination of ligands bearing enantiopure spacers with isoforms of streptavidin provided significantly more diversity in term of genetic optimization. In some cases, it was shown that combination of avidin with chiral-spacer ligands outperformed streptavidin as a host. This may be interesting for the future use, as avidin is much cheaper than streptavidin. Another interesting feature of the second-generation

artificial hydrogenases is the organic solvent tolerance. This remarkable property was not observed in the first generation of artificial hydrogenases bearing achiral spacer-ligands. A high-tolerance towards organic solvents is crucial in the design of metalloenzymes as most of the substrates are little soluble in water.

In the present work, we also demonstrated that it is possible to immobilize the host protein with commercially available biotin-sepharose. It was found that, again combination [Rh(COD)**Biot-(*R*)-Pro-1**)]$^+$ ⊂ Sav S112W emerged to catalyze nearly as efficiently as its homogeneous counterpart. Additionally, preliminary studies revealed that it is possible to recycle and reuse immobilized metalloenzymes.

Determination of reaction rates using Michaelis-Menten kinetics are presented and discussed in Chapter 3. It was found that all catalytic systems follow a Michaelis-Menten mechanism. An increase in reaction rate and in substrate-catalyst affinity was observed upon incorporation of metal-complexes within (strept)avidin. This suggests that the host protein contributes to increase both the rate and the selectivity of the reaction. Reactions performed in the presence of DMSO proceed with higher rates. This may be due to a higher solubility of dihydrogen in this solvent compared to that in water.

4.2. Outlook

Introduction of a chiral spacer between biotin moiety and diphosphine afforded second-generation artificial hydrogenases. Although the new class of ligands showed a high tolerance towards organic solvents, it remains still difficult to broaden the substrate scope and to increase the TON/TOF of the reaction. As stated previously, one of the most important factors in the design of the catalyst is the ligand scaffold. It thus will be interesting to design another ligand scaffold to achieve a wider substrate scope.

The future research may be focused on the use of other type of metal for enantioselective hydrogenation (Ruthenium instead of Rhodium) as high-air sensitivity is one of the major problems using Rh-diphosphine as metal precursor.

Biotin-sepharose allows the immobilization of the metalloenzymes and thus catalysis can be performed without using the purified protein. As protein purification is time-consuming, it is thus convenient to use directly the crude protein extract.

The creation of metalloenzymes using the biotin-(strept)avidin technology and its spectacular results are just a beginning. We have successfully demonstrated that some important chemical transformations (hydrogenation, transfer hydrogenation, allylic alkylation) are conveniently catalyzed by artificial metalloenzymes using biotin-(strept)avidin technology. In the near future, it is obvious that more challenging chemical transformations can be performed using artificial metalloenzymes: hydroformylation, epoxidation, sulfoxidation, Suzuki coupling, and so forth. We have taken advantage the power of Nature to induce the selectivity (and activity) for chemical transformations.

High-throughput screening and analysis can accelerate the procedure in finding the most versatile catalyst. The use of microdevices (e.g. microreactor) will allow a rapid identification and analysis of the outcome of the reaction; another advantage using the microdevices is that very small quantity of sample is required. A little more effort in optimization of the process will lead to industrial application of using artificial metalloenzymes.

SUPPORTING INFORMATION

5.1. Materials, instrumentation and techniques.

5.1.1. Abbreviation used

$BiotOC_6F_5$	biotin-pentafluorophenol ester
DMF	*N*,*N*'-dimethylformamide
CD	circular dichroism
CDMT	2-Chloro-4,6-dimethoxy-1,3,5-triazine
CH_2Cl_2	dichloromethane (DCM)
CH_3CN	acetonitrile
Conv.	conversion
d	day(s)
DMF	dimethylformamide
DMSO	dimethylsulfoxide
EtOAc	ethyl acetate
ee	enantiomeric excess
equiv	equivalent
ESI	electron spray ionization
EtOH	ethanol
g, mg	gram, milligram
GC	gas chromatography
h	hour(s)
HABA	2-(4'-hydroxyazoybenzene)benzoic acid
H_2O	water
HCl	hydrochloric acid
Hex	hexane
HPLC	high performance liquid chromatography
L, mL, mL	liter, milliliter, microliter
M, mM	molar ($mol \cdot liter^{-1}$), millimolar ($millimol \cdot liter^{-1}$)
MeOH	methanol
MES	2-morpholinoethanesulfonic acid ($pK_a = 6.15$)
min	minute(s)

MLCT	metal-to-ligand-charge transfer
mol, mmol, mmol	mole, milimole, micromole
MOPS	3-(*N*-morpholino)propanesulfonic acid (pK_a = 7.2)
MS	mass spectrometry
NaOH	sodium hydroxide
NH_4PF_6	amonium hexafluorophosphate
NMR	nuclear magnetic resonance
rt	room temperature
s	second(s)
Net_3	triethylenamine
TFA	trifluoroacetic acid
TOF	turnover frequency (mol of product/mol of catalyst/time)
TON	turnover number (mol of product/mol of catalyst)
UV-Vis	ultraviolet-visible
vs.	versus
WT	wild-type (native)

5.1.2. Reagents and solvents

Reagents and solvents used in this work are listed in the **Table 15**.

Table 15. Reagents and solvents used

Substance	Origin	Quality grade and purity
N-acetamidoacrylic acid	Acros	≥ 99%
N-acetamidocinnamic acid	Fluka	≥ 99%
Acetonitrile	Acros	≥ 99.9%
Ammonium Hexafluorophosphate	Fluka	≥ 98% (gravimetric)
Anisole	Fluka	≥ 99%
Avidin	Belovo	-
(+)-biotin (*D*-biotin)	Chanzou Huaren	≥ 99%
Biotin-sepharose	Affiland	In NaN_3 0.02% (w/v)
2,2'-bipyridine	Fluka	Purum ≥ 98% (NT)

Boc-(D)Phe-OH	Fluka	≥ 99%
Boc-(L)Phe-OH	Fluka	≥ 99%
Boc-(D)Pro-OH	Fluka	≥ 99%
Boc-(L)Pro-OH	Fluka	≥ 99%
(*R*)-1-Boc-2-piperidine carboxylic acid	Aldrich	98%
(*S*)-1-Boc-2-piperidine carboxylic acid	Aldrich	98%
(*R*)-1-Boc-glutamic acid benzyl ester	Senn	
(*S*)-1-Boc-glutamic acid benzyl ester	Fluka	98 %
(+)-O,O'-dibenzoyl-D-tartaric acid	Fluka	≥ 99%
(-)-O,O'-dibenzoyl-L-tartaric acid	Fluka	≥ 99%
N,*N*'-Diisopropylethylamine	Fluka	≥ 98%
N,*N*'-dimethylformamide	Fluka	≥ 99.8% (GC)
Dimethylformamide	Fluka	≥ 99.5% ($H_2O \leq 0.005$ %)
Dimethylsulfoxide	Acros	≥ 99.9%
Ethanol	Merck	p.a. ≥ 99.8% (GC)
Ethylene glycol	Fluka	≥ 99.5% (GC)
Ethylenediamine	Fluka	≥ 99%
Hydrochloric acid	Prochimie	Solution 32%
2-(4'-hydroxyazoybenzene) benzoic acid	Sigma	≥ 98% (TLC)
ketopantolactone	DSM Nutrition	≥ 99%
N-methylmorpholine	Fluka	≥ 98 %
2,3,4,5,6-pentafluorophenol	Fluka	≥ 99 % (GC)
Phosphate buffer	Merck	Titrisol® pH 7.0
Potassium hydroxide, pellets	Fluka	≥ 99%
$Rh(COD)_2BF_4$	Umicore	
Sephadex SP C-25	Pharmacia LKB	
Silica	Brunschwig	32-63 60Å
Sodium hydroxide, pellets	Fluka	Puriss. p.a ACS > 98%
Streptavidin	Own production	

Triethylenamine	Riedel-de-Haën	≥ 99% (GC)
Trifluoroacetic acid	Fluka	≥ 98%
Trimethylsulfonium hydroxide	Fluka	0.25 M in MeOH

5.1.3. Preparative methods: column chromatography

- Flash chromatography was carried out on silica gel 60, 32-63 mm.
- SP Sephadex C-25 was used for ion exchange chromatography.
- TLC (Thin Layer Chromatography) was performed on 0.2 mm silica gel 60 F254 aluminium sheets from Merck. All biotinylated compounds were revealed as red spots with a solution of DACA (4-dimethylaminocinnamaldehyde) in methanol containing 1% conc. H_2SO_4 [175, 176].

5.1.4. Analysis Instruments

5.1.4.1. Absorption Spectrophotometry (UV/Vis)

The measurements were performed on a UVIKON 930 spectrophotometer from Kontron/BioTech. The sample solutions were measured in 1 cm quartz cells. The spectrophotometric data were imported and treated with MS excel.

Indications in the spectroscopic data collection: λ_{max} [nm] (ε_{max} [$M^{-1}cm^{-1}$]).

5.1.4.2. Circular Dichroism (CD)

CD spectra were recorded on a J-710 spectropolarimeter from JASCO, Tokyo (J). The sample solutions were measured in 1 cm quartz cells. The spectrophotometric data were imported and treated in SPECFIT/32 package.

Indications in the spectroscopic data collection: λ_{max} [nm] ($\Delta\varepsilon_{max}$ [$M^{-1}cm^{-1}$]).

5.1.4.2. Mass spectrometry (MS)

Mass spectra were recorded on a mass spectrometer LCQ from ThermoFinnigan, San José (USA), and on a mass spectrometer FTMS 4.7T BioAPEX II from Bruker, Billerica (USA) (at University of Fribourg). The ionization mode was for both electron spray ionization (ESI). Indications in the spectroscopic data collection: Mr of species (relative intensity, attribution). The relative intensity is given in % with respect to the strongest peak of the spectrum.

5.1.4.3. Nuclear magnetic resonance (NMR)

Proton and carbon NMR spectra were recorded on spectrometer AMX-400 (400.00 MHz for ^{1}H, 100.58MHz for ^{13}C, 376.31MHz for ^{19}F, and 161.93MHz for ^{31}P) from Bruker, Billerica (USA). The samples were measured either in deuterated chloroform (99.8 % D) or deuterated dimethylsulfoxide (99.5 % D) from Cambridge Isotope Laboratories, Andover MA (USA).

Indication in the spectroscopic data collection: δ[ppm] relative to external standards TMS (^{1}H, ^{13}C), $CFCl_3$ (^{19}F) and H_3PO_4 (^{31}P) (multiplicity (^{1}H only, *J*[Hz](1H only), normalized integration values (^{1}H only), attribution (^{1}H and ^{13}C only). The following abbreviations were used: s for singlet, d for doublet, dd for doublet of doublet, ddd for doublet of doublet of doublet, dt for doublet of triplet, t for triplet, q for quadruplet and m for multiplet.

5.2. Synthesis Protocols

Synthesis and characterization of 5'-{2-[5-(2-Oxo-hexahydro-thieno[3,4-d]imidazol-4-yl)pentanoylamino]-ethylcarbamoyl}-2,2'-bipyridinyl-5-carboxylic acid ethyl ester (Biot-bpy)

The biotinylated ethylenediamine and activated ester were synthesized according the Li and Somlai's procedures [154, 155]. Meanwhile the synthesis of Δ-$[Ru(bpy)_2(py)_2][(+)$-O,O'-dibenzoyl-D-tartrate$] \cdot 12H_2O$ was achieved using von Zelewsky's method [157, 158]. The basic condition (pH = 8–9) is required to achieve a good solubility of tartaric acid [156]. The experimental detail was described in previous report of our group [20].

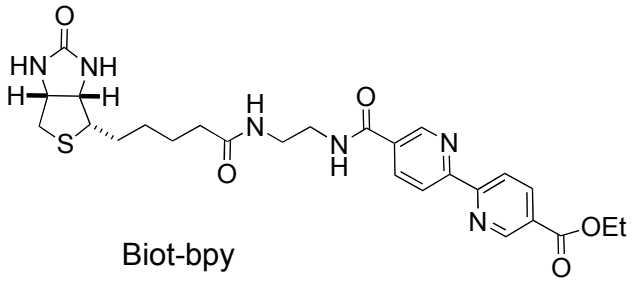

Biot-bpy

Synthesis of *rac*-$[Ru(bpy)_2(Biot\text{-}bpy)](PF_6)_2$ and diastereopures

The synthesis and full characterization of *rac*-$[Ru(bpy)_2(Biot\text{-}bpy)](PF_6)_2$, Δ-$[Ru(bpy)_2(Biot\text{-}bpy)](ClO_4)_2$ and Λ-$[Ru(bpy)_2(Biot\text{-}bpy)](ClO_4)_2$ were described in detail in previous report of our group [20].

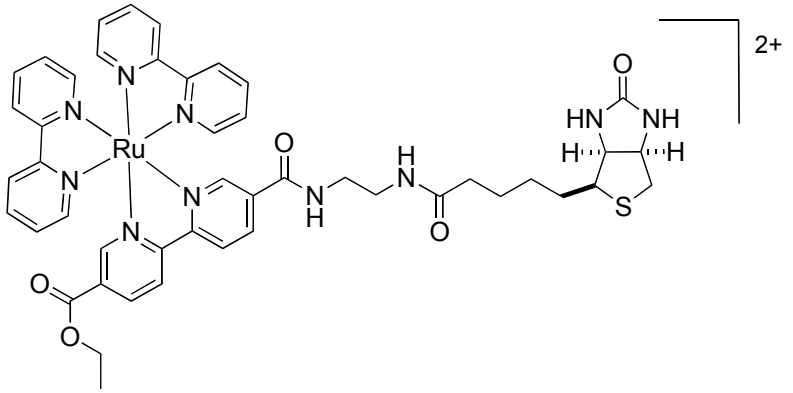

rac-[Ru(bpy)$_2$(Biot-bpy)]$^{2+}$

Diphosphine ligands synthesis and characterization

All ligands used herein were reported (synthesis and full characterization) in the supporting information of the preliminary communication 21, 164.

Synthesis of biotinylated amidodiphosphine Biot-1 and Biot-2

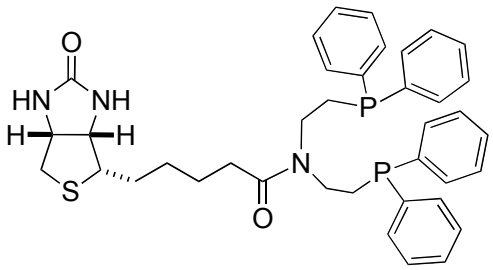

Biot-1

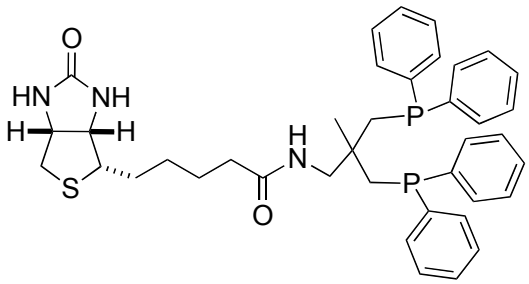

Biot-2

Biot-1 or **Biot-2** were prepared by the coupling of biotin *N*-Hydroxysuccinimide (**Biot**NHS) and **H–1** HCl or **H–2** according to the literature [21].

Synthesis of biotinylated amidodiphosphine ligands with 3^n or 4^q spacers

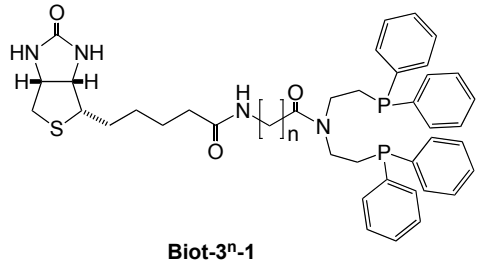

Biot-3^n-1
n = 1-5

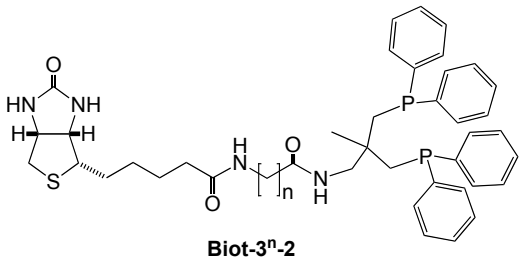

Biot-3^n-2
n = 1-5

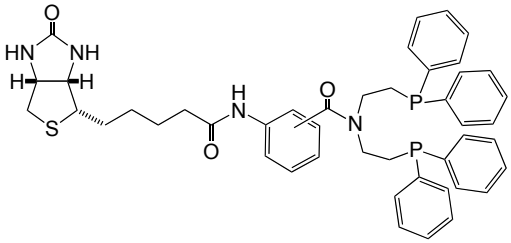

Biot-4^q-1
q = *ortho*-, *meta*- and *para*-

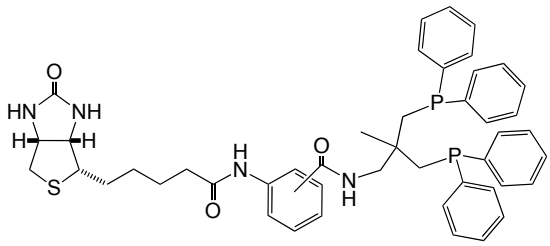

Biot-4^q-2
q = *ortho*-, *meta*- and *para*-

Biot-3^n-1, Biot-4^q-1, Biot-3^n-2, Biot-4^q-2 (n = 1-5, q = *ortho*-, *meta*- and *para*-) or **Biot-2** were prepared according to the literature [21], by the coupling between biotinylated aminoacid (**Biot-3^n** or **Biot-4^q** (n = 1-5, q = *ortho*-, *meta*- and *para*-)) and diphosphino-amine (**H–1** HCl or **H–2**).

Synthesis of second generation of aminodiphosphine with chiral spacers

The preparation of chiral spacers ligands were described in previous report of our group [22].

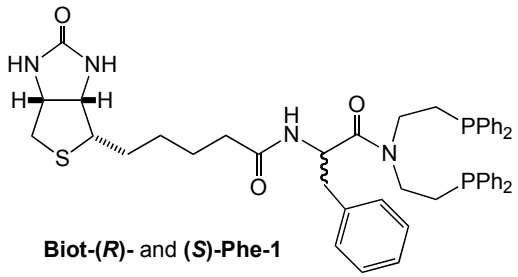

Biot-(*R*)- and **(*S*)-Phe-1**

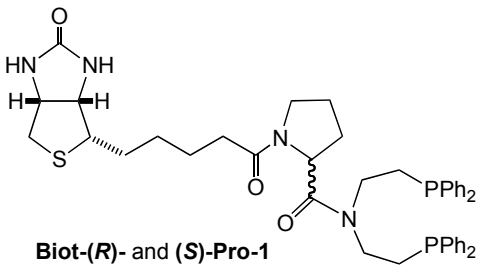

Biot-(*R*)- and **(*S*)-Pro-1**

In general, the synthesis of enantiopure chiral spacer ligands is achieved by following the procedure described below:

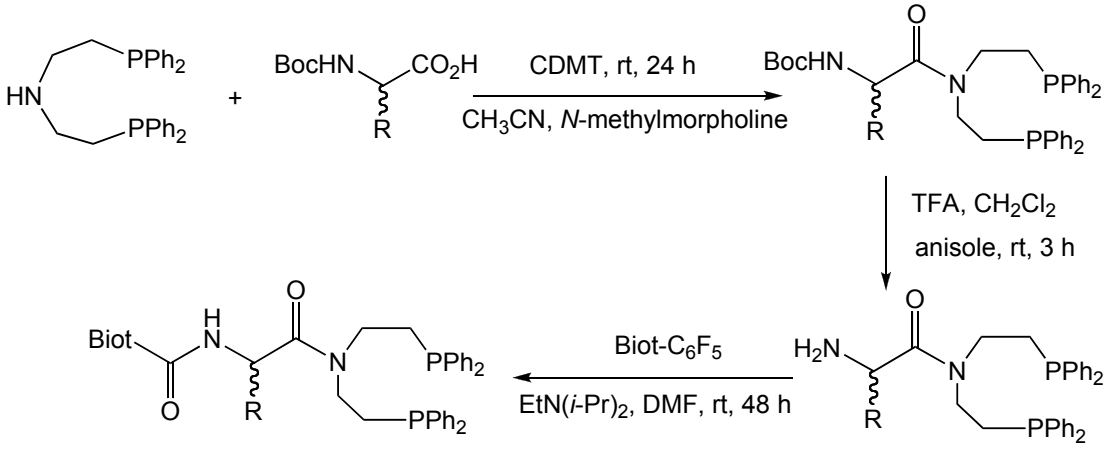

Scheme 46. Synthesis pathway of biotinylated-diphosphine ligands bearing an enantiopure amino acid spacer.

Synthesis of (*R*)–boc 2-((bis(2-diphenylphosphino)ethyl))carbamoyl piperidine-1-carboxylate (Boc-(*R*)-Pip-1)

The diphosphino-amine **H–1** HCl (1.0 g, 2.1 mmol), (*R*)-Boc 2-Piperidine Carboxylic Acid (0.49 g, 2.1 mmol) and CDMT (0.38 g, 2.3 mmol) were mixed in degassed acetonitrile (95 mL) and *N*-methylmorpholine (0.56 mL, 5.2 mmol) was added slowly (after 5 min). The slurry was stirred overnight at room temperature. The solvent was removed *in vacuo* and the crude precipitate was purified by column chromatography on silica gel 60 F254 using Hexane/EtOAc : 8/2 as eluent, allowing isolation of pure product as a white foam. (yield: 0.50 g, 0.76 mmol, 68%).

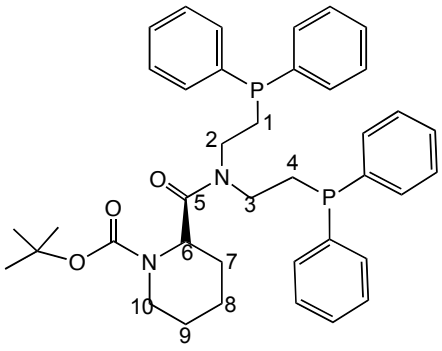

^{1}H NMR (200.00 MHz, $CDCl_3$, 20°C): δ [ppm] = 1.4 (s, 9H; **CH_3-Boc**), 1.5 (m, 6H; **H_9**, **H_8**, **H_7**), 1.6 (m, 4H; **H_1**, **H_4**), 3.3 (m, 4H; **H_2**, **H_3**), 3.5 (m, 2H; **H_{10}**), 4.6 (m, 1H; **H_6**), 7.3-7.4 (m, 20H; **PhH**).

^{31}P NMR (161.98 MHz, $CDCl_3$, 20°C): δ [ppm] = -19.3.

Synthesis of (*S*)–boc 2-((bis(2-diphenylphosphino)ethyl))carbamoyl)piperidine-1-carboxylate (Boc-(*S*)-Pip-1)

The diphosphino-amine **H–1** HCl (3.0 g, 6.3 mmol), (*S*)-Boc 2-Piperidine Carboxylic Acid (1.44 g, 6.3 mmol) and CDMT (1.22 g, 6.4 mmol) were charged into a 500 mL bottom flask containing degassed acetonitrile (280 mL) and after 5 min, a solution of *N*-methylmorpholine (1.7 mL, 15 mmol) was added slowly. The resulting slurry was stirred overnight at room temperature. The solvent was removed *in vacuo* and the crude precipitate was purified by column chromatography on silica gel 60 F254 using Hexane/EtOAc : 8/2 as eluent, allowing isolation of pure product as a white foam. (yield: 0.60 g, 0.92 mmol, 15%).

Synthesis of (*R*)–benzyl 5-(bis(2-diphenylphosphino)ethyl)amino)-4-(Boc)-5-oxopentanoate (Boc-(*R*)-Glu$^{5\text{-Bz}}$-1)

The diphosphino-amine **H–1** HCl (0.5 g, 1.1 mmol), (*R*)-Boc Glutamic Acid Benzyl Ester (0.35 g, 1.1 mmol) and CDMT (0.18 g, 1.1 mmol) were charged into a 100 mL bottom flask containing degassed acetonitrile (45 mL) and after 5 min, a solution of *N*-methylmorpholine (0.28 mL, 2.5 mmol) was added slowly. The resulting slurry was stirred overnight at room temperature. The solvent was removed *in vacuo* and the crude precipitate was purified by column chromatography on silica

gel 60 F254 using Hexane/AcOEt : 8/2 as eluent, allowing isolation of pure product as a white foam. (yield: 0.68 g, 0.89 mmol, 85%).

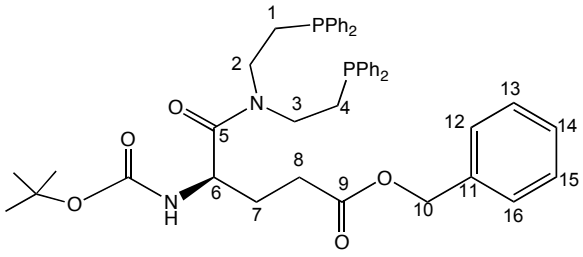

^{1}H NMR (400.00 MHz, $CDCl_3$, 20°C): δ [ppm] = 1.4 (s, 9H; **CH_3 Boc**), 1.9 (qd, 2H; **H_7**), 2.3 (m, 6H; **H_8**, **H_1**, **H_4**), 3.3 (m, 2H; **H_3**), 3.6 (m, 2H; **H_2**), 4.5 (td, 1H; *J* = 5.2, 3.8 Hz; **H_6**), 5.1 (dd, 2H; *J* = 12.2, 9.4 Hz; **H_{10}**), 5.3 (d, 1H, *J* = 8.6 Hz; **NH**), 7.3-7.5 (m, 25H; **PhH**, **H_{12}**, **H_{13}**, **H_{14}**, **H_{15}**, **H_{16}**).

^{13}C NMR (50 MHz, $CDCl_3$, 20°C): δ [ppm] = 26.6 (CH_2), 26.7 (CH_2), 28.5 (CH_2), 28.7 (CH_3 Boc), 30.2 (CH_2), 44.4 (CH_2), 45.7 (CH_2), 50.1 (CH-O), 66.8 (CH-O), 80.0 (C Boc), 128.7-133.4 (Ph–H), 136.3-137.8 (Ph–C), 155.8 (CO Boc), 171.9 (CO-N), 173.0 (CO-O).

^{31}P NMR (161.62 MHz, $CDCl_3$, 20°C): δ [ppm] = -19.7, -20.4.

Synthesis of (*S*)–benzyl 5-(bis(2-diphenylphosphino)ethyl)amino)-4-(Boc)-5-oxopentanoate (Boc-(*S*)-Glu$^{5\text{-Bz}}$-1)

The diphosphino-amine **H–1** HCl (0.5 g, 1.1 mmol), (*S*)-Boc Glutamic Acid Benzyl Ester (0.35 g, 1.1 mmol) and CDMT (0.18 g, 1.1 mmol) were added into a 45 mL degassed acetonitrile. After stirring for *ca*. 5 min, a solution of *N*-methylmorpholine (0.28 mL, 2.5 mmol) was added slowly to the mixture. The slurry was then stirred overnight at room temperature. The solvent was removed *in vacuo*

and the crude precipitate was purified by column chromatography on silica gel 60 F254 using Hexane/AcOEt : 8/2 as eluent, allowing isolation of pure product as a white foam. (yield: 0.61 g, 0.80 mmol, 76%).

General procedure of deprotection of *N*-boc amino acid diphosphine

The Boc group was removed by addition of 20 equiv TFA in dichloromethane (TFA/DCM: 0.5) and 2 equiv of anisole to the protected *N*-boc. All solvent was degassed before use for *ca*. 15 min. Upon stirring the reaction mixture (rt, 3 h approximately), the solvent was evaporated in *vacuo* to dryness. The resulting precipitate was used for coupling with biotin without further purification.

Synthesis of Biot-(*R*)-Pip-1

A solution of BiotOC_6F_5 (0.38 mg, 0.9 mmol) in DMF (45 mL) was added at room temperature to the deprotected aminodiphosphine H-(*R*)-Pip (0.5 g, 0.9 mmol). The reaction mixture was then stirred under N_2. A solution of *N*-*N*-Diisopropylethylamine (0.6 mL, 3.7 mmol) was added to the slurry. After 48 h of mixing, the solvent of resulting mixture was dried under vacuum. The product (white foam) was then purified by silica gel $CHCl_3$/MeOH = 12:1 (yield: 0.19 g, 0.24 mmol, 22%).

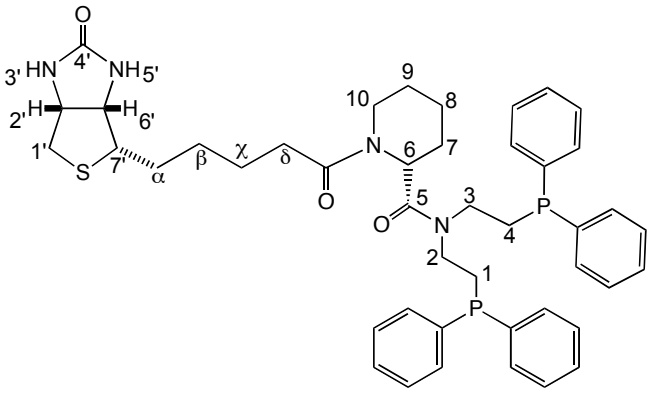

^{1}H NMR (400.00 MHz, $CDCl_3$, 20°C): δ [ppm] = 1.8-1.3 (m, 16H; $\mathbf{H_{\alpha}}$, $\mathbf{H_{\beta}}$, $\mathbf{H_{\chi}}$, $\mathbf{H_1}$, $\mathbf{H_4}$, $\mathbf{H_7}$, $\mathbf{H_8}$, $\mathbf{H_9}$), 2.3 (m, 2H; $\mathbf{H_{\delta\chi}}$), 2.7 (dd, 1H, *J* = 12.8 Hz, *J* = 4.8 Hz; $\mathbf{H_{1',b}}$), 2.8 (dd, 1H, *J* = 12.8 Hz, *J* = 4.8 Hz; $\mathbf{H_{1',a}}$), 3.1 (m, 1H; $\mathbf{H_{7'}}$), 3.3 (m, 2H; $\mathbf{H_{10}}$), 3.7 (m, 4H; $\mathbf{H_2}$, $\mathbf{H_3}$), 4.2 (m, 1H; $\mathbf{H_{6'}}$), 4.3 (m, 1H; $\mathbf{H_{2'}}$), 4.4 (dd, 1H, *J* = 7.7 Hz, *J* = 4.6 Hz; $\mathbf{H_6}$), 6.5-5.7 (s, 1H; $\mathbf{H_{3'}}$, $\mathbf{H_{5'}}$**),** 7.3-7.5 (m, 20H; **PhH**).

^{13}C NMR (50 MHz, $CDCl_3$, 20°C): δ [ppm] = 25.0-33.6 (CH_2; C_1, C_4, C_7, C_8, C_9, C_{α}, C_{β}, C_{χ}, C_{δ}), 40.8 (CH_2-S), 45.6 (CH_2), 43.9 (CH_2; C_2, C_3), 50.1 (CH-N), 55.9 (CH-S), 60.7 ($C_{2'}$), 62.3 ($C_{6'}$), 128.9-133.5 (Ph–H), 136.3-140.1 (Ph–C), 164.3 (N-CO-N), 172.7 (CO), 174.7 (Cε).

^{31}P NMR (161.62 MHz, $CDCl_3$, 20°C): δ [ppm] = -19.9, -20.2.

ESI MS $C_{44}H_{52}N_4O_3P_2S$ (778.32): 779.3 (100%) $[M+H]^+$.

Synthesis of Biot-(*S*)-Pip-1

A solution of BiotOC_6F_5 (0.4 mg, 1.03 mmol) in DMF (50 mL) was added at room temperature to the deprotected aminodiphosphine H-(*S*)-Pip (0.57 g, 1.03 mmol). The reaction mixture was then stirred under N_2. A solution of *N*-*N*-Diisopropylethylamine (0.7 mL, 5.4 mmol) was then added to the slurry. Upon mixing (for *ca*. 48 h), the solvent of resulting mixture was dried under vacuum. The product (white foam) was then purified by silica gel CH_2Cl_2/MeOH = 12:1 (yield: 0.36 g, 0.46 mmol, 44%).

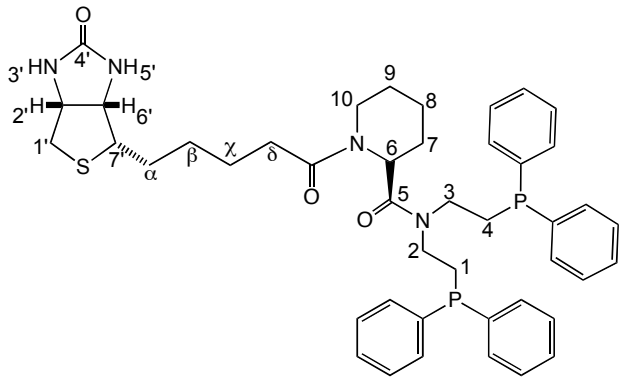

^{1}H NMR (400.00 MHz, $CDCl_3$, 20°C): δ [ppm] = 1.7-1.4 (m, 16H; **H_{α}**, **H_{β}**, **H_{χ}**, **H_1**, **H_4**, **H_7**, **H_8**, **H_9**), 2.3 (m, 2H; **H_{δ}**), 2.7 (m, 1H; **$H_{1',b}$**), 2.8 (m, 1H; **$H_{1',a}$**), 3.1 (m, 1H; **$H_{7'}$**), 3.3 (t, 2H, *J* = 5.3 Hz; **H_{10}**), 3.7 (m, 4H; **H_2**, **H_3**), 4.2 (dd, 1H, *J* = 12.8 Hz, *J* = 4.5 Hz; **$H_{6'}$**), 4.4 (dd, 1H, *J* = 12.8 Hz, *J* = 4.5 Hz; **$H_{2'}$**), 4.9 (m, 1H; **H_6**), 5.5-6.1 (s, 1H; **$H_{3'}$, $H_{5'}$),** 7.3-7.4 (m, 20H; **PhH**).

^{13}C NMR (50 MHz, $CDCl_3$, 20°C): δ [ppm] = 19.2-33.2 (CH_2; C_1, C_4, C_7, C_8, C_9, C_{α}, C_{β}, C_{χ}, C_{δ}), 40.3 (CH_2-S), 43.6 (CH_2; C_2, C_3), 45.6 (CH_2; C_{10}), 50.0 (CH-N), 55.4 (CH-S), 60.4 ($C_{2'}$), 61.9 ($C_{6'}$), 128.5-133.0 (Ph–H), 135.5-139.7 (Ph–C), 164.0 (N-CO-N), 172.1 (CO), 174.2 (Cε).

^{31}P NMR (161.62 MHz, $CDCl_3$, 20°C): δ [ppm] = -20.98, -21.17.

ESI MS $C_{44}H_{52}N_4O_3P_2S$ (778.32): 779.3 (100%) $[M+H]^+$.

Synthesis of Biot-(*R*)-Glu$^{5\text{-Bz}}$-1

BiotOC_6F_5 (0.44 mg, 1.06 mmol) was dissolved in DMF (59 mL). The slurry was added at room temperature to the deprotected aminodiphosphine H-(*R*)-Glu$^{5\text{-Bz}}$ (0.58 g, 1.06 mmol) under N_2. A solution of *N*-*N*-Diisopropylethylamine (0.6 mL, 3.7 mL) was added to the slurry. After 48 h of mixing, the solvent of resulting mixture

was dried under vacuum. The product (white foam) was then purified by silica gel CH_2Cl_2/EtOH = 30:1 (yield: 0.16 g, 0.18 mmol, 17%).

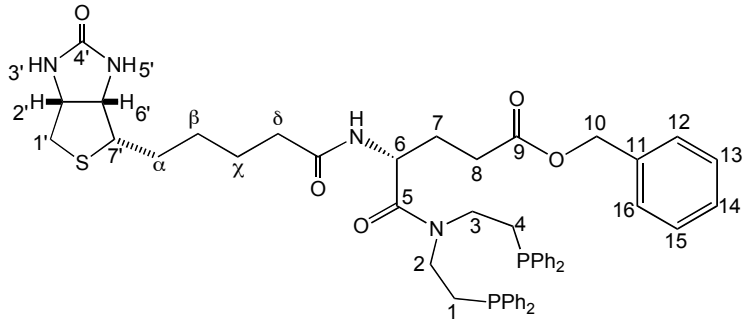

^{1}H NMR (400.00 MHz, $CDCl_3$, 20°C): δ [ppm] = 1.2-1.9 (m, 9H; **H_α**, **H_β**, **H_χ**, **H_1**, **H_4**), 2.2-2.4 (m, 6H; **H_δ**, **H_7**, **H_8**), 2.8 (dd, 2H, J = 8.00 Hz, J = 4.8 Hz; **$H_{1'}$**), 3.2 (m, 1H; **$H_{7'}$**), 3.5 (m, 4H; **H_2**, **H_3**), 4.2 (dd, 1H, J = 3.4 Hz, J = 4.4 Hz; **$H_{6'}$**), 4.3 (dd, 1H; J = 4.8 Hz, J = 4.4 Hz; **$H_{2'}$**), 4.7 (m, 1H; **H_6**), 5.0 (m, 2H; **H_{10}**), 6.7 (s, 2H; **$H_{3'}$**, **$H_{5'}$**), 7.3-7.5 (m, 25H; **PhH, H_{12}**, **H_{13}**, **H_{14}**, **H_{15}**, **H_{16}**) 8.0 (s, 1H; **NH**).

^{13}C NMR (50 MHz, $CDCl_3$, 20°C): δ [ppm] = 25.9-35.9 (CH_2; C_1, C_4, C_7, C_8, C_9, C_α, C_β, C_χ, C_δ), 40.9 (CH_2-S), 44.4 (CH_2; C_2, C_3), 48.7 (CH-N), 55.9 (CH-S), 60.8 ($C_{2'}$), 61.9 ($C_{6'}$), 66.8 (CH_2-O), 128.7-133.6 (Ph–H), 136.3-138.3 (Ph–C), 165,2 (N-CO-N), 172.8 (CO-N).

^{31}P NMR (161.62 MHz, $CDCl_3$, 20°C): δ [ppm] = -20.22, -20.3.

ESI MS $C_{50}H_{56}N_4O_5P_2S$ (886.34): 887.3 (100%) $[M+H]^+$.

Synthesis of Biot-(*S*)-Glu$^{5\text{-Bz}}$-1

$BiotOC_6F_5$ (0.33 mg, 0.79 mmol) was dissolved in DMF (45 mL). The mixture was then added at room temperature to the deprotected aminodiphosphine H-(*S*)-Glu$^{5\text{-Bz}}$ (0.44 g, 0.79 mmol). The reaction mixture was then stirred under N_2. A solution of *N*-*N*-Diisopropylethylamine (0.52 mL, 3.2 mmol) was added at last. Upon

stirring (for *ca*. 48 h), the solvent of resulting mixture was dried under vacuum. The product (white foam) was then purified by silica gel using 100 mL $CHCl_3$, 150 mL $CHCl_3$/MeOH = 30:1, and 200 mL $CHCl_3$/MeOH = 15:1 (yield: 0.25 g, 0.28 mmol, 35%).

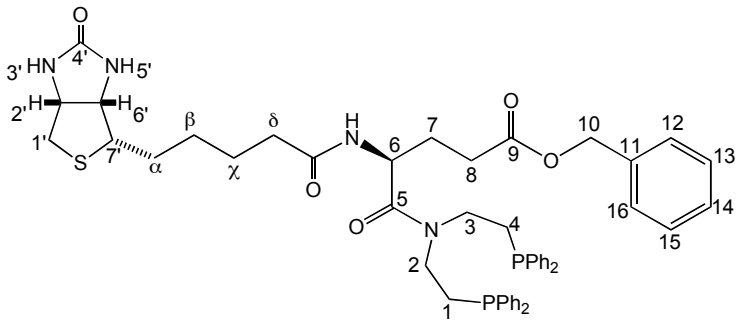

^{1}H NMR (400.00 MHz, $CDCl_3$, 20°C): δ [ppm] = 1.3-1.8 (m, 9H; $\mathbf{H_\alpha}$, $\mathbf{H_\beta}$, $\mathbf{H_\chi}$, $\mathbf{H_1}$, $\mathbf{H_4}$), 2.2-2.4 (m, 6H; $\mathbf{H_\delta}$, $\mathbf{H_7}$, $\mathbf{H_8}$), 2.8 (dd, 2H, J = 7.9 Hz, J = 4.8 Hz, $\mathbf{H_{1'}}$), 3.2 (m, 1H, $\mathbf{H_{7'}}$), 3.4 (m, 4H; $\mathbf{H_2}$, $\mathbf{H_3}$), 4.2 (dd, 1H, J = 3.2 Hz, J = 4.6 Hz, $\mathbf{H_{6'}}$), 4.4 (dd, 1H; J = 4.8 Hz, J = 3.6 Hz, $\mathbf{H_{2'}}$), 4.7 (dd, J = 4.7 Hz, J = 8.4 Hz, 1H; $\mathbf{H_6}$), 5.1 (m, 2H; $\mathbf{H_{10}}$), 7.1 (s, 2H; $\mathbf{H_{3'}}$, $\mathbf{H_{5'}}$**),** 7.3-7.5 (m, 25H; **PhH**, $\mathbf{H_{12}}$, $\mathbf{H_{13}}$, $\mathbf{H_{14}}$, $\mathbf{H_{15}}$, $\mathbf{H_{16}}$).

^{13}C NMR (50 MHz, $CDCl_3$, 20°C): δ [ppm] = 25.8-36.2 (CH_2; C_1, C_4, C_7, C_8, C_9, C_α, C_β, C_χ, C_δ), 40.8 (CH_2-S), 44.5 (CH_2; C_2, C_3), 48.8 (CH-N), 56.2 (CH-S), 60.7 ($C_{2'}$), 62.44 ($C_{6'}$), 66.7 (CH_2-O), 128.7-133.6 (Ph–H), 136.3-138.3 (Ph–C), 165,1 (N-CO-N), 172.9 (CO-N).

^{31}P NMR (161.62 MHz, $CDCl_3$, 20°C): δ [ppm] = -20.36, -20.41.

ESI MS $C_{50}H_{56}N_4O_5P_2S$ (886.34): 887.3 (100%) $[M+H]^+$.

5.3. Production and purification of streptavidin

The expression of mutant proteins Sav S112X has been described in the previous reports [21, 164]. Whereas, WT Avi was purchased from Belovo.

5.4. Enantioselective hydrogenation reactions

5.4.1. General Aspects

All aqueous and organic solvents were flushed with nitrogen during at least *three hours*. All manipulations were performed in a nitrogen atmosphere glove box. The metal source $[Rh(COD)_2]BF_4$ was dissolved in DMSO (4 mg, 16 mL DMSO), 1.56 mmol of this solution was added to the appropriate aliquoted ligand (2.02 mmol, 1.3 equiv with respect to the metal source). This solution was stirred for *ca*. 10 min.

5.4.2. Hydrogenation in Monophasic media (9%, 27%, 45% DMSO)

A Pyrex tube (volume *ca*. 3 mL) was placed in an autoclave and charged with an *N*-acetamidoacrylic acid solution in MES buffer 0.38 M (130 μL of a 23.85 mM solution, 3.10 μmol), and an *N*-acetamidocinnamic acid solution in MES buffer 0.38M (130 μL of a 23.85 mM solution, 3.10 μmol). The volume was adjusted with water (or with DMSO, depending on the ratio of DMSO to be used) to 900 μL. The protein solution in water was then added (100 μL of a 0.207 mM solution, 0.0207 μmol of the tetramer). The precatalyst solution in DMSO (100 μL, 0.062 μmol) was added last. The resulting mixture was vortexed, removed from the glove box and hydrogenated at 5 bars H_2 for 15 h.

5.4.3. Hydrogenation in Biphasic Media (EtOAc)

A Pyrex tube (volume *ca*. 3 mL) was placed in an autoclave and charged with an *N*-acetamidoacrylic acid solution in EtOAc (550 µL of a 5.66 mM solution, 3.10 µmol), and an *N*-acetamidocinnamic acid solution in EtOAc (550 µL of a 5.66 mM solution, 3.10 µmol). The buffer solution (580 µL of a 0.38 M solution) was added and the volume of the aqueous phase was adjusted with water to 900 µL. The protein solution in water was then added (100 µL of a 0.207 mM solution, 0.0207 µmol of the tetramer). The precatalyst solution in DMSO (100 µL, 0.062 µmol) was added last. The resulting mixture was vortexed and hydrogenated at 5 bars H_2 for 15 h using orbital shaking (*ca*. 200 rpm).

Note: In the case of hydrogenation without protein, the volume of the protein solution was replaced by H_2O.

All experiments were performed using MES buffer only. This change does not influence significantly the activity and enantioselectivity of experiments using avidin as the host protein.

5.4.4. Hydrogenation procedure for Immobilized Artificial Metalloenzymes

The commercial suspension of D-biotin-sepharose CL-4B (105 mL, which corresponds to 0.031 mmol biotin, capable of immobilizing 0.031 mmol tetrameric (strept)avidin) (Affiland, Belgium, suspension in TBS buffer pH 7.4, NaN_3 0.02% (w/v)) was decanted and washed with water to afford wet beads, which were resuspended in water (105 mL total volume). The protein solution (0.062 mmol, 2 equiv vs. biotin sepharose, 300 mL) was added. After *ca*. 10 min incubation, the immobilized protein (containing 0.031 mmol of protein, corresponding to 0.093 mmol, free active sites) was washed at least three times with H_2O to remove the

unbound protein and flushed with nitrogen for three hours. The precatalyst solution in DMSO (100 μL, 0.062 μmol, 0.66 equiv with respect to the free biotin-binding sites) was added last and was incubated with the immobilized protein for 10 min. The immobilized catalyst was subjected to several cycles of washing and decanting. The catalytic runs were performed according to the standard orbital shaking procedure.

5.4.5. Hydrogenation procedure for the determination of Michaelis-Menten parameters

A 15-mL glass vessel was charged with a quantity (depending on the number of equivalent of substrates used) α-acetamidoacrylic acid in MES buffer (0.1 M, pH = 5.5). The volume was adjusted with water to 9 mL followed by addition of (strept)avidin in H2O (1 mL, 0.207 mM solution, 0.207 mmol of tetramer). The catalyst precursor $[Rh(COD)(spacer)]^+$ in DMSO (1 mL, 0.62 mmol) was added last. The resulting mixture was stirred for *ca.* 2 min to ensure a homogeneous medium. The reactor was closed and was removed from the glove box and pressurized to 2 bars H_2 and stirred mechanically at room temperature. Aliquots (*ca*. 0.5 mL) were sampled at given times.

The initial conversions were collected for each concentration of substrate. The initial rate of the reaction (ν) can be calculated by:

$\nu = ([substrate]_0 \cdot conversion)/t$

This value gives observed initial rate. The calculated initial rate can be obtained by employing the following equation: $\nu = \frac{V_{max}[S]}{K_M + [S]}$

with: $V_{max} = k_{cat}[E]_0$

ν = initial rate of reaction

V_{max} = maximum rate of reaction (kinetic saturation)

[S] = concentration of substrate

$[E]_0$ = initial concentration of enzyme (catalyst)

K_M = Michaelis-Menten (dissociation of substrate-catalyst complex) constant

k_{cat} = rate constant (turnover number) of reaction

The initial guessed values of both unknowns (K_M and V_{max}) were introduced in the calculation. Thereafter, a least squares-minimization was performed to obtain the calculated initial rate **ν** of the reaction and the Michaelis-Menten parameters.

5.4.6. Kinetics experiments using Michaelis-Menten models

Conversions of the reaction were collected from the independent experimental by varying the concentration of the substrate. The observed initial rate can thus be calculated by dividing the initial conversion with time. The calculated initial rate can be computed by introducing the initial guess values of Michaelis parameters (k_{cat} and K_M). To minimize the error between observed and calculated initial rate, a least-squares minimization was performed resulting k_{cat} and K_M. The ensemble data are collected and summarized in **Table 16**-21.

Table 16. Kinetic experiments data of $[Rh(COD)(\textbf{Biot-1})]^+ \subset$ WT Sav

C[a] substrate [mM]	time (min)	conv. (%)	$\nu_{initial}$ ($mM \cdot min^{-1}$)	$\nu_{initial}$ calc[b] ($mM \cdot min^{-1}$)
0.00	0	0	0.00	0.00
2.83	2	8	0.11	0.12
3.96	3	11	0.15	0.14
5.09	3	9	0.15	0.16
5.65	5	15	0.17	0.16
11.30	5	9	0.20	0.20
16.95	10	12	0.20	0.21
28.25	10	8	0.23	0.23
33.90	10	7	0.24	0.23

[a]C = concentration; [b]calc = calculated

Table 17. Kinetic experiments data of [Rh(COD)(**Biot-1**)]$^+$

C[a] substrate [mM]	time (min)	conv. (%)	$v_{initial}$ (mM·min^{-1})	$v_{initial}$ calc[b] (mM·min^{-1})
0.00	0	0	0.00	0.00
2.83	5	8	0.05	0.05
5.09	6	8	0.07	0.07
5.65	10	13	0.07	0.07
11.30	10	10	0.11	0.10
16.95	10	7	0.12	0.12
28.25	10	5	0.14	0.14
33.90	15	6	0.14	0.14

[a]C = concentration; [b]calc = calculated

Table 18. Kinetic experiments data of [Rh(COD)(**Biot-(*R*)-Pro-1**)]$^+$ ⊂ WT Sav in the presence of 30% DMSO

C[a] substrate [mM]	time (min)	conv. (%)	$v_{initial}$ (mM·min^{-1})	$v_{initial}$ calc[b] (mM·min^{-1})
0.00	0	0	0.00	0.00
2.83	3	22	0.21	0.23
5.09	5	31	0.32	0.33
5.65	5	33	0.37	0.34
11.30	5	20	0.45	0.45
16.95	5	15	0.51	0.49
28.25	10	19	0.54	0.54
33.90	15	24	0.54	0.56

[a]C = concentration; [b]calc = calculated

Table 19. Kinetic experiments data of [Rh(COD)(**Biot-(*R*)-Pro-1**)]$^+$ ⊂ WT Sav in the presence of 30% DMSO

C[a] substrate [mM]	time (min)	conv. (%)	$v_{initial}$ (mM·min^{-1})	$v_{initial}$ calc[b] (mM·min^{-1})
0.00	0	0	0.00	0.00
2.83	3	23	0.22	0.27
5.09	5	38	0.39	0.37
5.65	5	37	0.42	0.39
11.30	5	23	0.52	0.50
16.95	5	17	0.58	0.55
28.25	10	21	0.59	0.60
33.90	15	26	0.59	0.62

[a]C = concentration; [b]calc = calculated

Table 20. Kinetic experiments data of [Rh(COD)(**Biot-(*R*)-Pro-1**)]$^+$

C[a] substrate [mM]	time (min)	conv. (%)	$\nu_{initial}$ (mM·min^{-1})	$\nu_{initial}$ calc[b] (mM·min^{-1})
0	0	0	0	0
2.83	5	6	0.034	0.038
5.09	6	6	0.051	0.057
5.65	10	12	0.068	0.060
11.3	10	8	0.090	0.084
16.95	15	8	0.090	0.097
28.25	15	6	0.113	0.110
33.9	15	5	0.113	0.114

[a]C = concentration; [b]calc = calculated

Table 21. Kinetic experiments data of [Rh(COD)(**Biot-(*R*)-Pro-1**)]$^+$ in the presence of 30% DMSO

C[a] substrate [mM]	time (min)	conv. (%)	$\nu_{initial}$ (mM·min^{-1})	$\nu_{initial}$ calc[b] (mM·min^{-1})
0	0	0	0	0
2.83	3	5	0.047	0.053
5.09	5	7	0.071	0.077
5.65	5	8	0.090	0.082
11.3	5	5	0.113	0.112
16.95	5	4	0.136	0.128
28.25	10	5	0.141	0.145
33.9	15	6.5	0.147	0.149

[a]C = concentration; [b]calc = calculated

As comparison to linearization methods, we describe hereafter the linearization data treatment using Lineweaver-Burk plot [174]. The kinetics parameters then can be compiled by modifying the Michaelis-Menten equations.

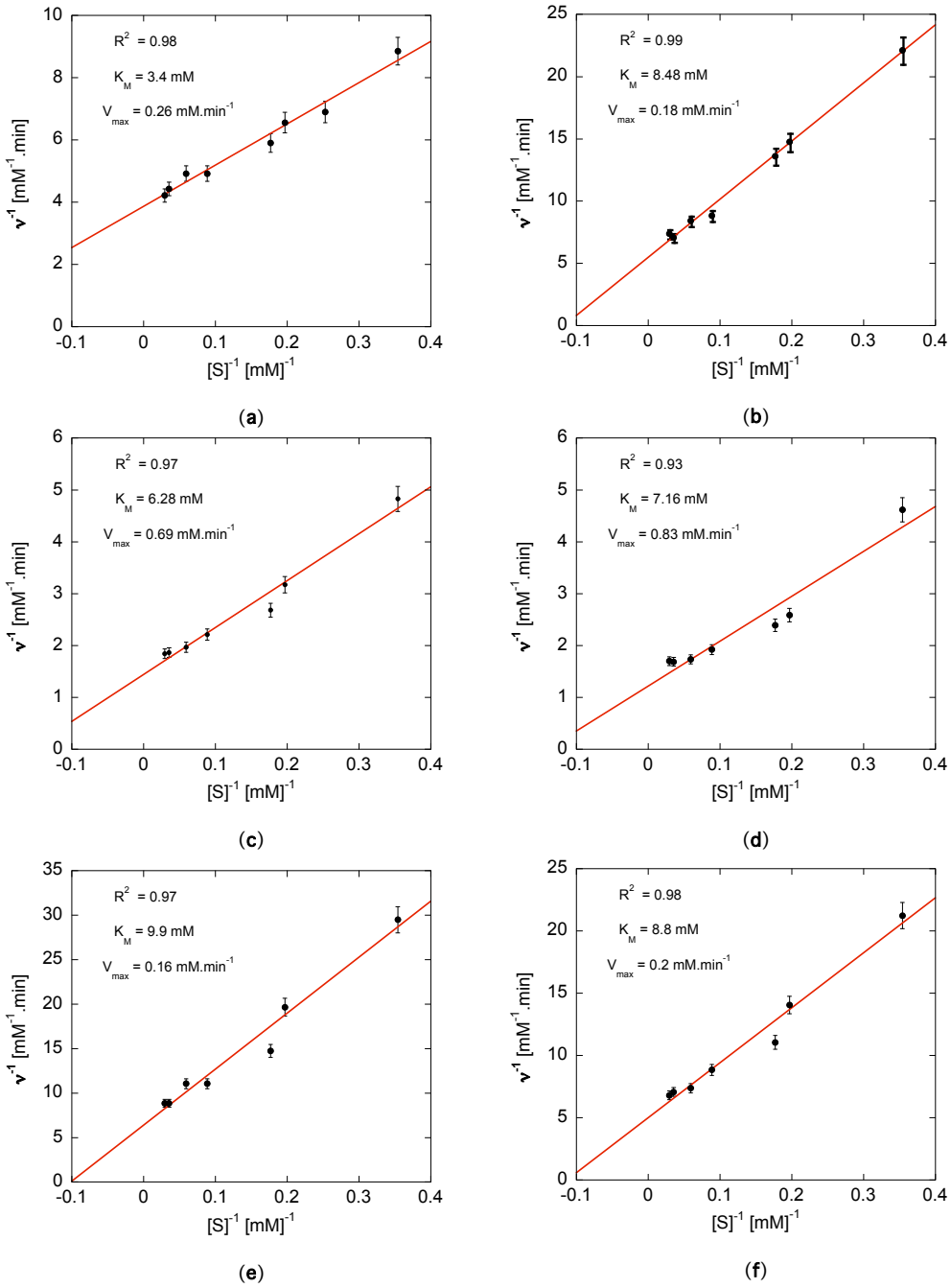

Figure 16. Lineweaver-Burk plot for each of the following system: [Rh(COD)(**Biot-1**)]$^+$ ⊂ WT Sav (a); [Rh(COD)(**Biot-1**)]$^+$ (b); [Rh(COD)(**Biot-(*R*)-Pro-1**)]$^+$ ⊂ WT Avi 30 % DMSO (c); [Rh(COD)(**Biot-(*R*)-Pro-1**)]$^+$ ⊂ WT Sav 30 % DMSO (d); [Rh(COD)(**Biot-1**)]$^+$ (e); [Rh(COD)(**Biot-(*R*)-Pro-1**)]$^+$ 30 % DMSO (f). Model equation is highlighted in red line in comparison with the observed data with calculated parameters (V_{max}, K_M, and R^2).

5.4.7. Analytical data for reduction products

Permabond-*L*-Chirasyl-Val (Macheray-Nagel), 25 m x 0.25 mm column: He carrier gas: 1.2 bar, inlet injector 280°C, oven (85°C; 10 min, 8°C/min; 135°C; 0 min, 10°C/min; 180°C; 35min), FID detector 200 °C; retention time:

Methyl *N*-acetylacetamidoacrylate: 9.3 min,

Methyl (*R*)-*N*-acetylacetamidoalanine: 17.2 min,

Methyl (*S*)-*N*-acetylacetamidoalanine: 18.5 min,

Methyl (*R*)-*N*-acetylacetamidophenylalanine: 35.4 min,

Methyl (*S*)-*N*-acetylacetamidophenylalanine: 36.1 min,

Methyl *N*-acetylacetamidocinnamate: 53.2 min.

Lipodex E, 25 m x 0.25 mm column: He carrier gas: 0.6 bar, inlet injector 280°C, oven (120°C; 10 min, 8°C/min; 10°C/min; 180°C; 10 min), FID detector 250 °C; retention time:

ketopantolactone: 23.7 min,

(*R*)-(-)-pantolactone: 25.0 min,

(*S*)-(-)-pantolactone: 25.3 min.

5.5. Titration Procedure

The activity of the host protein was determined using Gruber's protocol based on the fluorescence quenching of biotinylated fluorescein upon incorporation in (strept)avidin 49, 159.

All solutions were prepared and measured at room temperature in a phosphate buffer (pH = 7.0, I = 0.15 M). All aliquots were added using micropipettes. The collected data were analyzed and fitted using the programs SPECFIT/32 [160-162].

Aliquots of a Λ- or Δ-$[Ru(bpy)_2(Biot\text{-}bpy)]^{2+}$ solution (0.96 mM for Λ-$[Ru(bpy)_2(Biot\text{-}bpy)]^{2+}$ and 0.64 mM for Δ-$[Ru(bpy)_2(Biot\text{-}bpy)]^{2+}$) were added to (strept)avidin (8 μM initial concentration, 2400 μL, 19.2 nmol) in 0.25 equiv steps (5 μL per step, up to 6 equiv) relative to the tetrameric protein. The CD measurements (250-500 nm, band width 2 nm, step resolution 0.5 nm, response time 4 s, 3 accumulations) were recorded at 50 nm/min after thorough vortex mixing (1 min at rt).

5.6. Data treatment using SPECFIT/32

5.6.1. Spectra of each species

Spectra of each absorbing species obtained from SPECFIT/32 are depicted in **Figure 17** and **Figure 18**. As can be appreciated, the observed spectra of biotinylated complexes and apo-protein fit very well with the calculated spectra.

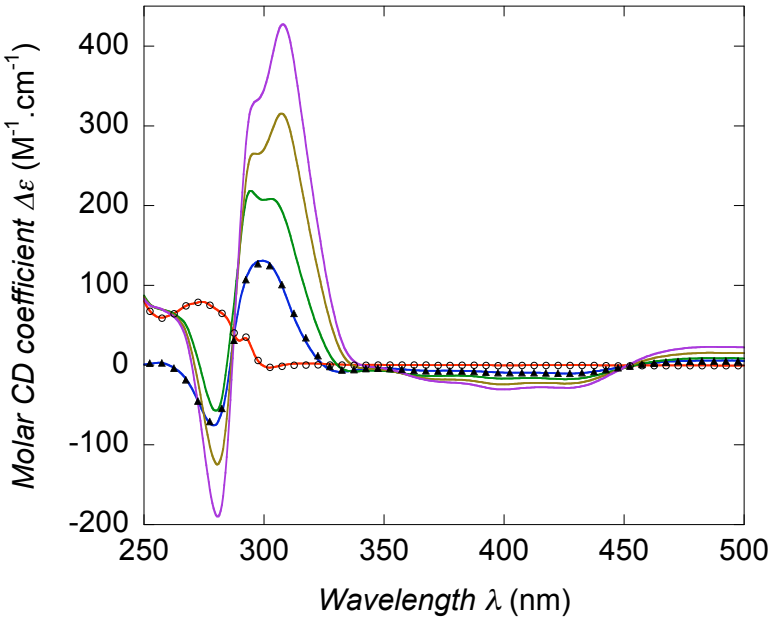

Figure 17. Refined CD spectra for each absorbing species for $(\Lambda\text{-}\mathbf{1})_x \subset$ streptavidin, $x = 0$: red line, $x = 2$: green line, $x = 3$: brown line and $x = 4$: violet line. For comparison, the measured spectra for the host protein and for the biotinylated guest Λ-**1** are displayed as open circles and full triangles respectively, overlaid with the corresponding refined spectra (thin lines).

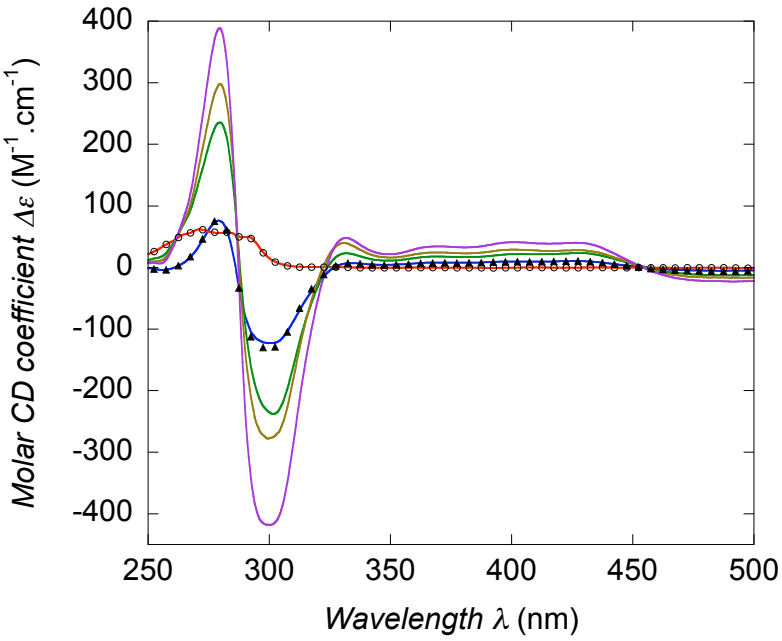

Figure 18. Refined CD spectra for each absorbing species for (Δ-**1**)$_x$ ⊂ avidin, x = 0: red line, x = 2: green line, x = 3: brown line and x = 4: violet line. For comparison, the measured spectra for the host protein and for the biotinylated guest Δ-**1** are displayed as open circles and full triangles respectively, overlaid with the corresponding refined spectra (thin lines).

5.6.2. Simulations for the Δ-1 ⊂ streptavidin system using SPECFIT/32

Simulated data sets were generated with SPECFIT/32 using a constant noise level and the following conditions:

[streptavidin]$_0$ = 7 × 10^{-6} M

[Δ-**1**]$_0$ = 9.6 × 10^{-4} M

Initial volume of streptavidin solution: V_0 = 2400 µL.

The solution of ruthenium complex Δ-[Ru(bpy)$_2$(Biot-bpy)]$^{2+}$ *Δ*-**1** is added in 0.005 mL increments up to 26 aliquots.

Equilibrium constants derived from **Table 3** (Chapter 2) were rounded off. Values were as follows:

streptavidin + Δ-**1** ⇆ (Δ-**1**) ⊂ streptavidin log $\beta_1 = 8$ (1)

streptavidin + 2 Δ-**1** ⇆ $(\Delta\text{-}\mathbf{1})_2$ ⊂ streptavidin log $\beta_2 = 19(2)$

streptavidin + 3 Δ-**1** ⇆ $(\Delta\text{-}\mathbf{1})_3$ ⊂ streptavidin log $\beta_4 = 28(3)$

streptavidin + 4 Δ-**1** ⇆ $(\Delta\text{-}\mathbf{1})_4$ ⊂ streptavidin log $\beta_4 = 36(4)$

Figure 19 shows a distribution diagram of the various species formed under these conditions during the simulated experiment.

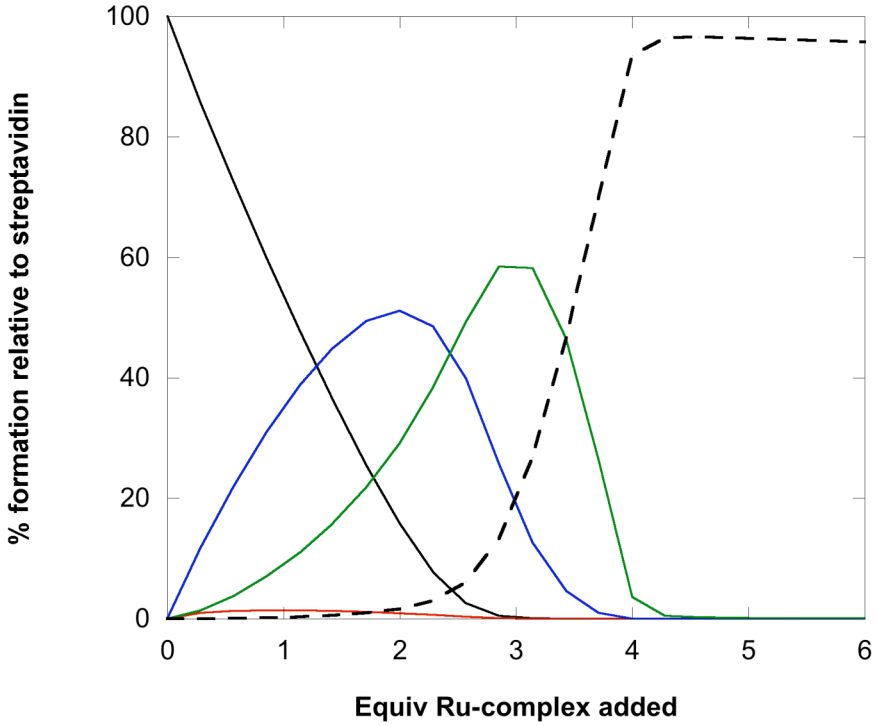

Figure 19. Species distribution diagram calculated for the above mentioned conditions (For each absorbing species for $(\Delta\text{-}[Ru(bpy)_2(Biot\text{-}bpy)]^{2+})_x \subset$ streptavidin ($(\Delta\text{-}[Ru(bpy)_2(Biot\text{-}bpy)]^{2+})_x \subset$ streptavidin). $x = 0$: black solid line, $x = 1$:red line, $x = 2$: blue line, $x = 3$: green line and $x = 4$: black dotted line.The fraction of the $(\Delta\text{-}[Ru(bpy)_2(Biot\text{-}bpy)]^{2+}) \subset$ streptavidin species does not exceed 1.4 %.

The individual CD spectra corresponding to each species used to construct the artificial data are displayed in **Figure 20**. The CD molar absorption $\Delta\varepsilon$ for $(\Delta\text{-}[Ru(bpy)_2(Biot\text{-}bpy)]^{2+}) \subset$ streptavidin were deduced from the experimentally refined

spectra obtained for $(\Delta\text{-}[Ru(bpy)_2(Biot\text{-}bpy)]^{2+})_2 \subset$ streptavidin by dividing the corresponding CD molar absorption $\Delta\varepsilon$ values by a factor of 2.

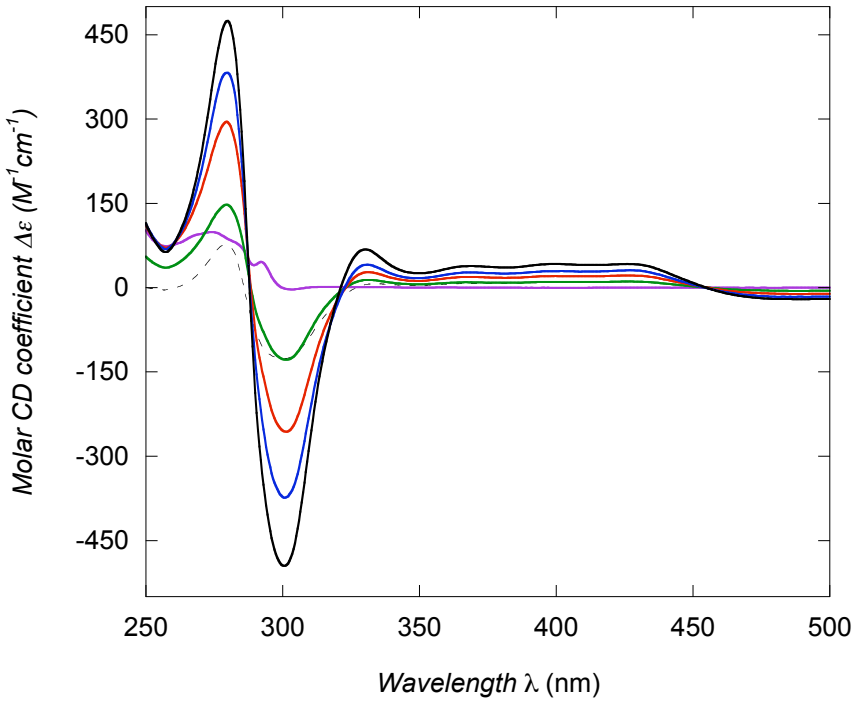

Figure 20. Fixed CD spectra used to generate the artificial data sets. For each absorbing species for $(\Delta\text{-}[Ru(bpy)_2(Biot\text{-}bpy)]^{2+})_x \subset$ streptavidin ($(\Delta\text{-}[Ru(bpy)_2(Biot\text{-}bpy)]^{2+})_x \subset$ streptavidin). $x = 0$: violet line, $x = 1$: green line, $x = 2$: red line, $x = 3$: blue line and $x = 4$: black solid line. The spectrum of $\Delta\text{-}[Ru(bpy)_2(Biot\text{-}bpy)]^{2+}$ is displayed as a dotted black line.

5.7. Experimental data of enantioselective hydrogenation

Table 22. Numerical results of enantioselective hydrogenation

Entry	Ligand	Protein	ee[a] *N*-AcPhe	Conv. *N*-AcPhe	ee[a] *N*-AcAla	Conv. *N*-AcAla
1	**Biot–(*R*)-Pro–1**	WT Avi	-89	quant. [b]	-87	quant. [b]
2	**Biot–(*S*)-Pro–1**	WT Avi	20	75	12	quant. [b]
3	**Biot–(*R*)-Phe–1**	WT Avi	-10	60	-5	quant. [b]

4	**Biot–(*S*)-Phe–1**	WT Avi	-12	98	-12	quant. [b]	
5	**Biot–(*R*)-Pro–1**	WT Sav	-91	quant. [b]	-87	quant. [b]	
6	**Biot–(*S*)-Pro–1**	WT Sav	23	quant. [b]	21	quant. [b]	
7	**Biot–(*R*)-Phe–1**	WT Sav	63	quant. [b]	65	quant. [b]	
8	**Biot–(*S*)-Phe–1**	WT Sav	-64	87	-73	quant. [b]	
9	**Biot–(*R*)-Pro–1**	S112A	-82	85	-69	quant. [b]	
10	**Biot–(*S*)-Pro–1**	S112A	6	70	22	quant. [b]	
11	**Biot–(*R*)-Phe–1**	S112A	44	51	61	quant. [b]	
12	**Biot–(*S*)-Phe–1**	S112A	-50	85	-65	quant. [b]	
13	**Biot–(*R*)-Pro–1**	S112C	-88	46	-88	quant. [b]	*
14	**Biot–(*S*)-Pro–1**	S112C	0	86	21	quant. [b]	
15	**Biot–(*R*)-Phe–1**	S112C	36	67	62	quant. [b]	
16	**Biot–(*S*)-Phe–1**	S112C	-3	98	-16	quant. [b]	
17	**Biot–(*R*)-Pro–1**	S112D	-81	72	-85	quant. [b]	
18	**Biot–(*S*)-Pro–1**	S112D	0	31	9	quant. [b]	
19	**Biot–(*R*)-Phe–1**	S112D	53	48	61	quant. [b]	
20	**Biot–(*S*)-Phe–1**	S112D	-68	90	-85	quant. [b]	
21	**Biot–(*R*)-Pro–1**	S112E	-55	16	-79	quant. [b]	
22	**Biot–(*S*)-Pro–1**	S112E	-11	16	1	91	
23	**Biot–(*R*)-Phe–1**	S112E	70	88	76	quant. [b]	
24	**Biot–(*S*)-Phe–1**	S112E	-70	85	-84	quant. [b]	
25	**Biot–(*R*)-Pro–1**	S112F	-93	91	-84	quant. [b]	

26	**Biot–(*S*)-Pro–1**	S112F	24	37	44	quant. [b]	*
27	**Biot–(*R*)-Phe–1**	S112F	41	48	62	quant. [b]	
28	**Biot–(*S*)-Phe–1**	S112F	63	75	63	quant. [b]	
29	**Biot–(*R*)-Pro–1**	S112G	-47	18	-56	quant. [b]	
30	**Biot–(*S*)-Pro–1**	S112G	37	95	54	quant. [b]	
31	**Biot–(*R*)-Phe–1**	S112G	13	88	53	quant. [b]	
32	**Biot–(*S*)-Phe–1**	S112G	-48	quant. [b]	0	quant. [b]	
33	**Biot–(*R*)-Pro–1**	S112H	-77	93	-78	quant. [b]	
34	**Biot–(*S*)-Pro–1**	S112H	-26	8	25	quant. [b]	
35	**Biot–(*R*)-Phe–1**	S112H	69	33	78	quant. [b]	
36	**Biot–(*S*)-Phe–1**	S112H	-78	65	-87	quant. [b]	*
37	**Biot–(*R*)-Pro–1**	S112I	-57	52	-57	quant. [b]	
38	**Biot–(*S*)-Pro–1**	S112I	1	69	17	quant. [b]	
39	**Biot–(*R*)-Phe–1**	S112I	74	80	84	quant. [b]	*
40	**Biot–(*S*)-Phe–1**	S112I	50	99	27	quant. [b]	*
41	**Biot–(*R*)-Pro–1**	S112K	-84	36	-88	quant. [b]	*
42	**Biot–(*S*)-Pro–1**	S112K	-35	12	0	86	
43	**Biot–(*R*)-Phe–1**	S112K	67	64	79	quant. [b]	
44	**Biot–(*S*)-Phe–1**	S112K	-48	62	-59	quant. [b]	
45	**Biot–(*R*)-Pro–1**	S112L	-55	13	-20	81	
46	**Biot–(*S*)-Pro–1**	S112L	-15	99	7	quant. [b]	
47	**Biot–(*R*)-Phe–1**	S112L	74	88	83	quant. [b]	*

48	**Biot–(*S*)-Phe–1**	S112L	66	quant. [b]	36	quant. [b]	
49	**Biot–(*R*)-Pro–1**	S112M	-82	63	-85	quant. [b]	
50	**Biot–(*S*)-Pro–1**	S112M	3	61	26	quant. [b]	
51	**Biot–(*R*)-Phe–1**	S112M	75	94	86	quant. [b]	*
52	**Biot–(*S*)-Phe–1**	S112M	87	quant. [b]	73	quant. [b]	*
53	**Biot–(*R*)-Pro–1**	S112N	-86	88	-89	quant. [b]	
54	**Biot–(*S*)-Pro–1**	S112N	6	16	15	quant. [b]	
55	**Biot–(*R*)-Phe–1**	S112N	62	38	70	quant. [b]	
56	**Biot–(*S*)-Phe–1**	S112N	-68	73	-88	quant. [b]	*
57	**Biot–(*R*)-Pro–1**	S112P	-79	18	-85	92	
58	**Biot–(*S*)-Pro–1**	S112P	54	20	62	quant. [b]	
59	**Biot–(*R*)-Phe–1**	S112P	61	23	72	quant. [b]	
60	**Biot–(*S*)-Phe–1**	S112P	-34	24	-50	quant. [b]	
61	**Biot–(*R*)-Pro–1**	S112Q	-87	52	-88	quant. [b]	*
62	**Biot–(*S*)-Pro–1**	S112Q	11	74	9	quant. [b]	
63	**Biot–(*R*)-Phe–1**	S112Q	76	82	81	quant. [b]	*
64	**Biot–(*S*)-Phe–1**	S112Q	-31	98	-54	quant. [b]	
65	**Biot–(*R*)-Pro–1**	S112R	-88	54	-92	quant. [b]	
66	**Biot–(*S*)-Pro–1**	S112R	-31	73	-12	quant. [b]	
67	**Biot–(*R*)-Phe–1**	S112R	82	75	84	quant. [b]	*
68	**Biot–(*S*)-Phe–1**	S112R	-33	66	-31	quant. [b]	
69	**Biot–(*R*)-Pro–1**	S112T	-68	88	-68	quant. [b]	

70	**Biot–(*S*)-Pro–1**	S112T	-2	95	17	quant. [b]	
71	**Biot–(*R*)-Phe–1**	S112T	49	94	67	quant. [b]	
72	**Biot–(*S*)-Phe–1**	S112T	-62	quant. [b]	-61	quant. [b]	
73	**Biot–(*R*)-Pro–1**	S112V	-56	74	-77	quant. [b]	
74	**Biot–(*S*)-Pro–1**	S112V	-42	53	-2	quant. [b]	
75	**Biot–(*R*)-Phe–1**	S112V	28	44	59	quant. [b]	
76	**Biot–(*S*)-Phe–1**	S112V	-66	92	-54	quant. [b]	
77	**Biot–(*R*)-Pro–1**	S112W	-95	quant. [b]	-95	quant. [b]	*
78	**Biot–(*S*)-Pro–1**	S112W	-2	20	5	quant. [b]	
79	**Biot–(*R*)-Phe–1**	S112W	66	56	74	quant. [b]	
80	**Biot–(*S*)-Phe–1**	S112W	27	51	38	quant. [b]	*
81	**Biot–(*R*)-Pro–1**	S112Y	-93	97	-92	quant. [b]	*
82	**Biot–(*S*)-Pro–1**	S112Y	35	74	27	quant. [b]	
83	**Biot–(*R*)-Phe–1**	S112Y	63	61	76	quant. [b]	
84	**Biot–(*S*)-Phe–1**	S112Y	73	90	67	quant. [b]	*

[a]ee in %, positive ee values in favor of the (*R*)-enantiomer, negative ee values in favor of the (*S*)-enantiomer; [b]quantitative; *selected results for Table 6 in Chapter 3; *N*-AcPhe = *N*-acetamidophenylalanine, *N*-AcAla = *N*-acetamidoalanine.

REFERENCES

1. Fish, R. H., *Bioorganometallics* **2006**, 321.
2. Nevo, Y.;Nelson, N., *Biochim. Biophys. Acta* **2006,** 1763, 609.
3. Kent, J. A.;Editor, *Riegel's Handbook of Industrial Chemistry, Tenth Edition*. 2003; p 1374 pp.
4. Bailey, J. E.;Editor, *Ullmann's Encyclopedia of Industrial Chemistry, 6th Edition: 1999 Electronic Release*. 1999; p No pp given.
5. Green, N. M., *Biochem. J.* **1965,** 94, 23c.
6. Green, N. M., *Biochem. J.* **1966,** 101, 774.
7. Rao, J.;Lahiri, J.;Isaacs, L.;Weis, R. M.;Whitesides, G. M., *Science* **1998,** 280.
8. Nair, H. K.;Lee, K.;Quinn, D. M., *J. Am. Chem. Soc.* **1993,** 115, 9939.
9. Green, N. M., *Adv. Protein Chem.* **1975,** 29, 85.
10. Green, N. M., Avidin and Streptavidin. In *Avidin-Biotin Technology*, Wilchek, M.; Bayer, E. A., Eds. Academic Press: San Diego, 1990; Vol. 184, pp 51.
11. Livnah, O.;Bayer, E. A.;Wilchek, M.;Sussman, J. L., *Proc. Natl. Acad. Sci. USA* **1993,** 90, 5076.
12. Livnah, O.;Bayer, E. A.;Wilchek, M.;Sussman, J. L., *FEBS Lett.* **1993,** 328, 165.
13. Weber, P. C.;Ohlendorf, D. H.;Wendoloski, J. J.;Salemme, F. R., *Science* **1989,** 243, 85.
14. Weber, P. C.;Wendoloski, J. J.;Pantoliano, M. W.;Salemme, F. R., *J. Am. Chem. Soc.* **1992,** 114, 3197.
15. Lin, C.-C.;Lin, C.-W.;Chan, A. S. C., *Tetrahedron: Asymmetry* **1999,** 10, 1887.
16. Lo, K. K.-W.;Chan, J. S.-W.;Lui, L.-H.;Chung, C.-K., *Organometallics* **2004,** 23, 3108.
17. Lo, K. K.-W.;Hui, W.-K., *Inorg. Chem.* **2005,** 44, 1992.
18. Lo, K. K.-W.;Hui, W.-K.;Ng, D. C.-M., *J. Am. Chem. Soc.* **2002,** 124, 9344.
19. Lo, K. K.-W.;Lee, T. K.-M., *Inorg. Chem.* **2004,** 43, 5275.
20. Loosli, A.;Rusbandi, U. E.;Gradinaru, J.;Bernauer, K.;Schlaepfer, C. W.;Meyer, M.;Mazurek, S.;Novic, M.;Ward, T. R., *Inorg. Chem.* **2006,** 45, 660.
21. Skander, M.;Humbert, N.;Collot, J.;Gradinaru, J.;Klein, G.;Loosli, A.;Sauser, J.;Zocchi, A.;Gilardoni, F.;Ward Thomas, R., *J. Am. Chem. Soc.* **2004,** 126, 14411.

22. Skander, M.;Malan, C.;Ivanova, A.;Ward, T. R., *Chem. Commun.* **2005**, 4815.

23. Slim, M.;Sleiman, H. F., *Bioconjugate Chem.* **2004,** 15, 949.

24. Thomas, C. M.;Letondor, C.;Humbert, N.;Ward, T. R., *J. Organomet. Chem.* **2005,** 690, 4488.

25. Thomas, C. M.;Ward, T. R., *Chem. Soc. Rev.* **2005,** 34, 337.

26. Ward, T. R., *Chem.Eur. J.* **2005,** 11, 3798.

27. Wilson, M. E.;Whitesides, G. M., *J. Am. Chem. Soc.* **1978,** 100, 306.

28. Zhou, X.;Shearer, J.;Rokita, S. E., *J. Am. Chem. Soc.* **2000,** 122, 9046.

29. Fukushima, H.;Taylor, D. M.;Morgan, H.;Ringsdorf, H.;Rump, E., *Thin Solid Films* **1995,** 266, 289.

30. Knox, S. J.;Goris, M. L.;Tempero, M.;Weiden, P. L.;Gentner, L.;Breitz, H.;Adams, G. P.;Axworthy, D.;Gaffigan, S.;Bryan, K.;Fisher, D. R.;Colcher, D.;Horak, I. D.;Weiner, L. M., *Clin. Cancer Res.* **2000,** 6, 406.

31. Hnatowich, D. J.;Virzi, F.;Rusckowski, M., *J. Nucl. Med.* **1987,** 28, 1294.

32. Kalofonos, H. P.;Rusckowski, M.;Siebecker, D. A.;Sivolapenko, G. B.;Snook, D.;Lavender, J. P.;Epenetos, A. A.;Hnatowich, D. J., *J. Nucl. Med.* **1990,** 31, 1791.

33. Van Osdol, W. W.;Sung, C.;Dedrick, R. L.;Weinstein, J. N., *J. Nucl. Med.* **1993,** 34, 1552.

34. Poston, R.;Ginon, I.;McGregor, J. Therapy of atherosclerosis. 99-EP2577 9952551, 19990415., 1999.

35. Cao, R.;Gu, Z.;Hsu, L.;Patterson, G. D.;Armitage, B. A., *J. Am. Chem. Soc.* **2003,** 125, 10250.

36. Caswell, K. K.;Wilson James, N.;Bunz Uwe, H. F.;Murphy Catherine, J., *J. Am. Chem. Soc.* **2003,** 125, 13914.

37. Richter, J.;Adler, M.;Niemeyer, C. M., *ChemPhysChem* **2003,** 4, 79.

38. Rivera, V. R.;Merrill, G. A.;White, J. A.;Poli, M. A., *Anal. Biochem.* **2003,** 321, 125.

39. Ruggiero, F. P.;Sheffield, J. B., *J. Histochem. Cytochem.* **1998,** 46, 177.

40. Weizmann, Y.;Patolsky, F.;Katz, E.;Willner, I., *J. Am. Chem. Soc.* **2003,** 125, 3452.

41. Wilchek, M.;Bayer, E. A.;Editors, *Methods in Enzymology, Vol. 184: Avidin-Biotin Technology*. 1990; p 746 pp.

42. Haddour, N.;Gondran, C.;Cosnier, S., *Chem. Commun.* **2004**, 324.

43. Schetters, H., *Biomol. Eng.* **1999,** 16, 73.

44. Nun, T. K.;Kroll, D. J.;Oberlies, N. H.;Soejarto, D. D.;Case, R. J.;Piskaut, P.;Matainaho, T.;Hilscher, C.;Wang, L.;Dittmer, D. P.;Gao, S.-J.;Damania, B., *Mol. Cancer Ther.* **2007,** 6, 2360.

45. Johnson, J. D.;Dennull, R. A.;Gerena, L.;Lopez-Sanchez, M.;Roncal, N. E.;Waters, N. C., *Antimicrob. Agents Chemother.* **2007,** 51, 1926.

46. Mackintosh, J. A.;Veal, D. A.;Karuso, P., *Proteomics* **2005,** 5, 4673.

47. Zhang, B.;Senator, D.;Wilson, C. J.;Ng, S.-C., *Anal. Biochem.* **2005,** 345, 326.

48. Kruger, W.;Gilbert, D.;Hawthorne, R.;Hryciw, D. H.;Frings, S.;Poronnik, P.;Lynch, J. W., *Neurosci. Lett.* **2005,** 380, 340.

49. Gruber, H. J.;Marek, M.;Schindler, H.;Kaiser, K., *Bioconjugate Chem.* **1997,** 8, 552.

50. Marek, M.;Kaiser, K.;Gruber, H. J., *Bioconjugate Chem.* **1997,** 8, 560.

51. Ercolani, G., *J. Am. Chem. Soc.* **2003,** 125, 16097.

52. Perlmutter-Hayman, B., *Acc. Chem. Res.* **1986,** 19, 90.

53. Cantor, C. R.;Schimmel, P. R., *Biophysical Chemistry*. W. H. Freemand and Company: San Francisco, 1979.

54. Tyuma, I.;Imai, K.;Shimizu, K., *Biochemistry* **1973,** 12, 1491.

55. Wang, H.;Tang, Y.;Lei, M., *Arch. Biochem. Biophys.* **2007,** 466, 85.

56. Hughes, A. D.;Anslyn, E. V., *Proc. Natl. Acad. Sci. U. S. A.* **2007,** 104, 6538.

57. Zhou, Z.;Bai, Y., *Nature* **2007,** 445, E16.

58. Williams, D. H.;Davies, N. L.;Zerella, R.;Bardsley, B., *J. Am. Chem. Soc.* **2004,** 126, 2042.

59. Zhang, Y.;Kobayashi, K.;Sasagawa, K.;Imai, K.;Kobayashi, M., *Zoolog. Sci.* **2003,** 20, 1087.

60. Sano, T.;Cantor, C. R., *J. Biol. Chem.* **1990,** 265, 3369.

61. Jones, M. L.;Kurzban, G. P., *Biochemistry* **1995,** 34, 11750.

62. Englander, S. W.;Englander, J. J.;McKinnie, R. E.;Ackers, G. K.;Turner, G. J.;Westrick, J. A.;Gill, S. J., *Science* **1992,** 256, 1684.

63. Knowles, W. S., *Angew. Chem., Int. Ed. Engl.* **2002,** 41, 1998.

64. Knowles, W. S., *Adv. Synth. Catal.* **2003,** 345, 3.

65. Noyori, R., *Angew. Chem., Int. Ed. Engl.* **2002,** 41, 2008.

66. Noyori, R., *Adv. Synth. Catal.* **2003,** 345, 15.

67. Sharpless, K. B., *Angew. Chem., Int. Ed. Engl.* **2002,** 41, 2024.

68. Kumobayashi, H.;Miura, T.;Sayo, N.;Saito, T.;Zhang, X., *Synlett* **2001**, 1055.

69. Jacobsen, E. N.;Pfaltz, A.;Yamamoto, H.;Editors, *Comprehensive Asymmetric Catalysis I-III, Volume 1*. 1999; p 487 pp.

70. Osborn, J. A.;Jardine, F. H.;Young, J. F.;Wilkinson, G., *J. Chem. Soc., Chem. Commun.* **1966**, 1711.

71. Osborn, J. A.;Wilkinson, G.;Young, J. F., *Chem. Commun.* **1965**, 17.

72. Knowles, W. S.;Sabacky, M. J., *Chemical Communications (London)* **1968**, 1445.

73. Knowles, W. S., *Asymmetric Synthesis* **2007**, 316.

74. Knowles, W. S., *Asymmetric Catalysis on Industrial Scale* **2004**, 23.

75. Kagan, H. B.;Dang Tuan, P., *J. Am. Chem. Soc.* **1972,** 94, 6429.

76. Blaser, H.-U.;Malan, C.;Pugin, B.;Spindler, F.;Steiner, H.;Studer, M., *Adv. Synth. Catal.* **2003,** 345, 103.

77. Miyashita, A.;Yasuda, A.;Takaya, H.;Toriumi, K.;Ito, T.;Souchi, T.;Noyori, R., *J. Am. Chem. Soc.* **1980,** 102, 7932.

78. Hoen, R.;Van den Berg, M.;Bernsmann, H.;Minnaard, A. J.;De Vries, J. G.;Feringa, B. L., *Org. Lett.* **2004,** 6, 1433.

79. Matsumura, K.;Saito, T. Process for producing an optically active amide from an alpha,beta-unsaturated amide derivative in the presence of a transition metal complex of an optically active phosphine-phospholane. 2002-291876 1279660, 20020724., 2003.

80. Van den Berg, M.;Haak, R. M.;Minnaard, A. J.;De Vries, A. H. M.;De Vries, J. G.;Feringa, B. L., *Adv. Synth. Catal.* **2002,** 344, 1003.

81. Hu, A.-G.;Fu, Y.;Xie, J.-H.;Zhou, H.;Wang, L.-X.;Zhou, Q.-L., *Angew. Chem., Int. Ed. Engl.* **2002,** 41, 2348.

82. Gridnev, I. D.;Yasutake, M.;Higashi, N.;Imamoto, T., *J. Am. Chem. Soc.* **2001,** 123, 5268.

83. Schmid, R.;Broger, E. A.;Cereghetti, M.;Crameri, Y.;Foricher, J.;Lalonde, M.;Muller, R. K.;Scalone, M.;Schoettel, G.;Zutter, U., *Pure Appl. Chem.* **1996,** 68, 131.

84. Noyori, R.;Ohkuma, T., *Angew. Chem., Int. Ed. Engl.* **2001,** 40, 40.

85. Togni, A.;Hayashi, T., *Ferrocenes, Homogeneous Catalysis - Organic Synthesis - Materials Science*. 1995; Vol. 34, p 395.

86. Gokel, G. W.;Ugi, I. K., *J. Chem. Educ.* **1972,** 49, 294.

87. Gokel, G.;Ugi, I. K., *Angew. Chem., Int. Ed. Engl.* **1971,** 10, 191.

88. Blaser, H.-U.;Brieden, W.;Pugin, B.;Spindler, F.;Studer, M.;Togni, A., *Top. Catal.* **2002,** 19, 3.

89. Burk, M. J., *Acc. Chem. Res.* **2000,** 33, 363.

90. Holz, J.;Heller, D.;Sturmer, R.;Borner, A., *Tetrahedron Lett.* **1999,** 40, 7059.

91. Tang, W.;Wu, S.;Zhang, X., *J. Am. Chem. Soc.* **2003,** 125, 9570.

92. Blaser, H.-U., *Chem. Commun.* **2003**, 293.

93. Blaser, H. U.;Spindler, F.;Studer, M., *Appl. Catal., A* **2001,** 221, 119.

94. Pugin, B.;Blaser, H.-U., *Adv. Synth. Catal.* **2006,** 348, 1743.

95. Corma, A.;Iglesias, M.;Del Pino, C.;Sanchez, F., *J. Chem. Soc., Chem. Commun.* **1991**, 1253.

96. Hems, W. P.;McMorn, P.;Riddel, S.;Watson, S.;Hancock, F. E.;Hutchings, G. J., *Org. Biomol. Chem.* **2005,** 3, 1547.

97. Buergi, T.;Baiker, A., *Acc. Chem. Res.* **2004,** 37, 909.

98. Raja, R.;Thomas, J. M.;Jones, M. D.;Johnson, B. F. G.;Vaughan, D. E. W., *J. Am. Chem. Soc.* **2003,** 125, 14982.

99. Blaser, H.-U.;Studer, M., *Green Chem.* **2003,** 5, 112.

100. Walsh, P. J.;Li, H.;de Parrodi, C. A., *Chem. Rev.* **2007,** 107, 2503.

101. Dwars, T.;Oehme, G., *Adv. Synth. Catal.* **2002,** 344, 239.

102. Wan, K. T.;Davis, M. E., *Tetrahedron: Asymmetry* **1993,** 4, 2461.

103. Wan, K. T.;Davis, M. E., *J. Chem. Soc., Chem. Commun.* **1993**, 1262.

104. Toth, I.;Hanson, B. E., *Tetrahedron: Asymmetry* **1990,** 1, 895.

105. Toth, I.;Hanson, B. E.;Davis, M. E., *Catal. Lett.* **1990,** 5, 183.

106. Toth, I.;Hanson, B. E.;Davis, M. E., *Tetrahedron: Asymmetry* **1990,** 1, 913.

107. Wan, K. T.;Davis, M. E., *J. Catal.* **1995,** 152, 25.

108. Sheldon, R., *Chem. Commun.* **2001**, 2399.

109. Pugin, B.;Studer, M.;Kuesters, E.;Sedelmeier, G.;Feng, X., *Adv. Synth. Catal.* **2004,** 346, 1481.

110. Jessop, P. G.;Ikariya, T.;Noyori, R., *Chem. Rev.* **1999,** 99, 475.

111. Segel, I. H., *Enzyme Kinetics: Behavior and Analysis of Rapid Equilibrium and Steady-State Enzyme Systems*. 1975; p 1024 pp.

112. Liese, A.;Filho, M. V., *Curr. Opin. Biotechnol.* **1999,** 10, 595.

113. Balkenhohl, F.;Ditrich, K.;Hauer, B.;Ladner, W., *J. Prakt. Chem.* **1997,** 339, 381.

114. Simon, H.;Rambeck, B.;Hashimoto, H.;Guenther, H.;Nohynek, G.;Neumann, H., *Angew. Chem.* **1974,** 86, 675.

115. Ohta, H.;Konishi, J.;Tsuchihashi, G., *Chem. Lett.* **1983**, 1895.

116. Ohta, H.;Konishi, J.;Tsuchihashi, G., *Agric. Biol. Chem.* **1985,** 49, 665.

117. Stuermer, R.;Hauer, B.;Hall, M.;Faber, K., *Curr. Opin. Chem. Biol.* **2007,** 11, 203.

118. Reetz, M. T., *Tetrahedron* **2002,** 58, 6595.

119. Martin-Matute, B.;Edin, M.;Bogar, K.;Backvall Jan, E., *Angew. Chem., Int. Ed. Engl.* **2004,** 43, 6535.

120. Martin-Matute, B.;Edin, M.;Bogar, K.;Kaynak, F. B.;Backvall Jan, E., *J. Am. Chem. Soc.* **2005,** 127, 8817.

121. Pamies, O.;Backvall, J.-E., *Curr. Opin. Biotechnol.* **2003,** 14, 407.

122. Paetzold, J.;Backvall Jan, E., *J. Am. Chem. Soc.* **2005,** 127, 17620.

123. Rissom, S.;Beliczey, J.;Giffels, G.;Kragl, U.;Wandrey, C., *Tetrahedron: Asymmetry* **1999,** 10, 923.

124. Stampfer, W.;Kosjek, B.;Moitzi, C.;Kroutil, W.;Faber, K., *Angew. Chem., Int. Ed. Engl.* **2002,** 41, 1014.

125. Groger, H.;Chamouleau, F.;Orologas, N.;Rollmann, C.;Drauz, K.;Hummel, W.;Weckbecker, A.;May, O., *Angew. Chem., Int. Ed. Engl.* **2006,** 45, 5677.

126. Kaiser, E. T.;Lawrence, D. S., *Science* **1984,** 226, 505.

127. Davies, R. R.;Distefano, M. D., *J. Am. Chem. Soc.* **1997,** 119, 11643.

128. Reetz, M. T.;Rentzsch, M.;Pletsch, A.;Maywald, M., *Chimia* **2002,** 56, 721.

129. Panella, L.;Broos, J.;Jin, J.;Fraaije, M. W.;Janssen, D. B.;Jeronimus-Stratingh, M.;Feringa, B. L.;Minnaard, A. J.;De Vries, J. G., *Chem. Commun.* **2005**, 5656.

130. Carey James, R.;Ma Steven, K.;Pfister Thomas, D.;Garner Dewain, K.;Kim Hyeon, K.;Abramite Joseph, A.;Wang, Z.;Guo, Z.;Lu, Y., *J. Am. Chem. Soc.* **2004,** 126, 10812.

131. Razavet, M.;Artero, V.;Cavazza, C.;Oudart, Y.;Lebrun, C.;Fontecilla-Camps, J. C.;Fontecave, M., *Chem. Commun.* **2007**, 2805.

132. Yamamura, K.;Kaiser, E. T., *J. Chem. Soc., Chem. Commun.* **1976**, 830.

133. Ueno, T.;Koshiyama, T.;Abe, S.;Yokoi, N.;Ohashi, M.;Nakajima, H.;Watanabe, Y., *J. Organomet. Chem.* **2007,** 692, 142.

134. Matsuo, T.;Hayashi, T.;Hisaeda, Y., *J. Am. Chem. Soc.* **2002,** 124, 11234.

135. Rosenberg, R. C.;Root, C. A.;Bernstein, P. K.;Gray, H. B., *J. Am. Chem. Soc.* **1975,** 97, 2092.

136. Kokubo, T.;Sugimoto, T.;Uchida, T.;Tanimoto, S.;Okano, M., *J. Chem. Soc., Chem. Commun.* **1983**, 769.

137. van de Velde, F.;Konemann, L.;van Rantwijk, F.;Sheldon, R. A., *Biotechnol. Bioeng.* **2000,** 67, 87.

138. Okrasa, K.;Kazlauskas, R. J., *Chem.Eur. J.* **2006,** 12, 1587.

139. Fernandez-Gacio, A.;Codina, A.;Fastrez, J.;Riant, O.;Soumillion, P., *ChemBioChem* **2006,** 7, 1013.

140. Bornscheuer Uwe, T.;Kazlauskas Romas, J., *Angew. Chem., Int. Ed. Engl.* **2004,** 43, 6032.

141. Kazlauskas, R. J., *Curr. Opin. Chem. Biol.* **2005,** 9, 195.

142. Yamaguchi, H.;Hirano, T.;Kiminami, H.;Taura, D.;Harada, A., *Org. Biomol. Chem.* **2006,** 4, 3571.

143. Roelfes, G.;Feringa, B. L., *Angew. Chem., Int. Ed. Engl.* **2005,** 44, 3230.

144. Ueno, T.;Suzuki, M.;Goto, T.;Matsumoto, T.;Nagayama, K.;Watanabe, Y., *Angew. Chem., Int. Ed. Engl.* **2004,** 43, 2527.

145. Letondor, C.;Humbert, N.;Ward, T. R., *Proc. Natl. Acad. Sci. U. S. A.* **2005,** 102, 4683.

146. Letondor, C.;Pordea, A.;Humbert, N.;Ivanova, A.;Mazurek, S.;Novic, M.;Ward, T. R., *J. Am. Chem. Soc.* **2006,** 128, 8320.

147. Letondor, C.;Ward, T. R., *ChemBioChem* **2006,** 7, 1845.

148. Landis, C. R.;Halpern, J., *J. Am. Chem. Soc.* **1987,** 109, 1746.

149. Blackmond, D. G., *Angew. Chem., Int. Ed. Engl.* **2005,** 44, 4302.

150. Blackmond, D. G., *Angew. Chem., Int. Ed. Engl.* **2006,** 45, 2162.

151. Boudart, M.;Djega-Mariadassou, G., *Catal. Lett.* **1994,** 29, 7.

152. Collot, J. Metalloenzymes Artificielles pour l'Hydrogénation Enantioselective basée sur la Technologie Biotin-Avidine. Université de Neuchâtel, Neuchâtel, 2004.

153. Collot, J.;Humbert, N.;Skander, M.;Klein, G.;Ward, T. R., *J. Organomet. Chem.* **2004,** 689, 4868.

154. Li, Z.;Ortega-Vilain, A.-C.;Patil, G. S.;Chu, D.-L.;Foreman, J. E.;Eveleth, D. D.;Powers, J. C., *J. Med. Chem* **1996,** 39, 4089.

155. Somlai, C.;Berenyi, M.;Maroy, P., *Z. Naturforsch., B: Chem. Sci.* **1993,** 48, 511.

156. Loosli, A. Investigation of Second Coordination Sphere Interactions between Biotinylated Coordination Complexes and (Strept)avidin: CD Spectroscopy as a Powerful Tool for Stability Constant Determinations. Université de Neuchâtel, Neuchâtel, 2004.

157. Hua, X.;Lappin, A. G., *Inorg. Chem.* **1995,** 34, 992.

158. Hua, X.;von Zelewsky, A., *Inorg. Chem.* **1995,** 34, 5791.

159. Gruber, H. J.;Kada, G.;Marek, M.;Kaiser, K., *Biochim. Biophys. Acta* **1998,** 1381, 203.

160. Gampp, H.;Maeder, M.;Meyer, C. J.;Zuberbühler, A. D., *Talanta* **1985,** 32, 95.

161. Gampp, H.;Maeder, M.;Meyer, C. J.;Zuberbühler, A. D., *Talanta* **1985,** 32, 251.

162. Gampp, H.;Maeder, M.;Meyer, C. J.;Zuberbühler, A. D., *Talanta* **1985,** 32, 1133.

163. Marquardt, D. W., *J. Soc. Indust. Appl. Math.* **1963,** 11, 431.

164. Collot, J.;Gradinaru, J.;Humbert, N.;Skander, M.;Zocchi, A.;Ward Thomas, R., *J. Am. Chem. Soc.* **2003,** 125, 9030.

165. Klein, G.;Humbert, N.;Gradinaru, J.;Ivanova, A.;Gilardoni, F.;Rusbandi, U. E.;Ward, T. R., *Angew. Chem., Int. Ed. Engl.* **2005,** 44, 7764.

166. Ward, T. R.;Collot, J.;Gradinaru, J.;Loosli, A.;Skander, M.;Letondor, C.;Joseph, E.;Klein, G., *Chimia* **2003,** 57, 586.

167. Knowles, W. S., *Acc. Chem. Res.* **1983,** 16, 106.

168. Skander, M. Métalloenzymes Artificielles: Nouvelle Génération de Catalyseurs Efficaces pour l'Hydrogénation Enantioselective. Université de Neuchâtel, Neuchâtel, 2005.

169. Reetz, M. T.;Peyralans, J. J. P.;Maichele, A.;Fu, Y.;Maywald, M., *Chem. Commun.* **2006**, 4318.

170. Deimling, A.;Karandikar, B. M.;Shah, Y. T.;Carr, N. L., *Chem. Eng. J.* **1984,** 29, 127.

171. Eadie, G. S., *J. Biol. Chem.* **1942,** 146, 85.

172. Fersht, A., *Structure and Mechanism in Protein Science*. 1999.

173. Hofstee, B. H. J., *Nature* **1959,** 184, 1296.

174. Lineweaver, H.;Burk, D., *J. Am. Chem. Soc.* **1934,** 56, 658.

175. McCormick, D. B.;Roth, J. A., *Methods Enzymol.* **1970,** 18, 383.

176. McCormick, D. B.;Roth, J. A., *Anal. Biochem.* **1970,** 34, 226.